Acta Numerica (1995), *pp.* 335–415

Numerical Solutions to Free Boundary Problems*

Thomas Y. Hou
Applied Mathematics,
California Institute of Technology,
Pasadena, CA 91125
E-mail: hou@ama.caltech.edu

Many physically interesting problems involve propagation of free surfaces. Vortex-sheet roll-up in hydrodynamic instability, wave interactions on the ocean's free surface, the solidification problem for crystal growth and Hele–Shaw cells for pattern formation are some of the significant examples. These problems present a great challenge to physicists and applied mathematicians because the underlying problem is very singular. The physical solution is sensitive to small perturbations. Naïve discretisations may lead to numerical instabilities. Other numerical difficulties include singularity formation and possible change of topology in the moving free surfaces, and the severe time-stepping stability constraint due to the stiffness of high-order regularisation effects, such as surface tension.

This paper reviews some of the recent advances in developing stable and efficient numerical algorithms for solving free boundary-value problems arising from fluid dynamics and materials science. In particular, we will consider boundary integral methods and the level-set approach for water waves, general multi-fluid interfaces, Hele–Shaw cells, crystal growth and solidification. We will also consider the stabilising effect of surface tension and curvature regularisation. The issue of numerical stability and convergence will be discussed, and the related theoretical results for the continuum equations will be addressed. This paper is not intended to be a detailed survey and the discussion is limited by both the taste and expertise of the author.

CONTENTS

* Research supported in part by an Office of Navel Research Grant N00014-94-1-0310, and a National Science Foundation Grant DMS-9407030.

1. Introduction

Many physically interesting problems involve propagation of free surfaces. Water waves, boundaries between immiscible fluids, vortex sheets, Hele–Shaw-cells, thin-film growth, crystal growth and solidification are some of the better-known examples. These problems present a great challenge to physicists and applied mathematicians because the underlying fluid-dynamic instabilities, such as the Kelvin–Helmholtz and the Rayleigh–Taylor instabilities, produce very rich and complex solution structures. Here we would like to review some of the recent advances in developing efficient and stable numerical approximations for these interfacial flows, and investigate the competing mechanism between fluid-dynamic instabilities and the physical regularising effects such as surface tension. In many applications, surface tension has an important effect on the dynamics of interfaces. It is especially central to understanding such fluid phenomena as pattern formation in Hele–Shaw cells, crystal growth and unstable solidification, the motion of capillary waves on free surfaces, the formation of fluid droplets and noise generation at the ocean surface Prosperetti, Crum and Pumphrey (1989).

We will divide this paper into three parts. The first part is concerned with numerical methods and their stability analysis for locally well-posed interface problems. This includes water waves, multi-fluid interfaces and Hele–Shaw cells with surface tension. The second part is concerned with numerical methods for ill-posed interface problems. This includes vortex sheets and multi-fluid interfaces without surface tension. Typically these problems experience the Kelvin–Helmholtz and/or Rayleigh–Taylor instabilities. The third part is concerned with the level-set approach which uses front capturing techniques. Using this approach, singularity formation and topological changes in the free surfaces can be computed naturally.

1.1. Stable discretisations for locally well-posed interfaces

In this part of the paper, we are concerned with stable numerical methods for water waves and multi-fluid interfaces with surface tension. Accurate simulation of these free surfaces presents a problem of considerable difficulty because the underlying physical problem is very singular and is sensitive to small perturbations. The boundary-integral method has been one of the most common approaches in solving these interfacial problems; see e.g. Pozrikidis (1992). The earliest attempt at using boundary-integral methods can be traced back to Rosenhead (1932) in his study of vortex-sheet roll-up.

In the early Sixties, Birkhoff (1962) extended this method to more general fluid interface problems. The first successful boundary integral method was developed by Longuet-Higgins and Cokelet (1976) to compute plunging breakers. Boundary-integral methods for the exact, time-dependent equations have been developed and used in many other works, including Vinje and Brevig (1981), Baker, Meiron and Orszag (1982), Pullin (1979), Roberts (1983), New, McIver and Peregrine (1985), and Dold (1992). We refer to Schwartz and Fenton (1982) and Yeung (1982) for a review of early works in this area. For small-amplitude surface waves, efficient numerical methods have also been developed based on perturbations about equilibrium in Eulerian variables. An expansion in powers of the surface height is used to calculate Fourier modes. These works include Stiassnie and Shemer (1984), West, Brueckner and Janda (1987), Dommermuth and Yue (1987), Glozman, Agnon and Stiassnie (1993), and Craig and Sulem (1993). The last paper has the advantage that the expansion is uniform in wave number.

The advantage of using boundary-integral methods is that they reduce the two-dimensional problem into a one-dimensional problem involving quantities along the interface only, consequently avoiding the difficulty of differentiating discontinuous fluid quantities across the fluid interface. However, numerical simulations using boundary-integral methods also suffer from sensitivity to numerical instabilities because the underlying problems are very singular (Longuet-Higgins and Cokelet 1976; Roberts 1983; Dold 1992). Straightforward discretisations may lead to numerical instabilities. This includes some of the existing boundary-integral methods. There are two possible sources of numerical instability. First, a certain compatibility is required between the choice of quadrature rule for the singular velocity integral *and* the choice of spatial derivative. This compatibility ensures that a delicate balance of terms at the continuous level is preserved at the discrete level. This balance is crucial for maintaining numerical stability. Second, the periodicity of the numerical solution introduces aliasing errors which affect adversely the balance of terms at the discrete level. Violation of this delicate balance of terms will result in numerical instability.

The key in obtaining stable discretisations is to identify the most singular (or the leading-order) contributions of the method, and to see how various terms balance one another. To this end, we need to study the symbols of discrete singular operators, such as the discrete Hilbert transform and its variants. By studying the leading-order discrete singular operators, we find that a certain amount of Fourier filtering on the interface variables is required for the compatibility of the quadrature and derivative rules, Beale, Hou and Lowengrub (to appear) and Beale *et al.* (1994). The amount of filtering is determined by the quadrature rule in approximating the velocity integral and the derivative rule being used. With this modification, we can prove stability of the boundary-integral method for water waves and multi-

fluid interfaces if surface tension effects are included. We also demonstrate that this modification is necessary for stability. Without this modification, the schemes using finite-order derivative operators are numerically unstable; see Subsection 3.2.

Linear analysis has contributed to understanding of numerical instabilities for boundary integral methods. Roberts (1983) showed how to remove a sawtooth instability. Baker and Nachbin (to appear) have performed Fourier analysis near equilibrium for various schemes for a vortex sheet with surface tension, identified sources of instability, and proposed new schemes which are free of linear instabilities. Dold (1992) emphasised the role of time discretisation with respect to instabilities.

While the spatial discretisations are proved to be stable and convergent, stability of the time discretisation is very difficult to obtain in the presence of surface tension. Surface tension introduces a large number of spatial derivatives through local curvature. If an explicit time integration method is used, these high-order derivative terms induce strong stability constraints on the time-step. For example, the time-step stability constraint for the Hele–Shaw flows is given by $\Delta t \leq Ch^3$, where Δt is the time step, and h is the minimum particle spacing. These stability constraints are time dependent, and become more severe by the differential clustering of points along the interface.

In (Hou, Lowengrub and Shelley, 1994) we have successfully removed this stiffness constraint by using an efficient implicit scheme based on a new reformulation of the problem. This reformulation introduces a dynamic change of variables from the (x, y) variables to the arclength metric and tangent angle variables. In this framework, the leading-order singular terms are shown to be linear and have constant coefficients (in space). Thus a Crank–Nicholson-type of discretisation can be used to eliminate the stiffness of the time discretisation. This reformulation greatly improves the stability constraint. For computations of the vortex sheet roll-up in an Euler flow with surface tension using a modest number of points (128), the time step can be chosen 250 times larger than that for an analogous explicit method. Many interfacial problems that were previously unobtainable are now solvable using our method, and new phenomena are discovered.

How to compute beyond the singularity time is a challenging task for the front tracking approach. Here we propose to use curvature regularisation in the boundary-integral formulation to continue beyond the singularity time. This borrows the idea from the level-set approach where curvature regularisation has been used successfully (Osher and Sethian, 1988). Curvature regularisation has an important property of preserving the index of a curve. Consequently, self-crossing of a curve is excluded under this regularisation. Moreover, the curvature regularisation is frame invariant. This is very different from putting an artificial viscosity in the Lagrangian variable. It turns

out that the reformulated system of the interface problem can be used most naturally with the curvature regularisation. In motion by mean curvature, the equation for the tangent angle is nonlinear hyperbolic in the absence of curvature regularisation. It is well-known that a smooth initial condition may develop a shock discontinuity at later times. An entropy condition is required to select the unique physical weak solution. The curvature regularisation plays the same role as the viscosity regularisation for hyperbolic conservation laws. Consequently a physical continuation is obtained with curvature regularisation. In practice, we can use high-order Godunov-type methods developed for conservation laws to discretise the equation for the tangent angle (parameterised in arclength variable). This has a similar effect to curvature regularisation. Curvature regularisation can also be used to regularise the ill-posed vortex-sheet problem, providing an attractive alternative to compute vortex-sheet roll-up (Hou and Osher, 1994).

The idea of using curvature regularisation to boundary-integral formulations combines the advantages of both front tracking and front capturing. By applying curvature regularisation to a free surface directly, we do not need to introduce one extra space dimension as in the level-set approach. More accurate numerical methods can be designed since we only deal with the free surface and don't have to differentiate across the free surface. Also, the stiffness can be removed easily using our reformulated system.

1.2. Boundary integral methods for ill-posed interface problems

Methods of boundary-integral type have also been used for the ill-posed cases of fluid-interface motion, including vortex sheets and Rayleigh–Taylor instabilities (Moore, 1981; Anderson, 1985; Baker *et al.*, 1982; Krasny, 1986a,b; Kerr, 1988; Tryggvason, 1988, 1989; Baker and Shelley, 1990; Shelley, 1992). Usually, either a regularisation or filtering of high wavenumbers is required to obtain numerical stability and to maintain an accurate solution. Surface tension and viscosity have been suggested and used as physical regularisations for these ill-posed problems. We refer to (Pullin, 1982; Rangel and Sirignano 1988; Tryggvason and Aref, 1983; Baker and Nachbin, to appear; Hou *et al.*, 1994a; Dai and Shelley, 1993) for numerical study of surface tension regularisation, and Pozrikidis (1992), Tryggvason (1991) for study using viscosity regularisations.

Study of singularity formation in vortex sheets has been an active subject in the past decade. The possibility of a finite-time singularity in vortex sheets was first conjectured by Birkhoff (1962). The first analytical evidence of singularity formation was given by Moore (1979, 1985) in an asymptotic analysis. He predicted that to leading order in the initial amplitude ϵ, the curvature of the vortex sheet blows up at a critical time and the interface forms a branch-point singularity of order 3/2. Using Taylor series in

time, Meiron, Baker and Orszag (1982) obtained results in agreement with Moore's. Krasny (1986) performed direct numerical simulations of vortex-sheet motion using the point-vortex approximation and a Fourier filter to control the growth of round-off errors. His results were also consistent with Moore's. Before the singularity time, the numerical solution converged, but convergence was lost after the singularity time. By using an infinite-order approximation combined with Krasny's Fourier filtering, Shelley (1992) has provided strong numerical evidence that the branch singularity of order 3/2 is chosen. Caflisch and Orellana (1989) have found a continuum of explicit solutions to the Birkhoff–Rott equation which display finite-time singularities. However, the physical interpretation of these constructed singularities is not clear since branch-type singularities were built explicitly in their initial data. The selection mechanism of a singularity for the general initial-value problems is not known. Caflisch, Ercolani, Hou and Landis (1993) studied propagation of singularities for the localised Moore's approximations. The 3/2 branch-point singularities were found to be generic. Singularity formation during the Rayleigh–Taylor instability has also been investigated by Baker, Caflisch and Siegel (to appear) using asymptotic and numerical methods.

To compute beyond the singularity time, certain numerical or physical regularisation is required. Moore (1978) has derived an evolution equation for a vortex layer of small thickness. Pullin (1992) has included surface tensions in the evolution equation. Pozrikidis and Higdom (1985) have numerically studied a periodically perturbed layer of constant vorticity. Krasny (Krasny, 1986b, 1987; Nitsche and Krasny, 1994) has used the vortex-blob method to study vortex-sheet roll-up and has obtained a number of interesting results. Baker and Shelley (1990) have considered regularisation of a thin vortex layer. Tryggvason (1989) has considered the vortex-in-cell as a grid-based vortex method, and has used an improved version of the VIC method to study vortex-sheet roll-up. Bell and Marcus (1992) used a second-order projection method for variable density flow to study Rayleigh–Taylor instability. These computational results using different regularisations all produced qualitatively similar results; at least they seem to agree outside the region of vorticity concentration.

The global existence of weak solutions for vortex-sheet initial data is not known in general. Motivated by the numerical studies of vortex sheets in Krasny (1986b, 1987) and Baker and Shelley (1990), DiPerna and Majda (1987a,b), introduced the concept of measure-valued solutions for vortex sheets. These measure-valued solutions may develop regions of vorticity concentration and may have a non-trivial set of defeat measure. If this is the case, the vortex-sheet solution does not satisfy the incompressible, inviscid Euler equations in the weak sense. In the special case of one-signed vorticity, Delort (1991) has recently proved that vortex sheets are global

weak solutions of the Euler equations. Using Delort's result, Liu and Xin (1994) have been able to prove that the vortex-blob calculation converges to a weak solution of the Euler equations provided that the initial vorticity is of the same sign. Other theoretical results for vortex-sheet motion assume analytic initial data. Existence and well-posedness of vortex-sheet motion have been established for analytic data for short times; see, for example, Sulem *et al.* (1981), Dochun and Robert (1986, 1988), Caflisch and Orellana (1988) and Ebin (1988).

1.3. Level-set approach

Although it is usually highly desirable to reformulate a problem into boundary-integral equations, there are certain applications for which the boundary-integral method has difficulty handling. For example, in crystal growth and thin-film growth, an initially smooth front can develop cusps and cracklike singularities, and isolated islands of film material can merge (Gray, Chisholm and Kaplan, 1993; Sethian and Strain, 1992; Snyder *et al.*, 1991; Spencer, Voorhees and Davis, 1991). In order to compute up to and continue beyond the singularity time, one has to use local-mesh refinement and local surgery techniques (Unverdi and Tryggvason, 1992). This often introduces some numerical instability and it is done in a somewhat unsatisfactory way. And it becomes increasingly difficult for three-dimensional problems.

The level-set approach developed by Osher and Sethian (1988) provides a powerful numerical method for capturing free surfaces in which topological singularities may form dynamically. The idea is to regard the free surface as a level set of a smooth function defined in one order higher space dimensions than the free surface. Only the information of the zeroth-level set is physically relevant to the free surface we want to compute. Thus we have sufficient freedom in specifying the level-set function away from the zeroth-level set. This freedom makes it possible to select a relatively smooth level-set function at all times. The free surface may form a singularity such as corners or cusps, but the level-set function still remains relatively smooth. Typically, we would like to choose the level-set function to be a signed distance function from the free surface. By viewing the surface as a level set, sharp corners and cusps are handled naturally, and changes of topology in the moving boundary require no additional effort. Furthermore, these methods work in any number of space dimensions.

Another important property of the level-set formulation is that it provides the correct equation of motion for a front propagating with curvature-dependent speed. This equation is of Hamilton–Jacobi type with a right-hand-side that depends on curvature effects. The limit of the right-hand-side as the curvature effect goes to zero satisfies an associated entropy condi-

tion. Thus high-order numerical approximations can be devised using techniques developed for the solution of hyperbolic conservation laws (Harten *et al.*, 1987; Colella and Woodward, 1984; Osher and Shu, 1991). Recently, this approach has been applied to computation of minimal surfaces (Chopp, 1993), compressible gas dynamics (Mulder, Osher and Sethian, 1992), crystal growth and dendritic solidification (Sethian and Strain 1992; Osher, private communication), and interaction of incompressible fluid bubbles (Chang *et al.*, 1994; Sussman, Smereka and Osher, 1994). In addition, theoretical analysis of mean curvature flow based on the level-set model presented in Osher and Sethian (1988) has been developed by Evans and Spruck (1991, 1992).

The rest of the paper is organised as follows. In Section 2, we introduce several important examples of free boundary-value problems arising from fluid dynamics and materials science. These include water waves, general two-fluid interfaces, Hele–Shaw cells, a model for crystal growth and unstable solidification. Their boundary-integral formulations will be given. In Section 3, we present a convergent boundary-integral method for water waves. A compatibility condition between the quadrature rule and the discrete derivative is given, and the stability property of the modified boundary-integral method is analysed. Examples of a class of unstable algorithms are given to illustrate why certain Fourier smoothings are necessary for our modified method to be stable. A numerical example of breaking-wave calculation supports the applicability of the method in the fully non-linear regime. In Section 4, we present several numerical methods for calculating vortex sheets and vortex-sheet roll-up. These include Krasny's filtering technique for the point-vortex method, vortex-blob desingularisation for vortex sheets, thin vortex-layer desingularisation and vortex-in-cell method calculations for vortex-sheet roll-up. In Section 5, the stabilising effect of surface tension is considered. We first consider a stable time-continuous discretisation. We then propose an efficient implicit time discretisation that completely removes the stiffness of surface tension by a dynamical reformulation of the interface problems. We also propose a new approach to compute beyond singularity time using our reformulated system together with curvature regularisation. Finally, in Section 6, we consider the level-set approach for computing topological singularities. The basic ideas of level-set approaches are reviewed. Applications to crystal growth and incompressible multi-fluid bubbles are discussed.

2. General two-fluid interfaces

In this section, we consider several examples of interfacial flows arising from fluid mechanics and materials science. They are water waves, stratified two-density interfacial flows, Hele–Shaw flows, crystal growth and solidification.

The stratified interfacial flows have been used as models to understand mixing of fluids, separation of boundary layers, generation of sounds (in bubbly flows) and coherent structures in turbulence models. Theoretical and numerical studies of Hele–Shaw flows and crystal growth have received renewed interest and increasing attention in recent years because of the rich phenomena in the physical solutions and the potential applications in pattern formation and materials science. These interfacial problems have one feature in common. The underlying physical instability generates a rapid growth in the high-frequency components of the solution. Without physical regularisations such as viscosity or surface tension, the problems are ill-posed in the Hadamard sense (except for water waves). It is the competition between the stabilising regularisation effect and the underlying physical instability that generates many fascinating solution structures. Since these problems are highly non-linear and non-local, it is usually difficult to obtain a complete understanding by using only analytical tools. Numerical simulations become essential in our study of these interfacial problems. It is not hard to imagine that this is a very difficult task.

2.1. Water waves without surface tension

Unsteady motion of water waves is one of the most familiar examples of free surfaces in our everyday experience, and it illustrates a rich variety of phenomena in wave motion. One of the spectacular properties of the sea surface is its capacity to turn over on itself and produce breaking waves. Mathematical difficulties in dealing with the exact equations are due to the free boundary, and the inherent non-linear, non-local nature of the problem. The usual linear theory and shallow-water theory for small-amplitude waves have been very useful in studying many important aspects of the wave motion. However, they are valid only where the fluid acceleration is sufficiently small compared to gravity. To obtain a better understanding of the large-amplitude wave interactions such as wave breaking, we need to develop effective numerical methods to compute free surface motion.

There are several different approaches that may be adopted to study free surface motion numerically. We refer to Yeung's (1982) paper for a partial review. The boundary-integral formulation of the equations of water waves leads to a natural approach for computing time-dependent motions. In this approach, the moving interface is tracked explicitly. Only quantities on the interface need be computed. However, high-frequency numerical instabilities are difficult to avoid, because of the non-local and non-linear nature of the problem, and the lack of dissipation.

Consider a two-dimensional incompressible, inviscid and irrotational fluid below a free interface. We parameterise the interface by $\mathbf{x} = (x(\alpha, t), y(\alpha, t))$, where α is a Lagrangian parameter along the interface. The kinematic con-

dition only requires that the normal velocity of the interface be equal to that of the fluid at the interface. There is no physical constraint on the tangential velocity of the interface. Tangential motions along the interface give only changes in frame for its parameterisation and are not physically specified as they do not affect its shape. Later, in Subsection 5.2, we will exploit this freedom in choosing a tangential motion to remove the stiffness of surface tension. Here, we use the usual convention of choosing the tangential velocity to be that of the fluid. Thus the interface is convected by the fluid velocity $\mathbf{u}$ at the interface:

$$\frac{\partial \mathbf{x}}{\partial t} = \mathbf{u}(\mathbf{x}(\alpha, t), t). \tag{2.1}$$

The fluid velocity $\mathbf{u}$ is determined by the incompressible Euler equations:

$$\rho\left(\frac{\partial \mathbf{u}}{\partial t} + \mathbf{u} \cdot \nabla \mathbf{u}\right) = -\nabla p - \rho g \mathbf{j} \tag{2.2}$$

with the incompressibility constraint $\nabla \cdot \mathbf{u} = 0$, where ρ and p are the fluid density and pressure, respectively, g is the constant of gravity and $\mathbf{j}$ is a unit vector in the y direction. In the absence of surface tension, the pressure is continuous across the interface. Since a vacuum is assumed above the interface, the pressure is equal to zero at the interface. To simplify the presentation, we only consider water waves with infinite depth in two space dimensions. One can easily modify the formulation to accommodate the bottom geometry if water waves with finite depth are considered, see, for example, Baker *et al.* (1982). Generalisation to three dimensions can also be carried out, see, for example Baker (1983) and Kaneda (1990).

Due to irrotationality, we can express velocity in terms of a velocity potential ϕ, that is, $\mathbf{u} = \nabla\phi$. Then incompressibility implies that

$$\Delta\phi = 0$$

in the interior flow region. Furthermore, the momentum equations (2.2) can be integrated to obtain Bernoulli's equation for the potential:

$$\frac{\partial \phi}{\partial t} + \frac{1}{2}|\nabla\phi|^2 + gy = 0. \tag{2.3}$$

Thus if $\phi(\alpha, 0) = \phi_0(\alpha)$ is given initially along the interface, then we can evaluate ϕ at later times according to (2.3). To compute the fluid velocity at the interface, we need to evaluate $\nabla\phi$ at the interface. It is easy to evaluate the tangential velocity component at the interface. But determining the normal velocity would require solving the interior problem for ϕ. This could be a difficult task since the relation between the Dirichlet value of ϕ and its normal derivative at the interface is non-local. There are several ways to relate the normal derivative of ϕ to its value at the interface, each involving a Fredholm integral equation of a different kind.

One way to relate the normal derivative of ϕ to its value at the interface is to use Green's third identity. This is the approach taken by Longuet-Higgins and Cokelet (1976), among others. This corresponds to using a single-layer potential representation. Denote by Γ the interface. Green's third identity gives

$$\int_\Gamma \frac{\partial \phi}{\partial n}(x(\alpha'))G(x(\alpha), x(\alpha'))\mathrm{d}x(\alpha') = \frac{1}{2}\phi(x(\alpha)) + \int_\Gamma \phi(x(\alpha'))\frac{\partial G}{\partial n}(x(\alpha), x(\alpha'))\mathrm{d}x(\alpha')), \quad (2.4)$$

where $\frac{\partial}{\partial n}$ is the exterior normal derivative and G is the Green's function for the Laplace equation. In two dimensions, we have $G(x, x') = \frac{1}{2\pi}\log|x - x'|$. If we prescribe ϕ at the interface, then (2.4) provides an integral relation to determine the normal derivative of ϕ at the interface. Equation (2.4) is a Fredholm integral equation of the first kind for the normal derivative of ϕ. Now the solution procedure is clear. Given $\mathbf{x}(\alpha, t)$ and $\phi(\alpha, t)$ at the interface, we can compute the normal derivative of ϕ by equation (2.4). This determines the normal velocity at the interface. The tangential velocity is given by $\phi_\alpha/|\mathbf{x}_\alpha|$. Then we can update $\mathbf{x}$ in time by (2.1), and update ϕ by Bernoulli's equation.

There are some disadvantages regarding this approach. To solve for $\partial\phi/\partial n$ from equation (2.4), we need to invert a dense N-by-N matrix if we discretise the integral by N grid points. Direct inversion of a $N \times N$ matrix requires $O(N^2)$ storage locations and $O(N^3)$ operation counts. For large N, this becomes prohibitively expensive. We must look for some fast iterative method to approximately invert the dense matrix. However, the matrix associated with a Fredholm integral of the first kind is usually not well conditioned and the number of iterations required increases rapidly with N.

An alternative approach is to use the dipole representation. Following Baker, Meiron and Orszag (1982) and Beale, Hou and Lowengrub (1993a), we express the complex potential by a double-layer representation. Denote by $\mu(\alpha, t)$ the dipole strength and denote the interface position by complex variable $z(\alpha, t) = x(\alpha, t) + \mathrm{i}y(\alpha, t)$. We can write the complex potential Φ in the fluid domain in terms of μ

$$\Phi = \frac{1}{2\pi\mathrm{i}}\int \frac{1}{z - z(\alpha', t)}\mu(\alpha', t)\mathrm{d}z(\alpha'),$$

for z away from the interface. The complex velocity $w = u - \mathrm{i}v$ can be obtained by differentiating the complex potential with respect to z and performing integration by parts. We get

$$w = \frac{\mathrm{d}\Phi}{\mathrm{d}z} = \frac{1}{2\pi\mathrm{i}}\int \frac{1}{z - z(\alpha')}\gamma(\alpha')\mathrm{d}\alpha',$$

where γ is the non-normalised vortex-sheet strength. It is given as the Lagrangian derivative of the dipole strength, that is, $\gamma = \mu_\alpha$. Using the Plemelj formula, we obtain the limiting velocity from the fluid region on the interface as

$$w(\alpha) = \frac{1}{2\pi \mathrm{i}} \int \frac{\gamma(\alpha')}{z(\alpha) - z(\alpha')} \mathrm{d}\alpha' + \frac{\gamma(\alpha)}{2 z_\alpha(\alpha)}. \tag{2.5}$$

Here the integral is the Cauchy principal-value integral. Denote by ϕ the real potential, $\phi = \mathrm{Re}(\Phi)$. We can determine γ from the condition $\phi_\alpha = \phi_x x_\alpha + \phi_y y_\alpha = \mathrm{Re}(w z_\alpha)$. Using (2.5) we obtain

$$\phi_\alpha = \frac{\gamma}{2} + \mathrm{Re}\left(\frac{z_\alpha(\alpha)}{2\pi \mathrm{i}} \int \frac{\gamma(\alpha')}{z(\alpha) - z(\alpha')} \mathrm{d}\alpha' \right).$$

This is a Fredholm integral equation of the second kind. The kernel is an adjoint double-layer potential.

It is customary to assume that the interface are periodic in the horizontal direction. Under this assumption, we can express $z(\alpha, t) = \alpha + s(\alpha, t)$, where $s(\alpha, t)$ and $\phi(\alpha, t)$ are periodic in α with period 2π. This also implies that the flow is at rest at infinity. We can sum the singular kernel $1/z$ over periodic intervals to obtain a periodic kernel $\frac{1}{2}\cot(z/2)$ defined over a single period. To summarise, we obtain a system of time-evolution equations for z and ϕ as follows:

$$\begin{aligned} \bar{z}_t = \frac{1}{4\pi \mathrm{i}} \int_{-\pi}^{\pi} \gamma(\alpha') \cot\left(\frac{z(\alpha) - z(\alpha')}{2} \right) \mathrm{d}\alpha' + \frac{\gamma(\alpha)}{2 z_\alpha(\alpha)} \\ \equiv u(\alpha, t) - \mathrm{i} v(\alpha, t), \end{aligned} \tag{2.6}$$

$$\phi_t = \frac{1}{2}(u^2 + v^2) - g \cdot y, \tag{2.7}$$

$$\phi_\alpha = \frac{\gamma}{2} + \mathrm{Re}\left(\frac{z_\alpha}{4\pi \mathrm{i}} \int_{-\pi}^{\pi} \gamma(\alpha') \cot\left(\frac{z(\alpha) - z(\alpha')}{2} \right) \mathrm{d}\alpha' \right), \tag{2.8}$$

where $\bar{z}$ is the complex conjugate of z. Equations (2.6)–(2.8) completely determine the motion of the system. We remark that Bernoulli's equation (2.7) is different from (2.3) because of the change to Lagrangian variables.

The advantage of using the dipole representation is that the Fredholm integral of the second kind has a globally convergent Neumann series (Baker, Meiron and Orszag, 1982; and Beale, Hou and Lowengrub, 1993a). This means that the equation for γ may be solved by iteration provided that the interface is reasonably smooth. For example, if γ^j is the jth iterate, then γ^{j+1} is computed by

$$\gamma^{j+1}(x) = 2\phi_\alpha(x) - 2\mathrm{Re}\left(\frac{z_\alpha}{4\pi \mathrm{i}} \int_{-\pi}^{\pi} \gamma^j(\alpha') \cot\left(\frac{z(\alpha) - z(\alpha')}{2} \right) \mathrm{d}\alpha' \right). \tag{2.9}$$

In general, only several iterations are required for high accuracy if we use the γ from the previous time level as our first iterate. By keeping values of γ at several previous time levels, an extrapolated first iterate can be found which will further reduce the number of iterations to typically 1 or 2. More iterations are required when the solution develops a high-curvature region such as in breaking surface waves. If the interface is not accurately resolved in the high-curvature region, the iteration scheme will eventually stop converging.

2.2. Stratified two-density fluid interfaces

Here we consider the motion of general two-density interfacial flows, that is, an interface separating two inviscid, incompressible and irrotational fluids in the presence of gravity and possibly surface tension in two space dimensions. In the following, the subscript 2 denotes the fluid above the interface and 1 denotes the fluid below the interface. In each fluid, we have Euler's equations

$$\rho_i[\partial_i \mathbf{u}_i + (\mathbf{u}_i \cdot \nabla)\mathbf{u}_i] = -\nabla \mathbf{p}_i - \rho_i g \mathbf{j}, \quad i = 1, 2.$$

The incompressibility and irrotationality constraints imply $\nabla \cdot \mathbf{u}_i = 0$ and $\nabla \times \mathbf{u}_i = 0$. Denote the interface by Γ. At the interface, we impose the Laplace–Young boundary condition which relates the pressure jump to the curvature of the interface, κ, by

$$[p]|_\Gamma = \tau\kappa,$$

where $[p]|_\Gamma$ denotes the jump of pressure across the interface Γ and τ is the surface-tension coefficient. The normal velocity is assumed to be continuous across the interface. As in the case of water waves, these interface problems have vortex-sheet representations. We refer to Birkhoff (1962) and Baker, Meiron and Orszag (1982) for a derivation of the governing equations.

The velocity at the interface is not uniquely defined since the tangential velocity in general has a jump discontinuity across the interface. It is customary to evolve the interface with the average velocity obtained from the limiting velocities above and below the interface. As before, we denote the interface position by complex variable $z(\alpha, t) = x(\alpha, t) + \mathrm{i}y(\alpha, t)$, where α is a Lagrangian parameter along the interface. Then, the interface evolves according to

$$\frac{\mathrm{d}\bar{z}}{\mathrm{d}t} = \frac{1}{2\pi \mathrm{i}} \int \frac{\gamma(\alpha', t)}{z(\alpha, t) - z(\alpha', t)} \mathrm{d}\alpha', \tag{2.10}$$

where the integral is understood as the Cauchy principal-value integral and γ is the unnormalised vortex-sheet strength. Equation (2.10) is also called the Birkhoff–Rott equation in the literature. The evolution equation for γ

can be obtained from Bernoulli's equations in both sides of the interface:

$$\frac{\mathrm{d}\gamma}{\mathrm{d}t} = -2A\left(\mathrm{Re}\left\{\frac{\mathrm{d}^2\bar{z}}{\mathrm{d}t^2}z_\alpha\right\} + \frac{1}{8}\partial_\alpha\left(\frac{\gamma^2}{|z_\alpha|^2}\right) + gy_\alpha\right) + \tau\kappa_\alpha, \tag{2.11}$$

where $A = (\rho_1 - \rho_2)/(\rho_1 + \rho_2)$ is the Atwood number. The curvature, κ, is evaluated by

$$\kappa = \frac{x_\alpha y_{\alpha\alpha} - x_{\alpha\alpha} y_\alpha}{(x_\alpha^2 + y_\alpha^2)^{3/2}}.$$

Note that equation (2.11) is actually a Fredholm integral equation of the second kind for $\mathrm{d}\gamma/\mathrm{d}t$. It has been shown that their Neumann series are globally convergent in the periodic case (Baker, Meiron and Orszag, 1982). The result also holds for unbounded domains (Beale, Hou and Lowengrub, 1993a). Therefore, the integral equation for $\mathrm{d}\gamma/\mathrm{d}t$ is invertible and can be solved by iteration. Equations (2.10) and (2.11) completely determine the motion of the interface.

2.3. Hele–Shaw flows

A closely related problem is the Hele–Shaw flow which describes the viscosity-dominant creeping flow confined between two closely spaced plates. The case in which one fluid displaces another has been studied extensively. This begins with the theoretical work of Saffman and Taylor (1958). They found exact self-similar fingers for the interface between the two fluids in a channel geometry when surface tension is absent. The subsequent works have mostly focused on the role of surface tension in the selection of finger width (see Pelcé, 1988, for a review). The dynamical behaviour of Hele–Shaw flows has received a lot of interests inspired by the complex patterns formed by an expanding bubble (Paterson, 1981, 1985; Rauseo, Barnes and Maher, 1987). It is believed that surface tension plays an essential role in producing these structures.

Consider an interface Γ that separates two Hele–Shaw fluids of different viscosities and densities. For simplicity, Γ is assumed periodic in the horizontal direction. The fluid below Γ is labelled fluid 1, and that above is labelled 2, and similarly for their respective viscosities and so forth. The velocity in each fluid is given by Darcy's law, together with the incompressibility constraint:

$$(u_j, v_j) = -\frac{b^2}{12\mu_j}\nabla(p_j - \rho_j g y), \quad \nabla \cdot \mathbf{u}_j = 0.$$

Here b is the gap width of the Hele–Shaw cell, μ_j is the viscosity, p_j is the pressure, ρ_j is the density and gy is the gravitational potential. The boundary conditions are exactly the same as for the two-density fluid interfaces. That is, the normal velocity is continuous across the interface, the jump in

the pressure across the interface is proportional to the local mean curvature, and velocity vanishes at infinity. Again, one can derive a boundary-integral formulation for the Hele–Shaw problem using the dipole representation; see, for example, Dai and Shelley (1993). The interface position will satisfy the same Birkhoff–Rott equation as in (2.10). The vortex-sheet strength γ satisfies

$$\gamma(\alpha,t) = -2A_\mu \mathrm{Re}\left\{\frac{z_\alpha}{2\pi \mathrm{i}} \int \frac{\gamma(\alpha',t)}{z(\alpha,t)-z(\alpha',t)} \mathrm{d}\alpha'\right\} + \tau\kappa_\alpha - Ry_\alpha.$$

Here $A_\mu = (\mu_1 - \mu_2)/(\mu_1 + \mu_2)$ is the Atwood ratio of the viscosities, τ is the non-dimensional surface tension and R is a signed measure of density stratification ($\rho_1 < \rho_2$ implies $R < 0$). As before, the equation for γ is a Fredholm integral of the second kind, and it has a globally convergent Neumann series.

2.4. Crystal growth and dendritic solidification

The last example we consider is concerned with crystal growth in unstable solidification. This problem has attracted considerable interest over the past decade from applied mathematicians, physicists and materials scientists. Here we only consider one particular model for this problem. There are many other interesting free-boundary problems arising from materials science that can be studied by numerical methods similar to those described in this paper. This includes the morphological instability in thin-film growth and the Ostwald ripening problem, see, for example, Gray, Chisholm and Kaplan (1993), Spencer, Voorhees and Davis (1991), Spencer and Meiron (1994), Voorhees *et al.* (1988) and Voorhees (1992).

Consider a container of the liquid phase of the material. Suppose we cool the box smoothly and uniformly below its freezing temperature. If this is done very carefully, the liquid does not freeze. The system is now in a 'metastable' state. A small disturbance, such as dropping a tiny seed of solid phase, will initiate a rapid and unstable process known as *dendritic solidification.* The solid phase will grow from the seed by sending out branching fingers. This growth process is unstable in the sense that small perturbations of the initial data can produce large changes in the solid/liquid boundary. One can model this phenomenon by a moving-boundary problem. The temperature field satisfies a heat equation in each phase, coupled through two boundary conditions on the unknown moving solid/liquid boundary. We refer to Langer (1980), Gurtin (1986) and Caginalp and Fife (1988) for derivations. Extensive asymptotic analysis for the solution has been carried out by several authors in the literature; see Langer (1986), Chadam and Ortoleva (1983), Kessler and Levine (1986), Benamar and Pomeau (1986), and Gaginalp and Fife (1988). It is also possible to reformulate the equations of motion in boundary-integral forms, as is done in Meiron (1986), Strain

(1989), Karma (1986), Kessler and Levine (1986) and Langer (1980). This yields accurate results for smooth boundaries.

The set-up of the problem described below follows the framework of Strain, Sethian and Strain (1992, 1989). Consider a square container, $B = [0,1] \times [0,1]$, filled with the liquid and solid phases of some pure substance. The unknowns are the temperature $u(x,t)$ for $x \in B$, and the solid/liquid boundary $\Gamma(t)$. The temperature field u is taken to satisfy the heat equation in each phase, together with an initial condition in B and boundary conditions on the container walls. Thus we have

$$\begin{aligned} u_t &= \Delta u && \text{in } B \text{ off } \Gamma(t), \\ u(x,t) &= u_0(x) && \text{in } B \text{ at } t = 0, \\ u(x,t) &= u_B(x) && \text{for } x \in \partial B. \end{aligned}$$

Since the position of the moving boundary $\Gamma(t)$ is unknown, two boundary conditions on $\Gamma(t)$ are required to determine u and $\Gamma(t)$. Let n be the outward normal to the boundary, pointing from solid to liquid. The first boundary condition is the classical Stefan condition:

$$[\partial u/\partial n] = -HV \quad \text{on} \quad \Gamma(t).$$

Here $[\partial u/\partial n]$ is the jump in the normal component of heat flux $\partial u/\partial n$ from solid to liquid across $\Gamma(t)$, V is the normal velocity of $\Gamma(t)$ and H is a constant. The second boundary condition on $\Gamma(t)$ is the classical Gibbs–Thomson relation,

$$u(x,t) = -\epsilon_\kappa(n)\kappa - \epsilon_V(n)V \quad \text{for} \quad x \in \Gamma(t),$$

where κ is the curvature at x on $\Gamma(t)$. Here we model the crystalline anisotropy by assuming that ϵ_κ and ϵ_V depend on the local normal vector n. Now we describe how to put the problem into a boundary-integral form. First we subtract the temperature field due to the initial condition u_0 and the boundary condition u_B. Let $U(x,t)$ be the solution to the heat equation

$$\begin{aligned} U_t &= \Delta U && \text{in } B, \\ U(x,0) &= u_0(x) && \text{at } t = 0, \\ U(x,t) &= U_B(x,t) && \text{for } x \in \partial B \text{ and } t > 0. \end{aligned}$$

Define $W = u - U$. Then W satisfies

$$W_t = \Delta W \quad \text{in } B - \Gamma(t), \tag{2.12}$$

$$W(x,0) = 0 \quad \text{at } t = 0, \tag{2.13}$$

$$W(x,t) = 0 \quad \text{for } x \in \partial B, \tag{2.14}$$

$$[\partial W/\partial n] = -HV \quad \text{on} \quad \Gamma(t), \tag{2.15}$$

$$W(x,t) = -\epsilon_\kappa(n)\kappa - \epsilon_V(n)V - U(x,t) \quad \text{for} \quad x \in \Gamma(t). \tag{2.16}$$

The temperature filed U can be obtained easily since there is no free boundary present. For example, we can use any standard numerical discretisation for the initial–boundary-value problem for the heat equation to obtain U. The difficult part is to compute W. We will formulate it as a boundary-integral equation. We use the kernel K of the heat equation to express the solution W to equations (2.12)–(2.16) as a single-layer potential. Given a function V on

$$\Gamma_T = \prod_0^T \Gamma(t) = \{(x,t) | x \in \Gamma(t), 0 \le t \le T\},$$

the single-layer heat potential SV is defined for (x,t) in $B \times [0,T]$ by

$$SV(x,t) = \int_0^t \int_{\Gamma(t')} K(x,x',t-t')V(x',t')\mathrm{d}x'\mathrm{d}t'.$$

Here the x' integration is over the curves comprising $\Gamma(t')$, and the Green function K of the heat equation in the box $B = [0,1] \times [0,1]$ with Dirichlet boundary conditions on the box walls is given by

$$\begin{aligned} K(x,x',t') \;=\; & \sum_{k_1=1}^{\infty} \sum_{k_2=1}^{\infty} \mathrm{e}^{-(k_1^2+k_2^2)\pi^2 t} \\ & \times \sin(k_1\pi x_1)\sin(k_2\pi x_2)\sin(k_1\pi x_1')\sin(k_2\pi x_2'), \end{aligned}$$

where $x = (x_1, x_2)$ and $x' = (x_1', x_2')$. The function SV defined above is a continuous function on $B \times [0,T]$, vanishing for $t = 0$ or on ∂B, and satisfying the heat equation every where off Γ_T. Across $\Gamma(t)$, $SV(x,t)$ has a jump in its normal derivative equal to V. Thus, $W(x,t) = H \cdot SV(x,t)$ is the solution to equations (2.12)–(2.16). All that remains is to satisfy the second boundary condition (2.16). This is equivalent to the boundary-integral equation

$$\epsilon_\kappa(n)\kappa + \epsilon_V V + U + H \int_0^t \int_{\Gamma(t')} K(x,x',t-t')V(x',t')\mathrm{d}x'\mathrm{d}t' = 0, \tag{2.17}$$

for $x \in \Gamma(t)$. Equation (2.17) is an integral equation for the normal velocity, V, of the moving boundary. We note that the velocity V of a point x on $\Gamma(t)$ depends not only on the position of $\Gamma(t)$ but also on its previous history. Thus in order to evaluate $V(x,t)$, we need to store information about the temperature in the previous history of the boundary.

The boundary-integral formulation of the problem requires the evaluation of the single-layer potential on a $M \times M$ grid in B. The computation of $SV(x,t)$ by a quadrature rule at M^2 points at N time steps would require $O(M^3N^2)$ work if there are $O(M)$ points on $\Gamma(t)$ at each time t. For M and N large, this becomes prohibitively expensive (Strain, 1989). A fast

algorithm has been developed by Greengard and Strain (1990) which reduces the operation count to $O(M^2)$ per time step. This greatly improves the speed of the calculation. A related, but different, fast method for solidification has also been proposed and implemented by Spencer and Meiron (1994). Recently, Osher and his coworker (private communication) have designed an extremely efficient numerical method based on level-set formulation which only involves a local heat equation solver without using boundary integral formulation. The preliminary results seem to be very promising.

2.5. Linear stability around equilibrium solutions

It is instructive to consider the linear stability of equilibrium solutions to (2.10) and (2.11). The equilibrium solution is the flat sheet: $z(\alpha, t) = \alpha, \gamma(\alpha, t) = \gamma_0$, where γ_0 is constant. Looking for solutions of (2.10) and (2.11) of the form $z = \alpha + \epsilon \dot{z}$ and $\gamma = \gamma_0 + \epsilon \dot{\gamma}$, and keeping only the linear terms in ϵ give the linearised equations

$$\begin{aligned} \frac{\mathrm{d}\dot{x}}{\mathrm{d}t} &= -\frac{\gamma_0}{2} H(\dot{y}_\alpha), \\ \frac{\mathrm{d}\dot{y}}{\mathrm{d}t} &= \frac{1}{2} H(\dot{\gamma}) - \frac{\gamma_0}{2} H(\dot{x}_\alpha), \\ \frac{\mathrm{d}\dot{\gamma}}{\mathrm{d}t} &= -A\gamma_0 \dot{\gamma}_\alpha + A\gamma_0^2 \dot{x}_{\alpha\alpha} - 2Ag\dot{y}_\alpha + \tau \dot{y}_{\alpha\alpha\alpha}, \end{aligned}$$

where $\dot{z} = \dot{x} + \mathrm{i}\dot{y}$. Notice that $\mathrm{d}\gamma/\mathrm{d}t$ is determined explicitly in the third equation. In the linear level, the integral equation contribution has dropped out. H is the Hilbert transform defined as

$$H(f)(\alpha) = \frac{1}{\pi} \int \frac{f(\alpha')\mathrm{d}\alpha'}{\alpha - \alpha'}.$$

It is easy to see that it has the Fourier symbol $\hat{H}(k) = -\mathrm{i}\mathrm{sgn}(k)$. The growth rates of the perturbations are determined by the eigenvalues of the perturbed system which can be calculated explicitly in the Fourier space as follows:

$$\lambda(k) = 0, \quad -\frac{A\gamma_0}{2}\mathrm{i}k \pm \sqrt{\frac{\gamma_0^2 k^2}{4}(1 - A^2) - Ag|k| - \tau|k|^3}.$$

The fact that the system admits zero eigenvalue implies that the interface does not change its shape by translating Lagrangian points along the interface. In the absence of surface tension, that is, $\tau = 0$, the other two eigenvalues may grow with large k. In fact, if $\gamma_0 \neq 0$, the interface experiences the Kelvin–Helmoltz instability, and the growth rate is proportional to $O(|k|)$ for large k. On the other hand, if $\gamma_0 = 0$, the stability of the perturbation depends on the sign of the Atwood number A. If $A > 0$, then the

interface is stable. If $A < 0$, then the interface experiences the Rayleigh–Taylor instability. The growth rate is proportional to $\sqrt{|k|}$. In general, due to baroclinic generation of vorticity at the interface, the vortex-sheet strength γ can be non-zero in some region even if it is equal to zero initially. Thus the Kelvin–Helholtz instability is always present for two-density interfaces as long as $A^2 \neq 1$, even if we have lighter fluid on top of a heavy fluid. In the case of positive surface tension, that is, $\tau > 0$, we can see that in the high-wavenumber regime, the surface-tension term dominates. The eigenvalues become imaginary, which can produce oscillations but no growth at the high modes. Thus surface tension is a dispersive regularisation of those instabilities. Of course, for small surface tension, there is still a band of modes below a certain critical wavenumber that can grow exponentially in time.

Similar linearised stability analysis for the Hele–Shaw flows indicates that the surface tension is a dissipative regularisation. For simplicity, we take $A_\mu = 0$. The eigenvalues are as follows:

$$\lambda(k) = 0, \quad -\frac{1}{2}(\tau|k|^3 + R|k|).$$

Therefore, if $R < 0$, there is a band of unstable modes near $k = 0$. This is a Mullins–Sekerka type of instability (1963), driven by the unstable density stratification. At higher wavenumbers, this instability is cut off by the surface-tension term which acts as a third-order dissipation.

3. A convergent boundary-integral method for water waves

The boundary-integral formulation of water waves is naturally suited for numerical computation. There are many ways one can discretise the boundary-integral equations, depending on how we choose to discretise the singular integral and the derivatives. These choices affect critically the accuracy and stability of the numerical method. Straightforward numerical discretisations of (2.6)–(2.8) may lead to rapid growth in the high wavenumbers. In order to avoid numerical instability, a certain compatibility between the choice of quadrature rule for the singular integral *and* that of the discrete derivatives must be satisfied. This compatibility ensures that a delicate balance of terms at the continuous level is preserved at the discrete level. Violation of this compatibility will lead to numerical instability.

We discretise the interval by choosing N equally spaced points $\alpha_j = jh$, where $h = 2\pi/N$. Denote by $z_j(t), \phi_j(t), \gamma_j(t)$ the discrete approximations of $z(\alpha_j, t), \phi(\alpha_j, t), \gamma(\alpha_j, t)$ respectively. To approximate the velocity integral, we use the alternating trapezoidal rule:

$$\int_{-\pi}^{\pi} \gamma(\alpha')\cot\left(\frac{z(\alpha_j) - z(\alpha')}{2}\right) \mathrm{d}\alpha' \simeq \sum_{\substack{k=-N/2+1 \\ (k-j)\ \text{odd}}}^{N/2} \gamma_k \cdot \cot\left(\frac{z_j - z_k}{2}\right) 2h, \quad (3.1)$$

The advantage of using this alternating trapezoidal quadrature is that the approximation is spectrally accurate. This and related quadrature rules have been used by several authors in the literature. Baker (1983) used the alternating quadrature rule for a desingularised integrand in water-wave calculations. It gives a quadrature similar to (3.1), but with a different (and desingularised) integrand. Sidi and Israeli (1988) analysed the spectral accuracy of a midpoint-rule approximation for a periodic singular integrand. They realised that the alternating quadrature rule applied to singular, periodic Cauchy kernels such as the integral in (3.1) gives spectral accuracy. Shelley (1992) used scheme (3.1) with Krasny's filtering in the context of studying the vortex-sheet singularity by the point-vortex method. By using the spectral accuracy of the alternating-trapezoidal rule, Hou, Lowengrub, and Krasny (1991) gave a simplified proof of convergence of the point vortex method for vortex sheets (Hou, Lowengrub and Krasny, 1991).

It seems natural to use the alternating-quadrature rule and a finite-order derivative operator (e.g. cubic spline) for the α-derivative. However, as will be seen later, the resulting scheme is numerically unstable at equilibrium; see Baker and Nachbin (to appear), Beale, Hou and Lowengrub (1993b) and Beale *et al.* (to appear). To see how standard schemes can be modified so that they become numerically stable, we use the discrete Fourier transform. For a discrete function $\{f_j\}$ on the periodic interval, the discrete transform and its inverse are (assuming N is even)

$$\hat{f}_k = \frac{1}{N} \sum_{j=-N/2+1}^{N/2} f_j e^{-ik\alpha_j}, \qquad f_j = \sum_{k=-N/2+1}^{N/2} \hat{f}_k e^{-ik\alpha_j}.$$

We will write a discrete derivative operator in the form

$$D_h^{(\rho)} f_j = \sum_{k=-N/2+1}^{N/2} \rho(kh) ik \hat{f}_k e^{ik\alpha_j}, \quad k = -N/2+1, ..., N/2, \tag{3.2}$$

where ρ is some non-negative, even function satisfying $\rho(0) = 1, \rho(\pi) = 0$. The choice of $\rho(\xi)$ varies depending on what kind of derivative operator is used. For example, we have $\rho_2(kh) = \sin(kh)/kh$ for the second-order centred differencing; $\rho_c(kh) = 3\sin(kh)/(kh(2+\cos(kh)))$ for the cubic spline approximation. It is easy to see that the order of accuracy is the order to which $\rho(\xi) \to 1$ as $\xi \to 0$. The spectral derivative without smoothing corresponds to the choice of $\rho \equiv 1$. We denote it by $D_h^{(1)}$. It is well known that the pseudo-spectral methods without smoothing may introduce aliasing errors which could lead to numerical instability (Kreiss and Oliger, 1979; Gottlieb and Orszag, 1977; Tadmor, 1987; and Goodman, Hou and Tadmor, 1994). To suppress aliasing errors, Fourier smoothing is often used. In that case,

ρ should satisfy (i) $\rho \geq 0, \rho(\pm\pi) = 0$; (ii) $\rho(x) = 1$ for $|x| \leq \lambda\pi$ for some $0 < \lambda < 1$; and (iii) ρ is smooth. Condition (ii) ensures spectral accuracy.

Once a derivative operator is chosen, we also use a smoothing based on ρ. For arbitrary periodic function f_j, we define $f_j^{(\rho)}$ by multiplying $\hat{f}_k$ by $\rho(kh)$ and taking the inverse Fourier transform. That is,

$$f_j^{(\rho)} = \sum_{k=-N/2+1}^{N/2} \rho(kh)\hat{f}_k e^{-ik\alpha_j}.$$

Thus, we have $D_h^{(\rho)} f_j = D_h^{(1)} f_j^{(\rho)}$. Similarly, we define $z_j^{(\rho)}$ by applying ρ to the transform of $z_j - \alpha_j$. It is clear that $f^{(\rho)}$ is an rth-order approximation to f if ρ corresponds to the rth-order derivative operator.

Now we can present our numerical algorithm for the water-wave equations (2.6)–(2.8) as follows:

$$\frac{d\bar{z}_j}{dt} = \frac{1}{4\pi i} \sum_{\substack{k=-N/2+1 \\ (k-j)\text{odd}}}^{N/2} \gamma_k \cot\left(\frac{z_j^{(\rho)} - z_k^{(\rho)}}{2}\right) 2h + \frac{\gamma_j}{2(D_h^{(\rho)} z)_j} \equiv u_j - iv_j, \quad (3.3)$$

$$\frac{d\phi_j}{dt} = \frac{1}{2}(u_j^2 + v_j^2) - g y_j, \quad (3.4)$$

$$D_h^{(\rho)} \phi_j = \frac{\gamma_j}{2} + \mathrm{Re}\left(\frac{D_h^{(\rho)} z_j}{4\pi i} \sum_{\substack{k=-N/2+1 \\ (k-j)\text{odd}}}^{N/2} \gamma_k \cot\left(\frac{z_j^{(\rho)} - z_k^{(\rho)}}{2}\right) 2h\right). \quad (3.5)$$

In practice, we solve for γ_j from (3.5) by iteration using (2.9).

Remark. The Fourier smoothing $z^{(\rho)}$ in (3.3) and (3.5) is to balance the high-frequency errors introduced by $D_h^{(\rho)}$. This will become apparent in the discussion of stability below. The choice of such smoothing is sharp. If we use finite-order derivative operators or Fourier smoothing for the spectral derivative, the use of smoothing on z is necessary for stability. We do not need to smooth on γ because γ defined by (3.5) has been smoothed implicitly through $D_h^{(\rho)}$ and $z^{(\rho)}$. We now state the convergence result; see Beale, Hou and Lowengrub (1993) and Beale *et al.* (to appear).

Theorem 1 (Convergence of a Boundary-Integral Method) Assume that $z(\cdot,t), \phi(\cdot,t) \in C^{m+2}[0,2\pi]$ *and* $\gamma(\cdot,t) \in C^{m+1}[0,2\pi]$ for $m \geq 3$, and $|z(\alpha,t) - z(\beta,t)| \geq c|\alpha - \beta|$ for $0 \leq t \leq T$ and $c > 0$. Furthermore, assume that

$$(u_t, v_t) \cdot n - (0,-g) \cdot n \geq c_0 > 0. \quad (3.6)$$

Here (u,v) is the Lagrangian velocity, n is the normal vector to the interface, pointing out of the fluid region, and c_0 is some constant. Then if $D_h^{(\rho)}$

corresponds to an rth-order-derivative approximation, we have for $h \leq h_0(T)$

$$\|z(t) - z(\cdot, t)\|_{l^2} \leq C(T)h^r, \tag{3.7}$$

Similarly, ϕ_j is accurate to order h^r, and γ_j is accurate to order h^{r-1} in the discrete L^2 norm defined by $\|z\|_{l^2}^2 = \sum_{j=1}^N |z_j|^2 h$. If $D_h^{(\rho)}$ corresponds to the spectral approximation, we have the same convergence result as above except for replacing h^r by h^m.

We remark that the sign condition (3.6) is required to prove well-posedness of the water-wave equations (Beale, Hou and Lowengrub, 1993a). It guarantees that the problem is stably stratified. It means that the interface is not accelerating downward, normal to itself, as rapidly as the normal acceleration of gravity. If (3.6) is violated, it would generate the Rayleigh–Taylor instability as if water were above the interface. It can be viewed as a natural generalisation of the criterion of Taylor (1950).

3.1. Discussion of stability analysis

Here we discuss some of the main ingredients in the stability analysis of the scheme given by (3.3)–(3.5). We will mainly focus on the linear stability. Once linear stability is established, non-linear stability can be obtained relatively easily by using the smallness of the error and an induction argument. The reader is referred to Beale, Hou and Lowengrub (to appear) and Beale *et al.* (to appear) for details.

To analyse linear stability, we write equations for the errors $\dot{z}_j(t) \equiv z_j(t) - z(\alpha_j, t)$, and so forth, and try to estimate their growth in time. If we compare the sum in (3.3) for the discrete velocity with the corresponding one for the exact velocity, the terms linear in $\dot{z}_j$, $\dot{\gamma}_j$ are

$$\frac{1}{2\pi \mathrm{i}} \sum_{(k-j)\text{odd}} \frac{\dot{\gamma}_k}{z(\alpha_j)^{(\rho)} - z(\alpha_k)^{(\rho)}} 2h$$

$$-\frac{1}{2\pi \mathrm{i}} \sum_{(k-j)\text{odd}} \frac{\gamma(\alpha_k)(\dot{z}_j^{(\rho)} - z_k^{(\rho)})}{(z(\alpha_j)^{(\rho)} - z(\alpha_k)^{(\rho)})^2} 2h,$$

where we have expanded the periodic sum, with k now unbounded. To identify the most singular terms, we use the Taylor expansion to obtain the most singular symbols

$$\frac{1}{z(\alpha_j) - z(\alpha_k)} = \frac{1}{z_\alpha(\alpha_j)(\alpha_j - \alpha_k)} + f(\alpha_j, \alpha_k),$$

where f is a smooth function. Thus, the most important contribution to

the first term is $(2iz_\alpha)^{-1}H_h\dot{\gamma}_j$, where H_h is the discrete Hilbert transform

$$H_h(\dot{\gamma}_j) \equiv \frac{1}{\pi} \sum_{(k-j)\text{odd}} \frac{\dot{\gamma}_k}{\alpha_j - \alpha_k} 2h. \tag{3.8}$$

Similarly, the most important contribution to the second term is $-\gamma(2iz_\alpha^2)^{-1}\Lambda_h(z_j^{(\rho)})$, where Λ_h is defined as follows:

$$\Lambda_h(\dot{f}_j) \equiv \frac{1}{\pi} \sum_{(k-j)\text{odd}} \frac{\dot{f}_j - \dot{f}_k}{(\alpha_j - \alpha_k)^2} 2h. \tag{3.9}$$

Let H and Λ be the corresponding continuous operators for H_h and Λ_h, respectively, that is, with the discrete sums replaced by continuous integrals. At the continuous level, it is easy to show that

$$\Lambda(f) = H(D_\alpha f), \tag{3.10}$$

where D_α is the continuous derivative operator. It turns out that in order to maintain numerical stability of the boundary-integral method, the quadrature rule for the singular integral and the discrete derivative operator $D_h^{(\rho)}$ must satisfy a compatibility condition similar to (3.10). That is, a given quadrature rule, which defines corresponding discrete operators H_h and Λ_h, and a discrete derivative $D_h^{(\rho)}$, must satisfy a compatibility condition similar to (3.10):

$$\Lambda_h(\dot{z}_i) = H_h(D_h^{(\rho)})(\dot{z}_i), \tag{3.11}$$

for $\dot{z}$ satisfying $\widehat{\dot{z}}_0 = \widehat{\dot{z}}_{N/2} = 0$. If (3.11) is violated, this will generate a singular operator of the form $(\Lambda_h - H_h(D_h^{(\rho)}))(\dot{z})$ in the error equations. This will generate numerical instability; see Subsection 2.6.

For the spectrally accurate alternating-trapezoidal-quadrature rule, the discrete Hilbert transform defined above has properties that are surprisingly similar to those of the continuum counterpart, that is,

$$\widehat{(H_h)}_k = -\text{isgn}(k), \quad \widehat{(\Lambda_h)}_k = |k|. \tag{3.12}$$

Thus the compatibility condition (3.11) would imply that a spectral derivative operator without smoothing should be used to obtain numerical stability. However, it is well known that aliasing errors can arise from products for spectral methods without smoothing. These aliasing errors will upset the high-mode balance of lower-order terms; see below.

By performing appropriate Fourier smoothing in the approximations of the velocity integral, we can ensure a variant of compatibility condition (3.11) is satisfied, that is,

$$\Lambda_h(\dot{z}_j^{(\rho)}) = H_h(D_h^{(\rho)})(\dot{z}_j). \tag{3.13}$$

This can be verified from the spectrum properties of H_h and Λ_h and the definition of the ρ smoothing. This modified compatibility condition is sufficient to ensure stability of our modified boundary-integral method. This explains why we need to smooth z in (3.3) and (3.5) when we approximate the velocity integral. The modified algorithm also allows use of non-spectral derivative operators.

The Fourier smoothing is also needed to eliminate aliasing errors in the discrete integral operator with smooth kernels. Typically, the lower-order terms are of the form $\sum_{(k-j)\text{odd}} f(\alpha_j, \alpha_k)\dot{z}_k 2h$ for a smooth function $f \in C^m$. In the continuous case, we have for any $\dot{z} \in L^2$

$$\int f(\alpha, \alpha')\dot{z}(\alpha')\mathrm{d}\alpha' = A_{-m}(\dot{z}),$$

where m is the degree of regularities of f and A_{-m} is a linear bounded operator from H^j to H^{j+m}, H^j being the Sobolev space of function with j derivatives in L^2. This is no longer true at the discrete level due to aliasing errors associated with the alternating-point-quadrature rule. For example, if we let $\dot{z}_j = \mathrm{e}^{\mathrm{i}(N/2-1)\alpha_j}$ and $f(\alpha, \alpha') = (\mathrm{e}^{\mathrm{i}2\alpha} - \mathrm{e}^{\mathrm{i}2\alpha'})/(\alpha - \alpha')$, we can show that

$$\sum_{(k-j)\text{odd}} f(\alpha_j, \alpha_k)\dot{z}_k 2h = -2\mathrm{i}\mathrm{e}^{\mathrm{i}(-N/2+1)\alpha_j},$$

which is of course no smoother than $\dot{z}$. This is a result of aliasing errors at the highest frequencies and is why we must use the Fourier smoothing to eliminate the aliasing errors in the high modes. With the ρ smoothing, we can prove that (Beale, Hou and Lowengrub, to appear)

$$\sum_{(k-j)\text{odd}} f(\alpha_j, \alpha_k)\dot{z}_k^{(\rho)} 2h = A_{-1}(\dot{z}).$$

With these observations, we can derive an error equation for $\dot{z}_j$ that is similar to the continuum counterpart in the linear well-posedness study (Beale, Hou and Lowengrub, 1993a)

$$\frac{\mathrm{d}\dot{z}_j}{\mathrm{d}t} = z_\alpha^{-1}(I - \mathrm{i}H_h)D_h^{(\rho)}\dot{F} + A_0(\dot{z}) + A_{-1}(\dot{\phi}) + O(h^r),$$

where $\dot{F} = \dot{\phi} - u\dot{x} - v\dot{y}$. This also suggests that we should project the error equation onto the local tangential and normal coordinate systems. In these local coordinates, the stability property of the error equations becomes apparent. Let $\dot{z}^N, \dot{z}^T$ be the normal and tangential components of $\dot{z}$ with respect to the underlying curve $z(\alpha)$, where N is the outward normal, and $\dot{\delta} = \dot{z}^T + H_h\dot{z}^N$. We obtain

$$\dot{z}_t^N = \frac{1}{|z_\alpha|}H_h D_h^{(\rho)}\dot{F} + A_{-1}(\dot{\phi}) + A_0(\dot{z}), \tag{3.14}$$

$$\dot{\delta}_t = A_{-1}(\dot{\phi}) + A_0(\dot{z}), \tag{3.15}$$

$$\dot{F}_t = -c(\alpha,t)\dot{z}^N A_{-1}(\dot{z}), \qquad c(\alpha,t) = (u_t, v_t + g)\cdot N, \tag{3.16}$$

where equation (3.16) is obtained by performing error analysis on Bernoulli's equation and using the Euler equations. In this form it is clear that only the normal component of $\dot{z}$ is important. Now it is a trivial matter to establish an energy estimate for the error equations. Note that $H_h D_h^{(\rho)}$ is a positive operator with a symbol $\rho(kh)|k|$. The problem is stable if the sign condition, $c(\alpha,t) > 0$, is satisfied. We refer to Beale, Hou and Lowengrub (to appear) for details.

3.2. Example of unstable schemes

In this section, we present a class of unstable schemes based on an equivalent boundary-integral formulation. We will demonstrate the numerical instability by performing a von Neumann stability analysis around the equilibrium (see also Baker and Nachbin (to appear)). Consider a boundary-integral formulation that uses the dipole strength μ. The vortex-sheet strength is defined in terms of μ by the relationship $\gamma = \mu_\alpha$. The evolution equations for z and ϕ are the same as before. The only difference is in the relation between ϕ and μ.

$$\phi = \frac{\mu}{2} + \mathrm{Re}\left(\frac{1}{4\pi \mathrm{i}}\int_{-\pi}^{\pi} \mu(\alpha')z_\alpha(\alpha')\cot\left(\frac{z(\alpha)-z(\alpha')}{2}\right)\mathrm{d}\alpha'\right). \tag{3.17}$$

It is clear that equation (2.8) is obtained by differentiating the relation (3.17) with respect to α and integrating by parts. A natural numerical approximation to the above equations is given by

$$\frac{\mathrm{d}\bar{z}_j}{\mathrm{d}t} = \frac{1}{4\pi \mathrm{i}}\sum_{(k-j)\mathrm{odd}} \gamma_k \cot\left(\frac{z_j - z_k}{2}\right)2h + \frac{\gamma_j}{2(D_h^{(\rho)} z_j)} \equiv u_j - \mathrm{i}v_j, \tag{3.18}$$

$$\frac{\mathrm{d}\phi_j}{\mathrm{d}t} = \frac{1}{2}(u_j^2 + v_j^2) - g y_j + \tau\kappa_j, \tag{3.19}$$

$$\phi_j = \frac{\mu_j}{2} + \mathrm{Re}\left(\frac{1}{4\pi \mathrm{i}}\sum_{(k-j)\mathrm{odd}} \mu_k D_h^{(\rho)} z_k \cot\left(\frac{z_j - z_k}{2}\right)2h\right), \tag{3.20}$$

$$\gamma_j = D_h^{(\rho)}\mu_j, \tag{3.21}$$

where $D_h^{(\rho)}$ can be any finite-order derivative approximation. As before, we denote its Fourier symbol as $\widehat{D_h^{(\rho)}}_k = \mathrm{i}k\rho(kh)$.

Now we perform a linear stability analysis around the equilibrium. Let

$$z = \alpha + \dot{z}; \phi = \dot{\phi}, \mu = 1 + \dot{\mu}.$$

Substituting the above expressions into the discrete equations (3.18)–(3.21), and using (3.12), we obtain to leading order

$$\frac{\mathrm{d}}{\mathrm{d}t}\bar{z}_j = \frac{1}{2i}H_h(D_h^{(\rho)}\dot{\mu}_j) + D_h^{(\rho)}\dot{\mu}_j/2, \tag{3.22}$$

$$\frac{\mathrm{d}}{\mathrm{d}t}\dot{\phi}_j = -g\dot{y}_j, \tag{3.23}$$

$$\dot{\phi}_j = \frac{\dot{\mu}_j}{2} + \frac{1}{2}(H_h(D_h^{(\rho)}\dot{y}_j) - \Lambda_h(\dot{y}_j)), \tag{3.24}$$

where H_h and Λ_h are defined as before. This system of equations has constant coefficients and it can be diagonalised in the Fourier space. The eigenvalues of the resulting system in the Fourier space give the growth rates of $\dot{x}, \dot{y}, \dot{\phi}$. They are explicitly given by

$$\lambda_1 = 0; \lambda_2, \lambda_3 = 0.5k^2\rho(1-\rho) \pm 0.5\sqrt{k^4\rho^2(1-\rho)^2 - 16g|k|\rho}.$$

Notice that if $\rho \neq 0, 1$, then $\lambda_2, \lambda_3 \simeq O(k^2)$ for large k. This indicates that the numerical high-mode instability is even stronger than that of Kelvin–Helmholtz! It is clear that the instability is caused by violating the compatibility condition (3.11), that is, $H_h D_h^{(\rho)} - \Lambda_h \neq 0$ (see (3.24)). If the Fourier smoothing is used as in (3.3) and (3.5), then this term vanishes and one can easily see that the modified method is stable. On the other hand, aliasing instabilities cannot be seen from this linear stability analysis around the equilibrium solution because there is no mode mixing for constant-coefficient problems. For computational evidences of numerical instabilities, we refer to Longuet-Higgins and Cokelet (1976); Roberts (1983); Dold (1992); Beale, Hou and Lowengrub (to appear); and Beale *et al.* (to appear).

There are other ways to perform smoothing to partially alleviate the difficulty due to high-mode instability, see Longuet-Higgins and Cokelet (1976), Roberts (1983) and Dold (1992). But they cannot completely eliminate the source of numerical instability since the modified schemes still fail to satisfy the compatibility constraint. So there is still a large number of intermediate to high modes that are numerically unstable. As the number of grid points increases, or as we compute further in time, the numerical scheme will suffer from the high-mode instability. This has been one of the major obstacles in computing free-surface waves.

3.3. A numerical calculation of wave breaking

Here we present a calculation of wave breaking to illustrate how well our modified boundary integral performs in the fully non-linear regime. For a survey of breaking waves; see Peregrine (1983). We use the following initial condition:

$$x(\alpha, 0) = \alpha, y(\alpha, 0) = 0.1\cos(2\pi\alpha), \gamma(\alpha, 0) = 1.0 + 0.1\sin(2\pi\alpha).$$

The gravity coefficient is chosen to be $g = 9.8$. Note that the vortex-sheet strength γ does not have zero mean in this case. This amounts to a convenient choice of frame of reference. Although the derivation of (2.6)–(2.8) was for the special case where ϕ is periodic and γ has zero mean, the formulation is still valid provided only that we apply $D_h^{(\rho)}$ to equation (2.7); only $D_h^{(\rho)}\phi$ is needed in (2.8). The time integration in this numerical example is the fourth-order explicit Adams–Bashforth method. The fourth-order Runge–Kutta method is used to initialise the first three time steps. Also, a fourth-order extrapolation in time is used to obtain a more accurate first iterate in the iterative scheme for γ, as suggested in Baker, Meiron and Orszag (1982). With this improved initial guess, the iteration will converge with an iteration error of order 10^{-10} in two iterations for most time until the wave is close to breaking. In this calculation, we use a 25th-order Fourier smoothing in the spectral derivative with ρ given by

$$\rho(kh) = \exp(-10 \cdot (2|k|/N)^{25}), \quad \text{for} \quad |k| \leq N/2.$$

In Figure 1, we present a series of interface profiles from $t = 0.28$ to $t = 0.5175$. In order to see clearly the time evolution of the water wave, we plot the solution at five different times in a single picture. The first curve from the top is obtained by adding 0.6 to the y coordinate; the successive ones are displaced by multiples of 0.3. Time increases from top to bottom. As we can see from Figure 1b, the interface becomes vertical around $t = 0.32$. After that, the wave turns over. In the mean time, the interface develops large curvature, and requires more-refined numerical resolution. With $N = 256$, we can compute up to $t = 0.5$ with six digits of accuracy in the interface positions. But in order to compute very close to the time of wave breaking, we need to increase our resolution to $N = 512$, or larger. Of course, beyond $t = 0.32$ when the interface becomes vertical, our convergence result will cease to be valid since it violates our condition (3.6) in Theorem 1. But one can see that our numerical calculations remain robust even after condition (3.6) is violated. Without additional filtering, our code can run up to $t \simeq 0.51$. In order to compute all the way up to the time of wave breaking, we need to use Krasny's filtering (see Subsection 4.1) beyond the time of wave turnover ($t \simeq 0.32$) to control the growth of round-off errors due to the Rayleigh–Taylor instability.

In Figure 1c, we plot the enlarged version of the wave fronts from $t = 0.5$ to 0.5175 when the wave is close to breaking. It is evident that the wave will break in finite time. In Figure 1d, we illustrate the number of computational particles near the wave front at the final time of our calculations. We can see that the interface is still well resolved and more particles are clustered near the head of the wave front where the curvature is the

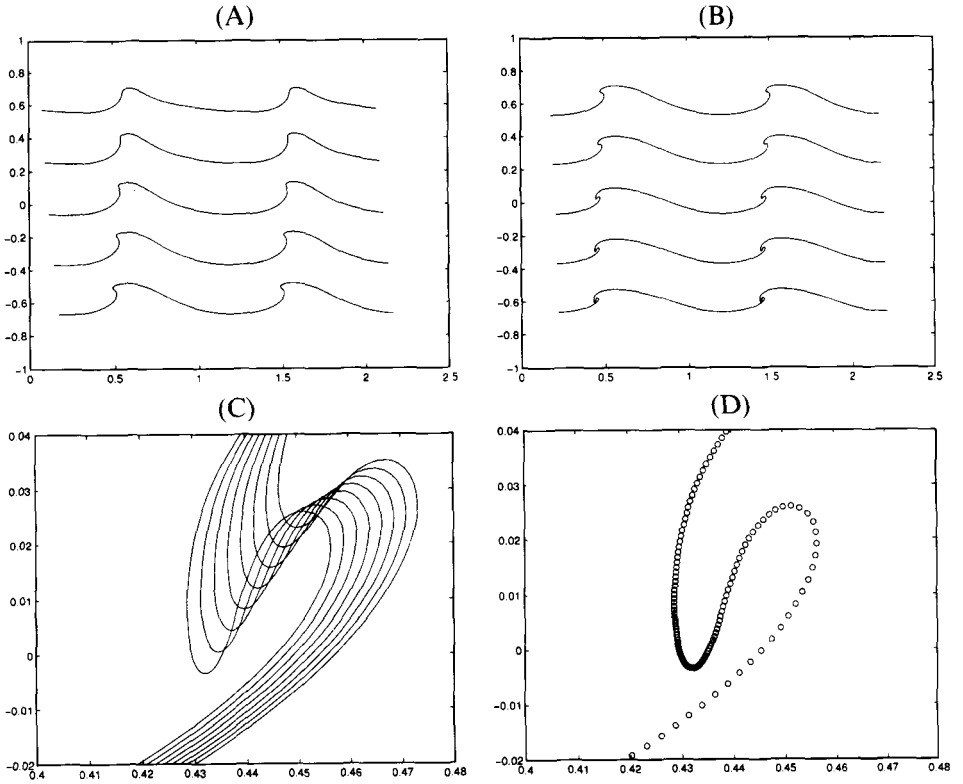

Fig. 1. (A) Water waves at $t = 0.28, 0.32, 0.36, 0.4, 0.44, N = 256, \Delta t = 0.001$. From Beale, Hou and Lowengrub (to appear). (B) Water waves at $t = 0.46, 0.48, 0.5, 0.51, 0.5175, N = 512, \Delta t = 0.00025$. From Beale, Hou and Lowengrub (to appear). (C) Enlarged view of wave fronts at $t = 0.5, 0.5025, ..., 0.5175, N = 512, \Delta t = 0.00025$. From Beale, Hou and Lowengrub (to appear). (D) Enlarged view of wave fronts at $t = 0.5175, N = 512, \Delta t = 0.00025$. From Beale, Hou and Lowengrub (to appear)

largest (about 800 in amplitude). This demonstrates the self-adaptive nature of the boundary-integral method. Details of the calculation and other computational examples can be found in Beale, Hou and Lowengrub (to appear).

4. Numerical computations of vortex-sheet roll-up

The idealisation of a shear layer as a vortex sheet separating two regions of potential flow has often been used as a model to study mixing properties, boundary layers and coherent structures of fluids. A vortex sheet corresponds to the case when the two fluid densities are the same on each side of the interface, but the tangential velocity across the interface has a jump discontinuity. Without physical regularisation such as surface tension or viscosity, the vortex-sheet problem is ill-posed in the Hadamard sense. Small

perturbations can lead to exponential growth in high wavenumbers due to the Kelvin–Helmholtz instability. Since the Kelvin–Helmholtz instability is a generic fluid-dynamical instability for multi-fluid interfaces (except for the case of unit Atwood number $A^2 = 1$), the understanding of the numerical and analytical difficulties of the vortex-sheet problem would shed useful light into the general multi-fluid interfaces. In fact, most of the numerical techniques we discuss in this section can be and have been extended to the study of Rayleigh–Taylor instability in multi-fluid interfaces.

Assume the interface is periodic in the horizontal direction, that is, $z(\alpha, t) = \alpha + s(\alpha, t)$ with $s(\alpha, t)$ being periodic in α. The vortex-sheet strength γ is also periodic. For a vortex sheet, the Atwood number is equal to zero. This greatly simplifies the equations of motion for the interface. The governing equations reduce to

$$\frac{\mathrm{d}\bar{z}}{\mathrm{d}t} = \frac{1}{4\pi \mathrm{i}} \int \gamma(\alpha', t) \cot\left(\frac{z(\alpha, t) - z(\alpha', t)}{2}\right) \mathrm{d}\alpha',$$

$$\frac{\mathrm{d}\gamma}{\mathrm{d}t} = 0.$$

This shows that γ is conserved along Lagrangian particle trajectories. If the initial vortex-sheet strength γ_0 is positive, then we can parameterise the interface by its circulation variable Γ. Then the above equations further reduce to a single equation for the interface position z:

$$\frac{\mathrm{d}\bar{z}}{\mathrm{d}t} = \frac{1}{4\pi \mathrm{i}} \int \cot\left(\frac{z(\Gamma, t) - z(\Gamma', t)}{2}\right) \mathrm{d}\Gamma', \tag{4.1}$$

Linear stability around equilibrium solution $z = \Gamma$ gives the dispersion relation

$$\lambda^2 = k^2/4, \tag{4.2}$$

so there is one growing eigenmode and one decaying eigenmode. Arbitrarily small perturbation can lead to unbounded exponential growth in high wavenumbers.

4.1. The point-vortex approximation

The point-vortex approximation to (4.1) was first introduced by Rosenhead (1932). The idea is to represent the vortex sheet by a collection of point sources. Let $z_j(t)$ denote the numerical approximation of $z(\Gamma_j, t)$, with $\Gamma_j = jh$, $h = 2\pi/N$. The integral on the right-hand side of (4.1) is approximated by the trapezoidal rule, which omits the infinite contribution due to the self-induced velocity at $\Gamma' = \Gamma$. This gives rise to a system of ordinary

differential equations for the particle trajectories

$$\frac{\mathrm{d}\bar{z}_j}{\mathrm{d}t} = \frac{1}{4\pi \mathrm{i}} \sum_{\substack{k=1 \\ k\neq j}}^{N} \cot\left(\frac{z_j - z_k}{2}\right) h \tag{4.3}$$

$$z_j(0) = \Gamma_j + s(\Gamma_j, 0). \tag{4.4}$$

Equations (4.3) have a Hamiltonian structure for the conjugate variables $x_j N^{-1/2}, y_j N^{-1/2}$. The Hamiltonian is given by

$$H_N(t) = \frac{-1}{4\pi N^2} \sum_{j=1}^{N} \sum_{k>j} \ln(\cosh(y_j - y_k) - \cos(x_j - x_k)). \tag{4.5}$$

One immediate consequence from the Hamiltonian is that if the variables $y_j(t)$ remain bounded, then the invariance of $H_N(t)$ implies that the point vortices remain separated (recall that we have assumed one signed vorticity distribution here).

The main issue here is the question of numerical stability of the point-vortex approximation. Using a sinusoidal initial perturbation with a small number of particles, Rosenhead integrated the vortex-sheet equation (4.3) and obtained the expected roll-up of the vortex sheet. These calculations were repeated by Birkhoff (1962). Birkhoff found that the point-vortex approximation did not converge as the number of particles increased. In fact, the increased number of points led to irregular motion of the points and early deterioration of the calculations. Some investigators have tried to use high-order discretisations to resolve this difficulty, and different smoothing techniques have been tried. But irregular motion still persists. We refer to van de Vooren (1980), Higdon and Pozrikidis (1985), Pullin (1982), Moore (1985) and Fink and Soh (1978) for more detailed discussions.

The source of numerical instability was later clarified by Krasny (1986a). Krasny found that there are two types of irregular motion that can occur in the numerical solution of the point-vortex equations for vortex sheets. The first one occurs at smaller times $t > 0$ as the value of N increases. The second type occurs only beyond the vortex-sheet's critical time regardless of the value of N. The second type of irregular motion is due to the loss of regularity of the solution beyond the critical time. Without additional physical or numerical regularisation, the point-vortex method will fail to converge beyond the singularity time. The first type of irregular motion is caused by round-off errors due to the computer's finite-precision arithmetic. Once these round-off error perturbations enter the calculations, they grow according to the equations' dynamics and are subject to the Kelvin–Helmholtz instability. Thus the highest modes will grow the fastest and the growth rate is exponential with increasing wavenumbers. This explains why increasing the number of grid points will lead to rapid growth and early-

time irregular motion. In order to control the growth of the round-off-error perturbations, Krasny introduced a non-linear filtering technique (1986a). That is, at every time step, before we evaluate the singular integral, we take the Fourier transform of the particle position z_j. Set to zero those Fourier coefficients that are below a certain cut-off level, say 10^{-13} if a 16-digit arithmetic is used. Then take the inverse Fourier transform.

More specifically, we can consider Krasny's filtering as a projection operator, denoted by P. Given an error tolerance τ, the projection operator P is given by

$$(\widehat{Pf})_k = \begin{cases} \hat{f}_k, & \text{if} \quad |\hat{f}_k| \geq \tau, \\ 0, & \text{otherwise}, \end{cases} \tag{4.6}$$

for any periodic function f. The filter P is non-linear because the wavenumbers at which it is applied depend on the solution. In order for this filtering operator to be effective, we assume that the underlying function, f, has a rapid decay in the Fourier space. Moreover, we want to take the filter level, τ, as small as possible for the sake of accuracy. So it is preferable to perform the numerical calculations in double-precision arithmetic. To illustrate the method, we take the forward Euler discretisation for the point-vortex method as an example. With Krasny's filtering, the numerical method becomes

$$\bar{z}_j^{n+1} = P\left\{\bar{z}_j^n + \Delta t \frac{1}{4\pi \mathrm{i}} \sum_{k \neq j} \cot\left(\frac{z_j - z_k}{2}\right) h\right\}. \tag{4.7}$$

The effect of this filtering is dramatic. With this filtering, the first type of irregular motion is eliminated. One can compute up to the time when the curvature singularity is formed. Since the filter level is very small (typically 10^{-13} in a 16-digit arithmetic), it does not affect the accuracy much in the smooth region. Comparison of the filtered calculation and the unfiltered 29-digit calculation shows very good agreement (Krasny, 1986a). Moreover, the filter does not suppress the growth of high-wavenumber modes. With the filtering, the high wavenumber modes can still grow through non-linear interactions. Once the modes grow larger than the filtered level, they are not affected by the filtering.

We include the calculations obtained by Krasny (1986a) for the initial data (note that the period is 1, not 2π):

$$x(\Gamma, 0) = \Gamma + 0.01 \sin 2\pi\Gamma, \; y(\Gamma, 0) = -0.01 \sin 2\pi\Gamma,$$

which is a small-amplitude perturbation of the equilibrium solution. The filtering technique was used in double precision (16-digit) with $N = 100$. The time step was set to be $\Delta t = 0.01$ for $t \leq 0.25$ and $\Delta t = 0.001$ for $t > 0.25$. A fourth-order Runge–Kutta method was used for time integration. The filter

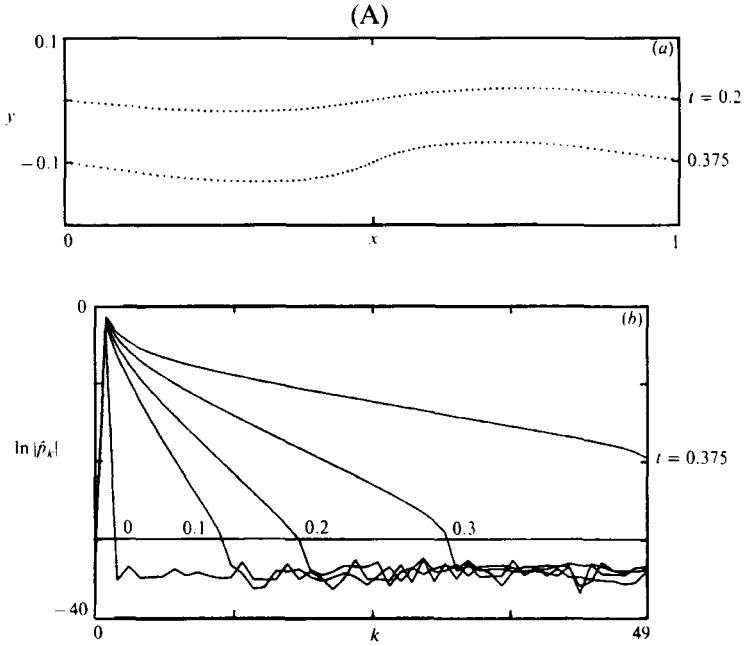

Fig. 2A. Double-precision (16-digit) calculation with filter level set at 10^{-13} (the horizontal line in (b)). This calculation used $N = 100$ and $\Delta t = 0.01$ for $t \leq 0.25$ and $\Delta t = 0.001$ for $t > 0.25$: (a) point-vortex positions; (b) log-linear plot of the Fourier coefficients. (2.2) amplitudes versus wavenumber. From Krasny (1986a)

level was set to 10^{-13}. In this case, the filter turned off at $t \simeq 0.35$. The resulting point positions and the Fourier coefficients are plotted in Figure 2A. In this calculation the Hamiltonian was also well conserved. There is no sign of the first type of irregular point motion which had appeared in the unfiltered 16-digit calculation at $t = 0.375$; Using filtering with $N = 200$ in double precision, Krasny can compute up to the singularity time $t = 0.375$; see Figure 2B (d). It is worth noting that without filtering even a 29-digit calculation yielded irregular motion at time $t = 0.375$ (see Fig 2B (c)), not to mention the calculations obtained used single and double precisions (Fig 2B (a) and (b)).

Shelley (1992) used the spectrally accurate alternating quadrature to re-examine the singularity formation in vortex-sheet motion, trying to acquire more precise information on the singularity structure. Shelley's calculations were performed in 30 digits of precision in conjunction with Krasny's filtering technique. The filter level was set to 10^{-25}. This high precision seems to be necessary to discern the asymptotic behaviour of the spectrum. It was found that Moore's asymptotic analysis is valid only at times well before the singularity time. Near the singularity time the form of the singularity

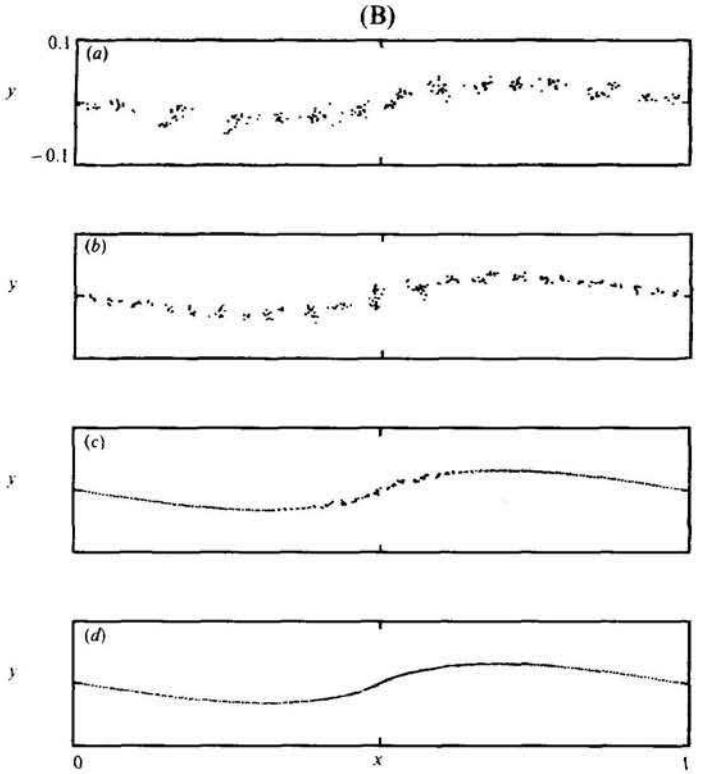

Fig. 2B. Point-vortex positions at $t = 0.375$ for $N = 200$: (a) single precision (7 digit); (b) double precision (16 digit); (c) CDC double precision (29 digit); (d) filtered at level 10^{-13}, double precision (16 digit). From Krasny (1986a).

departs significantly from that predicted by Moore. Moreover, the real and imaginary parts of the solutions behave differently near the singularity time. The form of the singularity also depends upon the amplitude of the initial disturbance.

Convergence of the point-vortex method for vortex sheets was first obtained by Caflisch and Lowengrub (1989) for analytic initial data. A simplified proof was later obtained by Hou, Lowengrub and Krasny (1991), using the spectral accuracy of the alternating quadrature rule. However, these convergence results are for short times, and do not consider the effect of round-off errors. In fact, with a simulated round-off-error term, the convergence result breaks down very quickly as the number of computational particles increases. Recently, Caflisch, Hou and Lowengrub (1994) have been able to prove convergence of the point-vortex method for vortex sheets with Krasny's filtering. The proof is in an analytic function class and uses a discrete form of the Cauchy–Kowalewski theorem. The proof is presented

for the case in which the sheet is initially near equilibrium and convergence is obtained nearly up to the singularity time. The analysis in this paper applies directly to other ill-posed problems such as Rayleigh–Taylor unstable interfaces in incompressible, inviscid and irrotational fluids, as well as to Mullins–Sekerka unstable interfaces in Hele–Shaw cells.

4.2. Vortex-blob calculations

In this section, we present a vortex-blob desingularisation to study vortex-sheet roll-up beyond the curvature singularity. The first application of vortex-blob methods for vortex-sheet roll-up was given by Chorin and Bernard (1973) in which they proposed to regularise the point-vortex method by smooth vortex blobs. Subsequently, Anderson (1985) applied vortex-blob methods to study vortex-sheet roll-up using the Bousinesqu approximation, and performed a careful numerical convergence study. In a series of papers (Krasny, 1986b; Krasny, 1987; Nitsche and Krasny, 1994), Krasny has used the vortex-blob method to study vortex-sheet roll-up and has obtained a number of interesting results. Some previous alternative desingularisations for vortex sheets have incorporated a stabilising physical mechanism into the model. Moore (1978) has derived an evolution equation for a vortex layer of small thickness. Pozrikidis and Higdom (1985) have numerically studied a periodically perturbed layer of constant vorticity. Baker and Shelley (1990) have considered regularisation of a thin vortex layer. Pullin (1982) has included surface tension in the evolution equation. We will come back to these other types of regularisation in later sections. Unlike these approaches, the specific form of desingularisation that is used in vortex-blob methods does not correspond precisely to a physical effect. It is a purely numerical regularisation.

The vortex-blob desingularisation for vortex sheets can be described as follows. Let δ be a non-negative real number. We will desingularise the Birkhoff–Rott equations by placing a cut-off in the singular kernel.

$$\frac{\partial x}{\partial t} = \frac{-1}{4\pi}\int_{-\pi}^{\pi} \frac{\sinh(y-y')}{\cosh(y-y')-\cos(x-x')+\delta^2}\mathrm{d}\Gamma', \tag{4.8}$$

$$\frac{\partial y}{\partial t} = \frac{1}{4\pi}\int_{-\pi}^{\pi} \frac{\sin(x-x')}{\cosh(y-y')-\cos(x-x')+\delta^2}\mathrm{d}\Gamma', \tag{4.9}$$

where $x = x(\Gamma,t)$, $x' = x(\Gamma',t)$. When $\delta = 0$, the integral is understood as the Cauchy principal-value integral. In that case, we recover the vortex-sheet equations in the periodic case.

A flat vortex sheet of constant strength is an equilibrium solution of the desingularised equations. It is easy to perform a linear stability analysis around the equilibrium solution. This helps us gain insight into the nature of the desingularisation. The growth rates of the perturbation can be computed

by Fourier transform. The dispersion relation is given by Krasny (1986b)

$$\omega^2 = \frac{k(1 - \mathrm{e}^{-k \cosh^{-1}(1+\delta^2)})\mathrm{e}^{-k \cosh^{-1}(1+\delta^2)}}{4\delta(2+\delta^2)^{1/2}}.$$

The positive branch of ω corresponds to the growing perturbations. For a fixed value of $\delta > 0$, there is a wavenumber k_m for which the growth rate $\omega(k_m)$ is maximum. In the limit $k \to \infty$ we have $\omega(k) \to 0$. For example, with $\delta = 0.05$, the maximum growth rate of the eigenvalue is about 3.5. The desingularised equations therefore do not exhibit the severe short wavelength instability of the exact vortex-sheet equations. As $\delta \to 0$ with a fixed wavenumber, we recover the exact dispersion relation $\omega^2 \simeq k^2/4$.

We can apply standard discretisation techniques to solve the initial value problem (4.8)–(4.9). For example, the trapezoidal quadrature of the integrals in (4.8)–(4.9) yields a system of ordinary differential equations in the case of period-one initial condition

$$\frac{\mathrm{d}x_j}{\mathrm{d}t} = \frac{-1}{2} \sum_{\substack{k=1 \\ k \neq j}}^{N} \frac{\sinh 2\pi(y_j - y_k)}{\cosh 2\pi(y_j - y_k) - \cos 2\pi(x_j - x_k) + \delta^2} h, \quad (4.10)$$

$$\frac{\mathrm{d}y_j}{\mathrm{d}t} = \frac{1}{2} \sum_{\substack{k=1 \\ k \neq j}}^{N} \frac{\sin 2\pi(x_j - x_k)}{\cosh 2\pi(y_j - y_k) - \cos 2\pi(x_j - x_k) + \delta^2} h. \quad (4.11)$$

If $\delta = 0$, then the above discretisation is the point-vortex approximation of Rosenhead (1932). As for the point-vortex system, for any $\delta \geq 0$, the equations (4.10),(4.11) form a Hamiltonian system for the conjugate variables $x_j \cdot N^{-1/2}$, $y_j \cdot N^{-1/2}$, with the Hamiltonian function given by

$$H_N(t) = \frac{-1}{4\pi N^2} \sum_{j=1}^{N} \sum_{k>j} \ln(\cosh 2\pi(y_j - y_k) - \cos 2\pi(x_j - x_k) + \delta^2). \quad (4.12)$$

Krasny (1986b) used the above vortex-blob method to compute vortex-sheet roll-up using the same initial condition as for the point-vortex method calculation

$$x_j(0) = \Gamma_j + 0.01 \sin 2\pi\Gamma_j, y_j(0) = -0.01 \sin 2\pi\Gamma_j. \quad (4.13)$$

The fourth-order Runge–Kutta method was used to perform time integration. There are now three parameters, $\delta, \Delta t$ and h. It turns out that if one simultaneously reduces all three parameters, one does not get a convergent result in general. The strategy, which was first used by Anderson (1985), is to first keep δ fixed, and then reduce Δt and h until we get a convergent solution of the δ equations. By repeating this process for several values of δ, one can extrapolate the limit $\delta \to 0$.

Krasny (1986b) showed that using the δ-desingularisation the vortex sheet

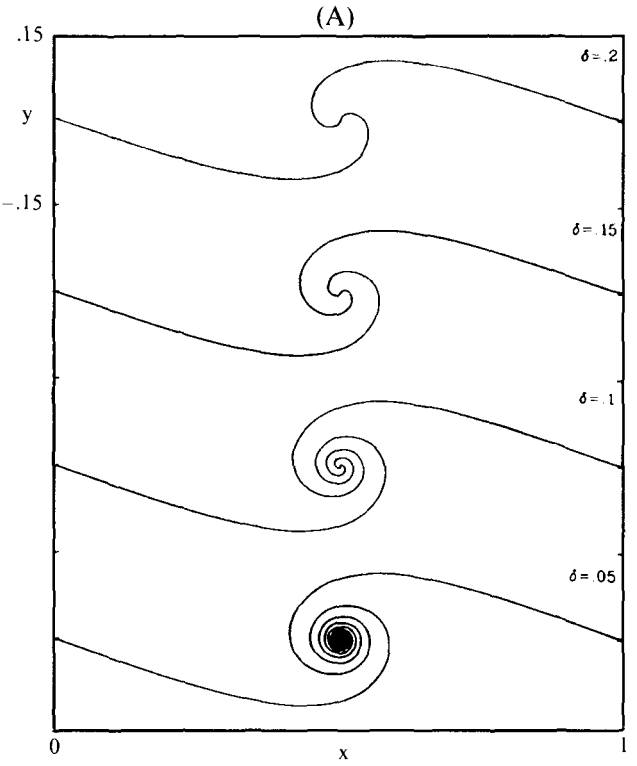

Fig. 3A. Vortex-blob-method solutions of the δ equation at $t = 1$, $N = 400$. From Krasny (1986b).

rolls up into a double-branched spiral past the critical time. The effect of decreasing δ at a fixed time ($t = 1$) beyond the critical time ($t_c = 0.375$) is shown in Figure 3A, which plots the interface for several values of δ between 0.2 and 0.05. These calculations used $N = 400$ and $\Delta t = 0.05$. In the case of $\delta = 0.05$, a smaller time step was used, $\Delta t = 0.01$, and the computation was performed in double-precision arithmetic (16 digits). As δ decreases with $t = 1$ in Figure 3A, more turns appear in the core. For $\delta = 0.05$, the core region is tightly packed. An enlarged view is shown in Figure 3B, which shows that each branch of the spiral contains five complete resolutions. The curve's outer region seems to converge as δ decreases. Some evidence was given in Krasny (1986b).

Krasny also used the vortex-blob method for several other applications, including computing the vortex-sheet roll-up in the Trefftz plane [95], and computing vortex sheet roll-up past a sharp edge to study separation [112]. The calculation of vortex ring formation at the edge of a circular tube in an axisymmetric 3-D vortex-sheet model seems to support the experimental findings (Nitsche and Krasny, 1994). Related numerical studies for axisym-

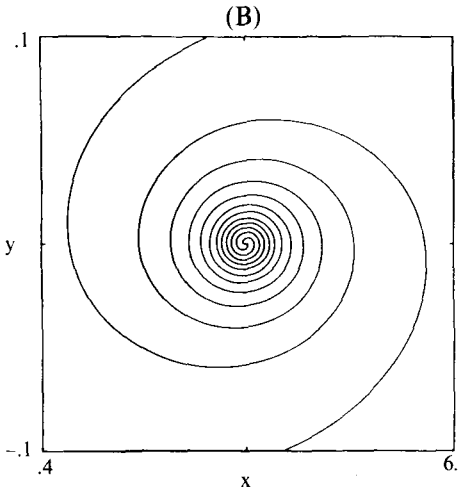

Fig. 3B. An enlarged view of the inner portion of the $\delta = 0.04$ case, $t = 1$, $N = 400$. From Krasny (1986b).

metric vortex-sheet motion have been carried out by Pullin (1979), Caflisch, Li and Shelley (1993), Pugh (1989), Kaneda (1990) and Dahm, Frieler and Tryggvason (1992).

Convergence of vortex-blob methods for vortex sheets has been established by Caflisch and Lowengrub (1989) for short times using analytic data. Following Delort's observation, Liu and Xin (to appear) have been able to prove that Krasny's vortex-blob calculation converges globally to a weak solution of the Euler equations if the initial vorticity does not change sign.

Finally, we remark that it is an easy matter to generalise the vortex-blob method to study Rayleigh–Taylor instability for general two-density interface problems; see, for example, Kerr (1988).

4.3. Thin-vorticity-layer regularisation of vortex sheets

Another approach to compute vortex-sheet motion beyond the singularity time is to study the motion of smoother solutions to the Euler equation. In 1990, Baker and Shelley approximated the vortex sheet by a thin layer of constant and finite vorticity of mean width H. The limiting behaviour of such vortex layers as $H \to 0$ was investigated to determine the possible nature of the vortex sheet past its singularity time. They found that the behaviour of an asymptotically thin vortex layer is given by a vortex sheet whose strength is the local layer width times the vorticity strength.

The problem of vortex layers with constant vorticity, also called vortex patches, is of interest in itself. Accurate and robust numerical methods for vortex-patch problems have been developed by Zabusky *et al.* (1979, 1983).

They referred to their methods as 'contour dynamics'. It has led to some interesting applications; see, for example, Dritschel (1989) for a review. The mathematical theory of vortex patches has attracted a lot of interest in recent years. The well-known result of Yudovich (1963) provides a theoretical framework for the vortex-patch problem. In particular, it guarantees the global existence of the flow. Yudovich's theory does not preclude the formation of singularities in the boundaries of vortex patches. Majda (1986) proposed the vortex-patch problem, in contour-dynamic form, as a model for the inviscid, incompressible creation of small scales. Motivated by analogy with the stretching of vorticity in three dimensions and by a simple model (1985, 1986), he suggested the possibility of finite-time singularities. In other words, some smooth initial contours might, in finite time, lead to loss of regularity such as infinite length, corners or cusps. This suggestion has been the subject of some debate in the computational literature (Buttke, 1989; Dritschel and McIntyre, 1990). Recently, Chemin (1993) proved that smooth contours stay smooth for all times provided that the initial condition is in $C^{1,\alpha}$ with $\alpha > 0$. A simplified proof was given by Bertozzi and Constantin (1993).

The set-up of the thin layer regularisation is as follows. Consider a periodic vortex layer surrounded by two interfaces. At $t = 0$, these two interfaces are symmetric with respect to the flat interface $y = 0$. The vortex layer is assumed to have mean width H and vorticity $-2U/H$. The lower interface, Γ_1, is parameterised as $z_1(\alpha)$, and the upper interface, Γ_2, as $z_2(\alpha)$, where $z_j(\alpha) = x_j(\alpha) + \mathrm{i}y_j(\alpha)$. The thin layer is assumed to be 2π-periodic in the x-direction. It can be shown that the velocity of the fluid at a point $z_j(\alpha, t)$ on the jth interface ($j = 1, 2$) is given by

$$\begin{aligned}\frac{\partial \bar{z}_j}{\partial t}(\alpha,t) &= \frac{2U}{4\pi H\mathrm{i}}\int_0^{2\pi}(y_1(\alpha,t)-y_j(\alpha'))\\ &\quad\times\cot\left(\frac{z_j(\alpha,t)-z_1(\alpha',t))}{2}\right)\frac{\partial z_1}{\partial\alpha'}(\alpha',t)\mathrm{d}\alpha' \qquad (4.14)\\ &\quad-\frac{2U}{4\pi H\mathrm{i}}\int_0^{2\pi}(y_2(\alpha,t)-y_j(\alpha'))\\ &\quad\times\cot\left(\frac{z_j(\alpha,t)-z_2(\alpha',t))}{2}\right)\frac{\partial z_2}{\partial\alpha'}(\alpha',t)\mathrm{d}\alpha'. \qquad (4.15)\end{aligned}$$

Note that the motion of vortex layers depends only upon information on the boundaries.

There have been many numerical studies in developing accurate quadrature rules for the boundary integrals in the above contour dynamic equations. Consider the case $j = 1$ as an example. The first integral in (4.14) has a smooth, periodic integrand due to a compensating zero in the function $y_1(\alpha, t) - y_1(\alpha', t)$. Thus the standard trapezoidal rule over equally spaced

collocation points gives spectral or infinite-order accuracy. Accuracy is then limited by the approximation to $\partial z_1/\partial \alpha'$ at the collocation points. In Baker and Shelly (1990), derivatives were approximated by periodic, quintic splines with an accuracy of $O(h^6)$. The approximation to the second integral can be derived similarly. It is even simpler in this case since the field point $z_1(\alpha)$ does not sit on the boundary Γ_2.

The numerical study of Baker and Shelley (1990) indicates that the motion of the vortex layer leads to the formation of regions of high curvature, and regions of rapid stretching in the bounding interfaces. To maintain resolution of the interfaces, the mesh was redistributed periodically to resolve the high-curvature regions and collocation points were kept in the regions of rapid stretching. The mesh redistribution was done through a smooth reparameterisation of the interfaces.

The initial conditions for layer interfaces considered in Baker and Shelley (1990) were given by

$$z_1(\alpha, 0) = \alpha - \mathrm{i}\frac{H}{2}(1 - a\cos\alpha), z_2(\alpha, 0) = \alpha + \mathrm{i}\frac{H}{2}(1 - a\cos\alpha),$$

with $a < 1$. The limit of the above initial data as $H \to 0$ corresponds to the vortex-sheet initial data considered by Meiron, Baker and Orszag (1982) in their study of the singularity structure of a vortex sheet. In particular, the vortex sheet acquires a curvature singularity at $\alpha = \pi$.

The evolution of vortex layers with $U = 1/2$ and $a = 1/2$ was calculated for various mean thicknesses, $H = 0.025, 0.05, 0.1$ and 0.2. The case $H = 0.025$ corresponds to an aspect ratio of 250 to 1. This was the smallest value of H that Baker and Shelley (1990) could compute reliably. The critical time of curvature singularity is about $t_c = 1.6$ (Shelley, 1992). Figure 4a shows the location of the layer interfaces with $H = 0.025$ at various times $t = 0, t = 2.0$ and $t = 2.4$. Figure 4b shows several sequences of layer profiles for various thicknesses. Each column gives a sequence of layers at various times with H fixed, and goes as far as the computation is reliable. For a fixed time beyond the critical time, the central region of the layer does not show a converging pattern, but at different times one can observe a similarity in the profiles. This non-uniformity behaviour makes it very difficult to extrapolate the limiting behaviour from the profiles of the layer.

A close examination reveals that the evolution generically occurs in three phases: First, the vorticity advects to the centre (i.e. $\alpha = \pi$), causing a further thickening near the centre. Second, the vorticity in the centre quickly reforms into a roughly elliptical core with trailing arms, which subsequently wrap around the core as it evolves. As the value of H becomes smaller, the vorticity becomes more intense, which leads to faster roll-up. For thinner layers the core structure becomes a smaller fraction of the total layer. The

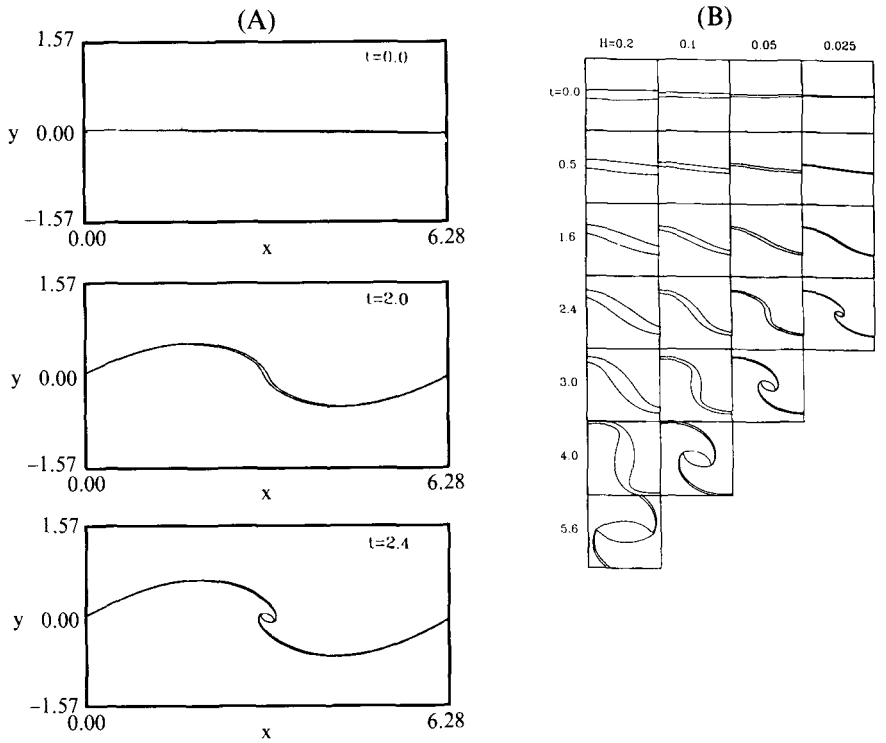

Fig. 4. (A) The location of the layer interfaces for $H = 0.025$ at various times. From Baker and Shelley (1990). (B) Thin-vortex-layer-solutions. The core region of the layer interfaces for various times and thicknesses. From Baker and Shelley (1990).

core seems to collapse to a point with no circulation but infinite vortex-sheet strength. Assuming such a limit exists, it would converge to a weak solution of the Euler equations described by DiPerna and Majda (1987a,b) and Delort (1991). The cores with their trailing arms are very similar to the structures observed by Zabusky *et al.* (1979) in their numerical study of the vortex patches. The simulations also agree qualitatively with the vortex-layer simulations done by Pozrikidis and Higdon (1985).

4.4. Vortex-in-cell method

Here we present the vortex-in-cell (VIC) method for computing vortex sheets by Tryggvason (1989), and compare with the vortex-blob calculations by Krasny (1986b). Usually the VIC method is used only as a device to speed up the calculation of the velocities from the vorticity. However, the grid-particle interpolations usually introduce some numerical smoothing. This smoothing is generally regarded as an unpleasant property of the VIC method because

it may suppress the small-scale interactions. On the other hand, one can also regard the VIC method as a grid-based vortex method with the blob size equal to the mesh size. It actually has regularisation properties similar to the vortex-blob method.

We begin with the two-dimensional vortex method for the Euler equation in the vorticity form:

$$\frac{\mathrm{D}\omega}{\mathrm{d}t} = 0, \quad \nabla^2\psi = -\omega, \quad \mathbf{u} = (\partial_y\psi, -\partial_x\psi), \tag{4.16}$$

where ω is the vorticity, ψ is the stream function and

$$\frac{\mathrm{D}}{\mathrm{d}t} = \frac{\partial}{\partial t} + \mathbf{u}\cdot\nabla$$

is the material derivative. In vortex methods, the vorticity field is approximated by a collection of discrete point vortices, each with circulation Γ_i. By (4.16), the circulation of each vortex is conserved in time. The Lagrangian particle positions can be found by integrating

$$\frac{\mathrm{d}\mathbf{x}_i}{\mathrm{d}t} = \mathbf{u}(\mathbf{x}_i, t).$$

To find the velocity from the vorticity, we need to solve the Poisson equation for the stream function. Traditional vortex methods make use of the Biot–Savart kernel, and the fact that the solution can be written as a sum over the singular point sources:

$$\mathbf{u}(\mathbf{x}) = \sum_i \mathbf{K}(\mathbf{x} - \mathbf{x}_i)\Gamma_i,$$

where $\mathbf{K}$ is the Biot–Savart kernel

$$\mathbf{K}(\mathbf{x}) = \frac{1}{2\pi}\frac{(-y, x)}{|\mathbf{x}|^2}, \quad \mathbf{x} = (x, y).$$

Due to the singularity of the Biot–Savart kernel, there has been concern about the possibility of producing unbounded velocity as two neighbouring particles approach each other. To alleviate this difficulty, Chorin (1973) and Chorin and Bernard (1973) introduced a vortex-blob method in which the singular Biot–Savart kernel is replaced by a desingularised kernel, that is,

$$\mathbf{K}_\delta(\mathbf{x}) = \mathbf{K} * \phi_\delta(\mathbf{x}),$$

where $\phi_\delta(\mathbf{x}) = \phi(\mathbf{x}/\delta)/\delta^2$ is an approximate Delta function, and $\phi(\mathbf{x})$ is its shape function. For example, we can take ϕ to be Gaussian. This modification gives a computationally more stable method than the point-vortex method. The method has been applied and extended to a variety of fluid-dynamical situations (Leonard, 1980). For smooth vorticity fields, it has been proved that the vortex-blob method converges provided that the

smoothing blob δ is much larger than the initial grid size h, see, for example, Hald (1979), Beale and Majda (1982), Anderson and Greengard (1985) and Cottet (1988) and the review paper (Hald 1991). For a long time, it has been widely believed that the point-vortex method is numerically unstable without additional regularisation. In Goodman, Hou and Lowengrub (1990), Hou and Lowengrub (1990) and Cottet, Goodman and Hou (1991), we proved a surprising result. The point-vortex method is stable and convergent with second-order accuracy for smooth vorticity fields in two and three space dimensions.

An alternative to the direct summation methods just described are grid-based methods, that work directly with the Poisson equation. The singular point-vortex distribution is approximated by a smoother grid vorticity and the elliptic equation in (4.16) is solved by a fast Poisson solver for difference methods. The grid velocity is obtained by numerical differentiation of ψ over the grid and the velocity of the point vortices is found by interpolating from the grid. Such grid-based methods are generally referred to as vortex-in-cell (or cloud-in-cell) methods, which were first introduced by Christiansen (1973). Since the velocity field is calculated from a smooth grid vorticity, vortex-in-cell methods may be considered as a type of vortex-blob method (Tryggvason, 1989). In 1987, Cottet presented a VIC method for which he was able to show convergence under similar conditions to the blob methods.

In Christiansen's original VIC method, the vorticity of the point vortices is assigned to the corners of the mesh block that each vortex is in by the so-called area–weight rule. This corresponds to giving each vortex an effective area of the order of one mesh block. Thus we may consider the VIC method as a type of vortex-blob method with blob size of the same order as the mesh size. However, since only the nearest four grid nodes are involved, vorticity is not evenly distributed to the nearest four grid nodes. The resulting blob is anisotropic, rather than symmetric, as the blobs in the vortex-blob methods. If the problem being simulated is sensitive to small-scale disturbances, this anisotropy can trigger small-scale Kelvin–Helmholtz instability. This small-scale instability has severely limited previous investigations of the effects of grid refinements (Baker, 1979). Tryggvason (1989) overcame this difficulty by making the blob slightly larger and spreading the vorticity over a larger area on the grid. By doing so, the small-scale anisotropy can be made significantly smaller. The shape function Tryggvason used is the interpolation function suggested by Peskin (1977) in a slightly different context. This conversion of the singular point vortex into a smooth grid vorticity can be viewed as approximating the δ-function by a smoother function. The smoother-shape function at the grid point (i, j) is expressed as a product of two one-dimensional functions:

$$\delta_{ij}(x, y) = \mathrm{d}(x - ih)\mathrm{d}(y - jh)$$

where

$$\mathrm{d}(r) = \begin{cases} (1/4h)(1+\cos(\pi r/2h), & \text{if } |r| < 2h \\ 0, & \text{if } |r| \geq 2h, \end{cases}$$

where h is the mesh size, and the point vortex is located at (x, y). The various aspects of this approximation are discussed in detail by Peskin (1977). Using this approximate Delta function, we approximate the vorticity field at the grid points from the vorticity field at the Lagrangian particle positions $(x_k(t), y_l(t))$ by

$$\omega(ih, jh) = \sum_{k,l} \mathrm{d}(ih - x_k(t))\mathrm{d}(jh - y_l(t))\omega(x_k(t), y_l(t))h^2.$$

Conversely, we interpolate the velocity field from the grid points to the Lagrangian particle positions by

$$\mathbf{u}(x_i(t), y_j(t)) = \sum_{k,l} \mathrm{d}(x_i(t) - kh)\mathrm{d}(y_j(t) - lh)\mathbf{u}(kh, lh)h^2.$$

This version of the VIC method has been used successfully by Tryggvason in his numerical study of the Rayleigh–Taylor instability and the vortex-sheet roll-up (Tryggvason, 1988, 1989).

In Figure 5, we present the computations of a vortex-sheet roll-up by Tryggvason (1989) using the VIC method described above. The result is compared with a similar calculation obtained using the vortex-blob method. The VIC simulation in Figure 5a was on a grid with 32 meshes per wavelength; the vortex-blob simulation in Figure 5b used 200 points and $\delta = 0.2$. The vertical dimension of the computational box in the VIC simulation was four times the horizontal one to keep the top and bottom boundaries well away from the interface. The initial conditions were

$$x_i = \mathrm{i}/N + 0.05 \sin\left(\frac{2\pi \mathrm{i}}{N}\right), \quad y_i = -0.05 \sin\left(\frac{2\pi \mathrm{i}}{N}\right),$$

which are the same as those used by Krasny (1986) except that the amplitude was five time larger. This larger amplitude was selected to allow comparisons with runs made by the original four-point VIC code. It was found that the original VIC method was very sensitive to small disturbances from the grid. These disturbances can cause the interface to roll up into more than one vortex.

In Figure 6 we demonstrate the numerical calculations (non-dimensional time equal to 1) obtained using several different methods. Figure 6a and 6b was calculated by the original four-point VIC method. In (a) 16 meshes per wavelength were used, and in (b) 32. Figure 6c and 6d was calculated by the smoother VIC method. In (c) 32 meshes per wavelength were used, and in (d) 64. Figure 6e and 6f was calculated by a vortex-blob method using the modified kernel K_δ. In (e) $\delta = 0.2$, and in (f) $\delta = 0.1$. Both runs

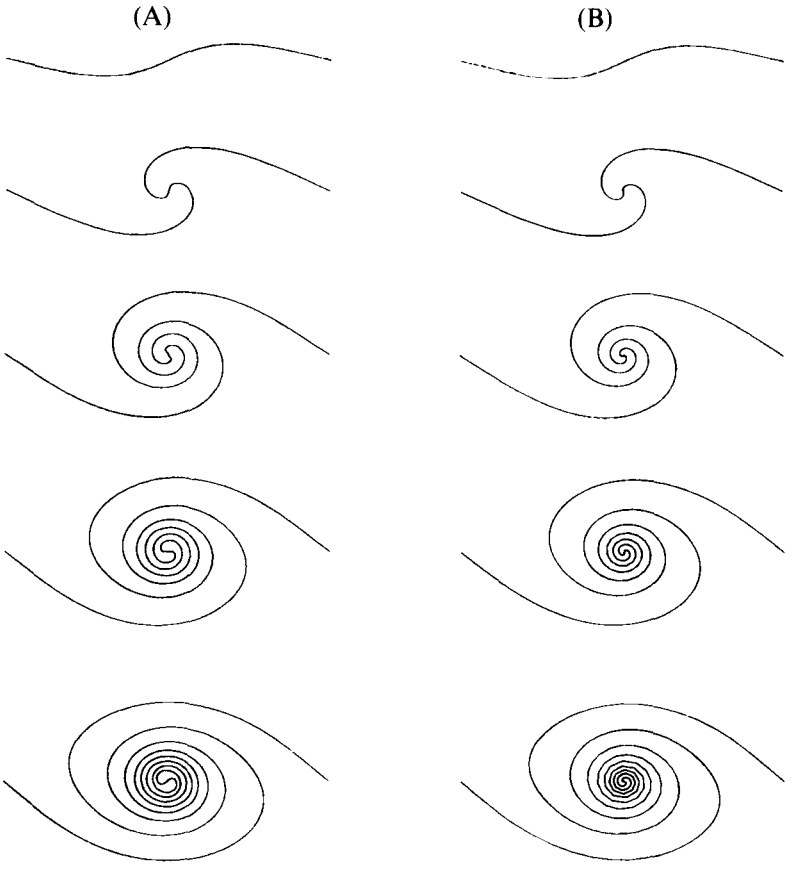

Fig. 5. The roll-up of a vortex sheet. The dimensionless times are 0.0, 0.5, 1.0, 1.5 and 2.0. (A) Calculation with an isotropic vortex-in-cell method. The grid is 32×128. (B) Calculations with a vortex-blob method with 200 points and $\delta = 0.2$. From Tryggvason (1989)

employed a sufficient number of points so that the results were independent of the resolution (in (e) $N = 200$; in (f) $N = 400$). It is evident that the smoother VIC method produces results very similar to those obtained by the vortex-blob method.

We note that several fast algorithms have been developed which give a much faster and accurate evaluation of the particle velocity in the vortex-blob methods. These do not introduce the grid-particle interpolation errors that are present in the VIC method. In (1986), Anderson introduced a fast summation algorithm based on local corrections. It has the advantage of reducing the computational cost of the direct summation without sacrificing the high-order accuracy of the vortex method. The operation count is approximately $O(M \log M) + O(N)$, where M is a constant independent

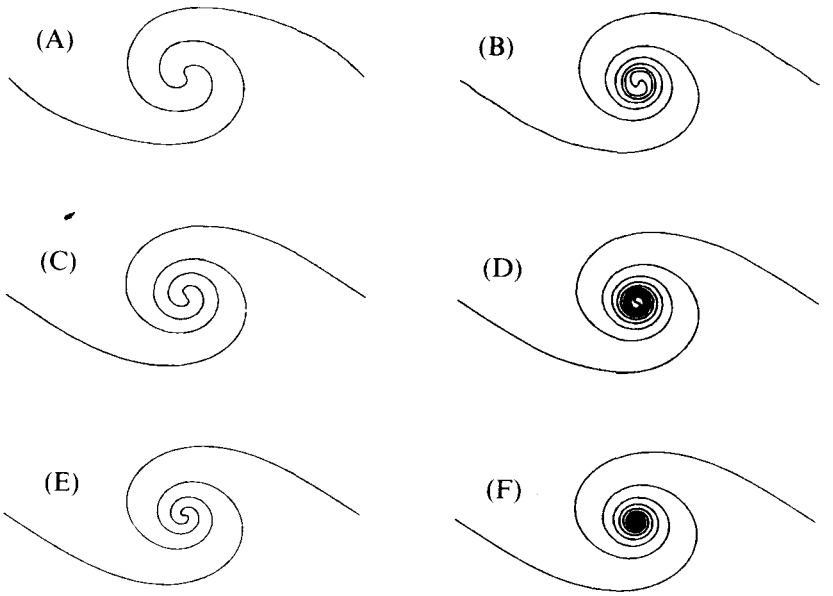

Fig. 6. The large-amplitude stage (at dimensionless time $t = 1.0$) calculated in different ways. (A) Original VIC method on a 16×64 grid. (B) Same as (A) but on a 32×128 grid. (C) Modified (isotropic) VIC method on a 32×128 grid. (D) Same as (C) but on a 64×256 grid. (E) Vortex-blob method 200 points and $\delta = 0.2$. (F) Same as (E) but with 400 points and $\delta = 0.1$. From Tryggvason (1989).

of the number of vortices. The fast multipole summation algorithm developed by Grenngard and Rokhlin (1989) has proved to be very useful. It reduced the operation count from the $O(N^2)$ for direct summation to $O(M \log M) + O(N)$, where M is a constant independent of the number of vortices. A similar fast algorithm has been proposed independently by van Dommelen and Rundensteiner (1989). A somewhat slower, but more flexible version of the fast algorithm based on Taylor expansions has been proposed recently by Draghicescu (1994). A well-vectorised version of the fast multipole algorithm has allowed vortex-method calculations with a large number of vortex particles. For example, in his study of flow past circular cylinders, Koumoutsakos (1993) has used up to $O(10^6)$ vortex particles by efficiently implementing the fast multipole algorithm for vector computer architectures. Fast algorithms have also been used in three-dimensional applications, see, for example, the work of Almgren, Buttke and Colella (1994).

5. Effect of surface tension

The surface tension at an interface between two immiscible fluids arises from the imbalance of their intermolecular cohesive forces. It is one of the most commonly used physical regularisations for interfacial flows. It is believed

that surface tension plays a central role in determining the length scales, selection mechanics and large time behaviour of interface dynamics. The understanding of the stabilising effect of surface tension will enhance our understanding of fluid phenomena such as pattern formation in Hele–Shaw cells, the motion of capillary waves on free surfaces, the formation of fluid droplets and the propagation of sound waves in a porous medium.

Surface tension has been used as a physical regularisation for the Kelvin–Helmholtz instability. With surface-tension regularisation, the interface problem is locally well posed. Pullin (1982) was the first to study the stabilising effect of surface tension for vortex sheets. Rangel and Sirignano (1988) also studied the effect of surface tension and density ratio on the nonlinear growth of the Kelvin–Helmholtz instability. Numerical calculations of fluid interfaces with surface tension are more susceptible to numerical instabilities since surface tension introduces high-order spatial derivatives into the governing equations. As in the case of water waves without surface tension, numerical stability requires a certain compatibility between the choice of quadrature rule for the singular integral and the approximation of derivative operators. Violation of this compatibility condition will lead to numerical instability.

5.1. Spatial discretisation

Here we only describe the time-continuous discretisation for general two-density interface problems. Similar discretisation applies to Hele–Shaw flows. Recall that the equations of motion for general two-density fluid interfaces are given by

$$\begin{aligned}\frac{\mathrm{d}\bar{z}}{\mathrm{d}t} &= \frac{1}{2\pi \mathrm{i}} \int \frac{\gamma(\alpha', t)}{z(\alpha, t) - z(\alpha', t)} \mathrm{d}\alpha', \\ \frac{\mathrm{d}\gamma}{\mathrm{d}t} &= -2A \left(\mathrm{Re} \left\{ \frac{\mathrm{d}^2 \bar{z}}{\mathrm{d}t^2} z_\alpha \right\} + \frac{1}{8} \partial_\alpha \left(\frac{\gamma^2}{|z_\alpha|^2} \right) + g y_\alpha \right) + \tau \kappa_\alpha,\end{aligned}$$

Define the derivative operator $D_h^{(\rho)}$ as in the case of water waves; see (3.2). Further, we discretise the singular integral by the alternating-point-trapezoidal rule. The numerical algorithm for which we can prove stability and convergence is given by

$$\frac{\mathrm{d}\bar{z}_j}{\mathrm{d}t} = \frac{1}{4\pi \mathrm{i}} \sum_{(k-j)\mathrm{odd}} \gamma_k^{(\rho)} \cot \left(\frac{z_j^{(\rho)} - z_k^{(\rho)}}{2} \right) 2h; \tag{5.1}$$

$$\frac{\mathrm{d}\gamma_j}{\mathrm{d}t} = -2A \, \mathrm{Re} \left(\frac{D_h^{(\rho)}}{4\pi \mathrm{i}} \sum_{(k-j)\mathrm{odd}} \frac{\mathrm{d}\gamma_k}{\mathrm{d}t} \cot \left(\frac{z_j^{(\rho)} - z_k^{(\rho)}}{2} \right) 2h \right) \tag{5.2}$$

$$+2A\ \mathrm{Re}\left(\frac{D_h^{(\rho)}}{4\pi \mathrm{i}}\sum_{(k-j)\mathrm{odd}}\gamma_k^{(\rho)}\sec^2\left(\frac{z_j^{(\rho)}-z_k^{(\rho)}}{2}\right)\cdot((z_j)_t-(z_k)_t)2h\right) \tag{5.3}$$

$$-\frac{A}{4}D_h^{(\rho)}\left(\frac{\gamma_j^2}{|D_h^{(\rho)}z_j|^2}\right)-2AgD_h^{(\rho)}y_j+\tau D_h^{(\rho)}\kappa_j, \tag{5.4}$$

where

$$\kappa_j=\left(D_h^{(\rho)}x_j^{(q)}(D_h^{(\rho)})^2y_j-D_h^{(\rho)}y_j^{(q)}(D_h^{(\rho)})^2x_j\right)/((D_h^{(\rho)}x_j^{(q)})^2+(D_h^{(\rho)}y_j^{(q)})^{3/2} \tag{5.5}$$

and $\hat{x}_k^{\rho}=\rho(kh)\hat{x}_k$ and $\hat{x}_k^{q}=q(kh)\hat{x}_k$, where $q(x)=\frac{\mathrm{d}}{\mathrm{d}x}(x\rho(x))$.

The use of x^q, y^q in the curvature computation is to balance the aliasing errors in the high modes due to the non-linearity of the curvature term. Its use is determined by the discrete product rule

$$D_h^{(\rho)}(f\dot{z})=fD_h^{(\rho)}\dot{z}+(D_h^{(\rho)}f)\dot{z}^q+hA_0(\dot{z}) \tag{5.6}$$

for any smooth function f. To illustrate the algorithm for a practical example, we take the second-order finite-difference derivative operator as an example. Note that $\rho(x)=\sin(x)/x$ and $q(x)=\cos(x)$ if $D_h^{(\rho)}$ corresponds to the second-order centred difference derivative. It is easy to see that

$$f_j^q=\frac{1}{2}(f_{j+1}+f_{j-1}), \tag{5.7}$$

$$D_h^{(\rho)}f_j^q=\frac{f_{j+2}-f_{j-2}}{4h}=D_{2h}^{(\rho)}f_j, \tag{5.8}$$

$$(D_h^{(\rho)})^2f_j=\frac{f_{j+2}-2f_j+f_{j-2}}{h^2}. \tag{5.9}$$

Thus, equations (5.8)–(5.9) imply that we should simply use every other grid point when discretising the curvature.

In the presence of surface tension, a higher-order norm is used to estimate the growth rate of the errors. This requires a better control of aliasing errors introduced in the approximation of the singular integrals. For finite-order derivative approximations, $\rho'(\pm\pi)\neq 0$ in general, and so the natural filtering associated with $D_h^{(\rho)}$ is not strong enough to control the aliasing errors. We will need to apply an additional filtering to achieve this result. In equations (5.2)–(5.4), we need to replace $D_h^{(\rho)}$ by $\tilde{D}_h^{(\rho)}$, where

$$\tilde{D}_h^{(\rho)}x_j=D_h^{(\rho)}x_j^s \quad\text{and}\quad \hat{x}_k^s=s(kh)\hat{x}_k \tag{5.10}$$

where s satisfies

$$|s(kh)-1|\leq C(kh)^r, s(kh)>0 \quad\text{and}\quad s(\pm\pi)=0. \tag{5.11}$$

The evaluation of the curvature remains unchanged. It is computed exactly

the same as in equation (5.5). With these modifications, we can prove the convergence of the algorithm defined by (5.1)–(5.5) (Beale, Hou and Lowengrub, to appear).

Theorem 2 Convergence with Surface Tension Assume that $z(\cdot,t)$, $\phi(\cdot,t) \in C^{m+3}[0,2\pi]$ and $\gamma(\cdot,t) \in C^{m+2}[0,2\pi]$ for $t \le T$ and $m \ge 4$. If D_h corresponds to an rth-order derivative operator, with $r \ge 4$ and $h \le h_0(T)$, then

$$\|z.(t) - z(\cdot,t)\|_{H_h^1} \le C(T)h^r, \tag{5.12}$$

$$\|\gamma.(t) - \gamma(\cdot,t)\|_{H_h^{1/2}} \le C(T)h^{r-1}, \tag{5.13}$$

where

$$\|\phi\|_{H_h^{1/2}}^2 = \sum_{|k|\le N/2} (1+|k|\rho(kh))|\hat{\phi}_k|^2 \quad \text{and} \quad \|\phi\|_{H_h^1}^2 = \|\phi\|_{l^2}^2 + \|D_h\phi\|_{l^2}^2. \tag{5.14}$$

If $D_h^{(\rho)}$ corresponds to a spectral derivative approximation, the result is the same with r replaced by m.

As we can see, there are many choices of quadrature rule and derivative rule. Also, it is not clear which term needs to be smoothed, and which term need not be smoothed. Our analysis indicates that the combination of these choices must satisfy certain compatibility conditions in order to be stable. These compatibility conditions can be determined by performing linear stability analysis around the arbitrary smooth solution of the interface. In principle, such analysis is non-trivial and could be very messy. By studying the leading-order linear singular operators and projecting them into the appropriate local coordinates, a simplified system can be derived from which stability of the numerical method becomes apparent. We note that with surface-tension regularisation, the interface is locally well-posed (Craig, 1985; Beale, Hou and Lowengrub, 1993a). The sign of gravity plays no role. The convergence result holds even if the fluid is unstably stratified.

The proof of Theorem 2 relies on an estimate of the linearised error in the curvature. Let

$$\dot{\kappa}_j = \kappa_j - \kappa(\alpha_j). \tag{5.15}$$

Using the discrete product rule and the fact that $(fg)^q = gf^q + hA_0(f)$ for any smooth g, we can show that the linear part of $\dot{\kappa}_j$ is given by

$$\dot{\kappa}_j^L = \frac{1}{s_\alpha(\alpha_j)} D_h^{(\rho)} \left[\frac{1}{s_\alpha(\alpha_j)} D_h^{(\rho)} \dot{x}_j^N \right] + A_0(\dot{x}^T) + A_0(\dot{x}^N). \tag{5.16}$$

We refer the reader to Beale, Hou and Lowengrub (to appear) for details.

Performing a linear stability analysis similar to that for water waves, we obtain

$$\frac{d\dot{\phi}}{dt} = -\frac{\gamma\sigma^2}{2} D_h^{(\rho)} \dot{\psi} + A_0(\dot{\phi} + \dot{\psi}) + A_{-1}(\dot{\Gamma}), \tag{5.17}$$

$$\frac{d\dot{\psi}}{dt} = -2\sigma D_h^{(\rho)} \dot{\Gamma} - \frac{\gamma\sigma^2}{2} D_h^{(\rho)} \dot{\phi} - A\gamma\sigma^2 D_h^{(\rho)} \dot{\phi} + A_0(\dot{\phi} + \dot{\psi}) + A_{-1}(\dot{\Gamma}), \tag{5.18}$$

$$\frac{d\dot{\Gamma}}{dt} = \tau\sigma D_h^{(\rho)} \left(\sigma \left(\frac{\gamma^2\sigma}{4\tau} - \Lambda_h \right) \dot{\psi} \right) + A_0(\dot{\phi} + \dot{\psi} + \dot{\Gamma}), \tag{5.19}$$

where $\sigma = 1/s_\alpha$ and $D_h^{(\rho)}$ and Λ_h are defined as in (3.2) and (3.9). Here $\dot{\phi}$ denotes a variant of $D_h^{(\rho)} \dot{x}^T$, $\dot{\psi}$ denotes a variant of $\Lambda_h \dot{x}^N$ and $\dot{\Gamma}$ denotes a variant of $\dot{\gamma}$. Recall that the operator Λ_h is positive, that is, $\widehat{D_{hk}^{(\rho)}} = |k|\rho(kh)$. In deriving equations (5.17)–(5.19), we have changed variables so that the coupling between $\dot{\phi}$ and $\dot{\psi}$ changes from elliptic to hyperbolic. By doing this, we have successfully put the term responsible for the Kelvin–Helmholtz instability to the third equation. It appears as $\gamma^2\sigma/4\tau$ that is added to $-\Lambda_h$. The Λ_h term represents the dispersive effect of surface tension. We can see that the dispersive regularisation dominates the destabilising term for those wavenumbers k satisfying $|k| > \max_\alpha\{\gamma^2\sigma/4\tau\}$. This observation leads to our energy estimate and convergence proof. The details are given in Beale, Hou and Lowengrub (to appear); see also Beale, Hou and Lowengrub (to appear).

We remark that the numerical approximations discussed for two-density interfaces can easily be generalised for Hele–Shaw flows and other multi-fluid interfaces.

5.2. Removing the stiffness of surface tension for interfacial flows

It turns out that it is difficult to obtain a stable and efficient time integration scheme for fluid interfaces with surface tension. If an explicit time discretisation is used, there is a severe time-step stability constraint. This constraint arises because of the presence of surface tension, and is a major obstacle to performing high-resolution, long-time numerical simulations. In this section, we present a new approach that successfully removes the high-order time-step constraint induced by surface tension. This approach was developed in detail, and demonstrated through numerical simulations, in Hou, Lowengrub, and Shelley (1994a). Using our method, it is possible to perform accurate and large time integration of fluid interfaces with surface tension. Many previously untenable problems now become possible using our approach. The application of these methods has led to the discovery of interesting new phenomena. For example, numerical calculations of the vortex-sheet roll-up with surface tension, using up to 8192 points, reveal the

late time self-intersection of the interface, which creates trapped bubbles of fluid. This is very interesting. A collision of interfaces is a singularity in the evolution, and is of a type that has not been observed previously for such flows in 2-D. We will describe this further below. Our methods have also been applied recently to problems of topological singularity formation in Hele–Shaw flows (Goldstein, Pesci and Shelley 1993) and to studies of the effect of anisotropy in quasi-static solidification (Almgren, Dai and Hakim, 1993).

By stiffness, we mean the presence of strict time-step stability constraints. The stiffness is introduced by the curvature term in the Laplace–Young boundary condition. For incompressible fluid interfaces, it is especially difficult to remove the stiffness of surface tension because the stiffness enters non-linearly and non-locally. Straightforward implicit discretisation would not work since it could be as expensive to solve for the implicit solution. By performing the frozen coefficient Fourier analysis of the interface equations, we can derive the dynamic stability constraint

$$\Delta t < C \cdot (\bar{s}_\alpha h)^{3/2}/\tau, \tag{5.20}$$

where $\bar{s}_\alpha = \min_\alpha s_\alpha$. Therefore, the stability constraint is determined by the minimum grid spacing in arclength ($\Delta s \approx h s_\alpha$), which is strongly time dependent. Our experience is that the Lagrangian motion of the points can lead to 'point clustering' and hence to very stiff systems, even for flows in which the interface is smooth and the surface tension is small. For example, in previous calculations of the motion of vortex sheets with surface tension, a fourth-order (explicit) Runge–Kutta method was used to advance the system. An adaptive time-stepping strategy was used to satisfy the stability constraint. With $N = 256$, the time step had become as small as 10^{-6}, and soon thereafter the computation became too expensive to continue. For Hele–Shaw flows the situation is even worse. A similar analysis gives the constraint

$$\Delta t < C \cdot (\bar{s}_\alpha h)^3/\tau. \tag{5.21}$$

Our approach relies on two key observations. The first is to introduce a new set of variables for which curvature can be evaluated 'linearly' through these new variables. The second observation is to factor out the leading-order singular linear operators from the non-linear and non-local system. This gives rise to a much simplified leading-order system to which standard implicit methods such as the Crank–Nicholson scheme can be trivially applied.

Our new set of dynamical variables consists of the tangent angle, θ, and arclength metric, s_α, of the interface. This is strongly motivated by the formula $\kappa = \theta_s = \theta_\alpha/s_\alpha$. Furthermore, we would like to impose α as an arclength variable. This is equivalent to imposing s_α is a function of time

alone. By doing this, we need to reparameterise the interface dynamically, which amounts to a change of frame in time by introducing a particular tangential velocity T.

Given an equation of motion of a free interface,

$$(x(\alpha,t),y(\alpha,t))_t = Un + T\hat{s},$$

where n and $\hat{s}$ are the unit local normal and tangential vectors, respectively and U and T are the local normal and tangential components of the interface velocity. Define the tangent angle θ and the arclength metric s_α as $\tan\theta = y_\alpha/x_\alpha$, $s_\alpha = \sqrt{x_\alpha^2 + y_\alpha^2}$. It is easy to derive an equivalent equation of motion for θ and s_α

$$(s_\alpha)_t = T_\alpha - \theta_\alpha U, \tag{5.22}$$

$$\theta_t = \left(\frac{1}{s_\alpha}\right)(U_\alpha + \theta_\alpha T). \tag{5.23}$$

For most interface problems of practical interest, the motion of the interface is determined only by the normal velocity. The tangential velocity would determine the frame or parameterisation of the interface, but it does not affect the shape of the interface. We will exploit this degree of freedom in choosing T to derive a simpler evolution equation for s_α and θ. Ideally, we would like to choose a frame such that the moving particles $\{(x(\alpha_j,t),y(\alpha_j,t)\}_j$ are equally spaced at all times if they are so initially. This corresponds to imposing s_α to be independent of α, varying with time only. To achieve this, we choose the tangential velocity T such that

$$T_\alpha - \theta_\alpha U = \frac{1}{2\pi}\int_0^{2\pi}(T_\alpha - \theta_\alpha U)\mathrm{d}\alpha.$$

Since T is periodic with respect to α, we get

$$T(\alpha,t) = T(0,t) + \int_0^\alpha \theta_{\alpha'} U \mathrm{d}\alpha' - \frac{\alpha}{2\pi}\int_0^{2\pi}\theta_{\alpha'} U \mathrm{d}\alpha'. \tag{5.24}$$

This expresses T entirely in terms of θ and U. The spatial constant $T(0,t)$ just gives an overall temporal shift in frame. With this choice of T, the evolution equations for θ and s_α reduce to

$$(s_\alpha)_t = -\frac{1}{2\pi}\int_0^{2\pi}\theta_\alpha U \mathrm{d}\alpha. \tag{5.25}$$

$$\theta_t = \left(\frac{1}{s_\alpha}\right)(U_\alpha + \theta_\alpha T). \tag{5.26}$$

This system should be solved, together with the evolution equations governing other dynamical variables, such as vortex-sheet strength, velocity potential, etc. This is a complete reformulation of the evolution problem. Once we obtain s_α and θ in time, we can recover the interface position (x,y)

by an integration (up to a constant of integration). This formulation of plane curve motion is not new. See, for example, Strain (1989) in the context of unstable solidification.

Next we would like to factor out the leading-order linear singular operators in the evolution equations. To illustrate the idea, we take vortex sheets with surface tension as an example. It is important to note that the time-step stability constraint is a result of high-order derivative and singular operators. They enter only at small spatial scales or high-frequency components of the solution. Thus it is essential to single out the leading singular operators and high-order derivative terms, and treat these terms implicitly. Although the Birkhkoff–Rott equation is highly non-linear and non-local, its leading-order approximation at small scales is extremely simple. It can be expressed in terms of the Hilbert transform. With some manipulation, we find that for a vortex-sheet flow with surface tension, the normal velocity U behaves at small scales as

$$U \sim \frac{1}{2}\left(\frac{2\pi}{L}\right)\mathcal{H}[\gamma],$$

while for γ,

$$\gamma_t \sim \tau\kappa_\alpha.$$

It is worth noting that the Hilbert transform is diagonalisable under the Fourier transform. Now we can recompose the equations of motion to a form suitable for applying implicit time-integration methods. We will separate the leading-order singular operators from the smoother and lower-order operators. The leading-order terms dominate at small scales, and will be treated implicitly. The smoother and lower-order terms are non-linear and non-local. We will treat them explicitly. There is no stiffness in the equation for s_α since only the space-averaged quantity enters the equation. The stiffness of the system is in the coupling of the θ and γ equations. The recomposed system for θ and γ is given by

$$\theta_t = \left(\frac{1}{2s_\alpha^2}\right)\mathcal{H}[\gamma_\alpha] + P, \tag{5.27}$$

$$\gamma_t = \left(\frac{\tau}{2s_\alpha}\right)\theta_{\alpha\alpha} + Q. \tag{5.28}$$

The first term in each equation is the leading-order term, dominant at small scales. P and Q represent the smoother and lower-order terms. They are obtained by subtracting off the leading-order terms from the right-hand sides of the θ and γ equations respectively. We term this form of the equations of evolution *Small Scale Decomposition* (SSD). It is the leading terms that introduce the stiffness into the system. These leading terms diagonalise under the Fourier transform, and can be treated implicitly

very easily. A very similar, and simpler, recomposition can be found for Hele–Shaw flows.

A stable second-order integration can be obtained by discretising the leading-order stiff terms implicitly using a Crank–Nicholson discretisation, and leap-frogging on the non-linear terms. To simplify the notation, we denote $2\pi s_\alpha$ by $L(t)$. It is the total arclength of the interface. In Fourier space, this gives

$$\frac{\hat{\theta}^{n+1} - \hat{\theta}^{n-1}}{2\Delta t} = \frac{|k|}{4}\left(\left(\frac{2\pi}{L^{n+1}}\right)^2 \hat{\gamma}^{n+1} + \left(\frac{2\pi}{L^{n-1}}\right)^2 \hat{\gamma}^{n-1}\right) + \hat{P}^n(k), \quad (5.29)$$

$$\frac{\hat{\gamma}^{n+1} - \hat{\gamma}^{n-1}}{2\Delta t} = -\frac{\tau}{2}k^2\left(\frac{2\pi}{L^{n+1}}\hat{\theta}^{n+1} + \frac{2\pi}{L^{n-1}}\hat{\theta}^{n-1}\right) + \hat{Q}^n(k). \quad (5.30)$$

Given L^{n+1}, $\hat{\theta}^{n+1}(k)$ and $\hat{\gamma}^{n+1}(k)$ can be found explicitly by inverting a 2×2 matrix. By using an explicit method to integrate L (a non-stiff ODE), L^{n+1} is found before updating θ and γ. At most, a first-order CFL condition must be satisfied because of transport terms in the θ and γ evolutions. And indeed, numerical simulations of the fully non-linear flow show no high-order time-step constraint from the surface tension, but do reveal a first-order CFL constraint. Further details on implementation are found in Hou, Lowengrub and Shelley (1994). Recently, we have been able to prove convergence of the above reformulated boundary-integral method for general two-density interface problems with surface tension (Ciniceros and Hou, to appear). This includes Hele–Shaw flows and water waves.

A fourth-order implicit discretisation

We can also design a fourth-order implicit multistep discretisation in time. Motivated by the work of Ascher, Ruuth and Wetton (to appear), we propose the following fourth-order implicit discretisation in time:

$$\begin{aligned}
(25/12)\hat{\theta}^{n+1} &- 4\hat{\theta}^n + 3\hat{\theta}^{n-1} - (4/3)\hat{\theta}^{n-2} + (1/4)\hat{\theta}^{n-3} \\
&= \Delta t\left(\frac{|k|}{2}\left(\frac{2\pi}{L^{n+1}}\right)^2 \hat{\gamma}^{n+1} + 4\hat{P}^n(k)\right. \\
&\quad \left. - 6\,\hat{P}^{n-1}(k) + 4\hat{P}^{n-2}(k) - \hat{P}^{n-3}(k)\right) \\
(25/12)\hat{\gamma}^{n+1} &- 4\hat{\gamma}^n + 3\hat{\gamma}^{n-1} - (4/3)\hat{\gamma}^{n-2} + (1/4)\hat{\gamma}^{n-3} \\
&= \Delta t\left(-\tau k^2 \frac{2\pi}{L^{n+1}}\hat{\theta}^{n+1} + 4\hat{Q}^n(k)\right. \\
&\quad \left. - 6\,\hat{Q}^{n-1}(k) + 4\hat{Q}^{n-2}(k) - \hat{Q}^{n-3}(k)\right).
\end{aligned}$$

We have tested this fourth-order version of implicit discretisation. It indeed gave a fourth-order convergence with a CFL stability constraint which is about half of that in the second-order Crank–Nicholson discretisation

(Hou, Lowengrub and Shelley, to appear). The improved order of accuracy in time is very important for large time integration of free interfaces. And it is especially useful in our study of the formation of topological singularities; see; Hou, Lowengrub and Shelley (to appear).

We would like to emphasise that the equal arclength frame we described above is one convenient choice. This choice leads to a constant coefficient system to the leading order which makes the inversion explicit by using the fast Fourier transform. But there are other situations where we may want to choose a non-equal arclength frame that is adapted to the local property of the interface. For example, we may want to cluster computational particles near a singular region. This can be carried out in a similar way. In this case, the implicit solutions become a variable coefficient problem, which can be solved by some iterative methods such as the preconditioned conjugate gradient method. We refer to Hou, Lowengrub and Shelley (1994; to appear) for more discussions of the formulation and implementation issues.

5.3. Numerical examples

In this section, we present some very interesting numerical simulations that serve to demonstrate the utility of the SSD. The numerical methods are based on the Crank–Nicholson discretisation discussed above. This yields a stable, second-order in time, infinite-order in space discretisation. We are interested in understanding the competing effects of surface tension and the Kelvin–Helmholtz instability on the motion of a vortex sheet. In our calculation, $\tau = 0.005$, with the initial condition

$$x_0(\alpha) = \alpha + 0.01 \sin 2\pi\alpha, y_0(\alpha) = -0.01 \sin 2\pi\alpha, \gamma_0(\alpha) = 1. \tag{5.31}$$

This initial data was used by Krasny (1986a,b) in the absence of surface tension to study singularity formation through the Kelvin–Helmholtz instability. In the case of zero surface tension, a curvature singularity was shown to occur at the centre ($\alpha = 1/2$) at $t \approx 0.375$. With $\tau = 0.005$, the linear dispersion analysis gives approximately 16 linearly growing modes above $k = 0$. Modes higher than 16 are all linearly stable and are dispersively regularised by surface tension.

Figure 7 shows a sequence of interface positions, starting from the initial condition (Figure 7A). At early times, the interface steepens and behaves similarly to the zero-surface-tension case. However, it passes smoothly through the $\tau = 0$ singularity time, and becomes vertical at the centre at $t \approx 0.45$. At about this time, dispersive waves are generated at the centre and propagate outwards. By $t = 0.6$ (Figure 7B) the interface has rolled over and has begun to roll-up into a spiral. However, at later times (see Figure 7C and D), sections of interface within the inner turns of the spiral appear to be attracted towards one another, and in the process appear to

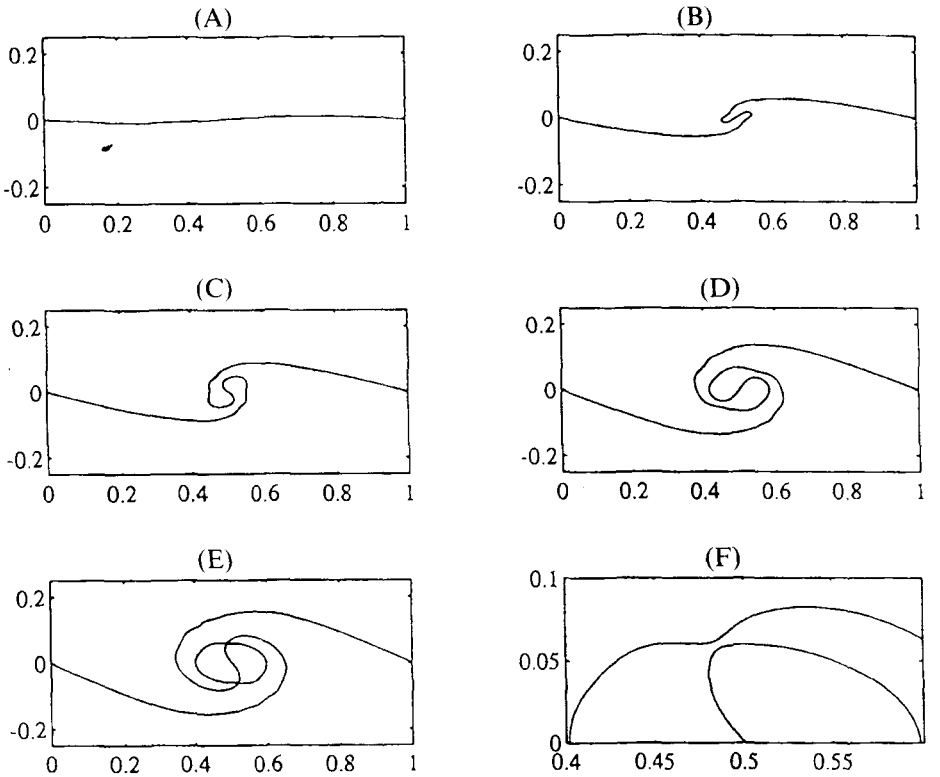

Fig. 7. Point-vortex-method solution of vortex sheets with surface tension, $\tau = 0.005, N = 1024, \Delta t = 1.25 \times 10^{-4}$. (A) $t = 0$; (B) $t = 0.6$; (C) $t = 0.8$; (D) $t = 1.2$; (E) $t = 1.4$; (F) close-up of top pinching region, $t = 1.4$. From Hou, Lowengrub and Shelley (1994)

pinch off interior 'bubbles' of fluid (see Figure 7E). A close-up of the pinch region is shown in Figure 7F.

These sections of interface in the pinching region appear to collide at a finite time. Figure 8 shows the minimum distance between the two sections of interface in the pinching region as a function of time for several spatial and temporal resolutions. Figure 8B shows that the total energy is conserved up to 6-digit accuracy very close to the time of pinching for $N \leq 2048$. This figure suggests strongly that the pinching occurs at a finite time. Moreover, the width apparently vanishes with infinite slope, which indicates that the pinching rate intensifies as the width narrows.

We remark that this apparent singularity is of a completely different type from that of the $\tau = 0$ singularity. This singularity is a *topological singularity*. Beyond the pinching singularity, change in the topology of the flow may occur. More fundamentally, with $\tau = 0$ the singularity occurs

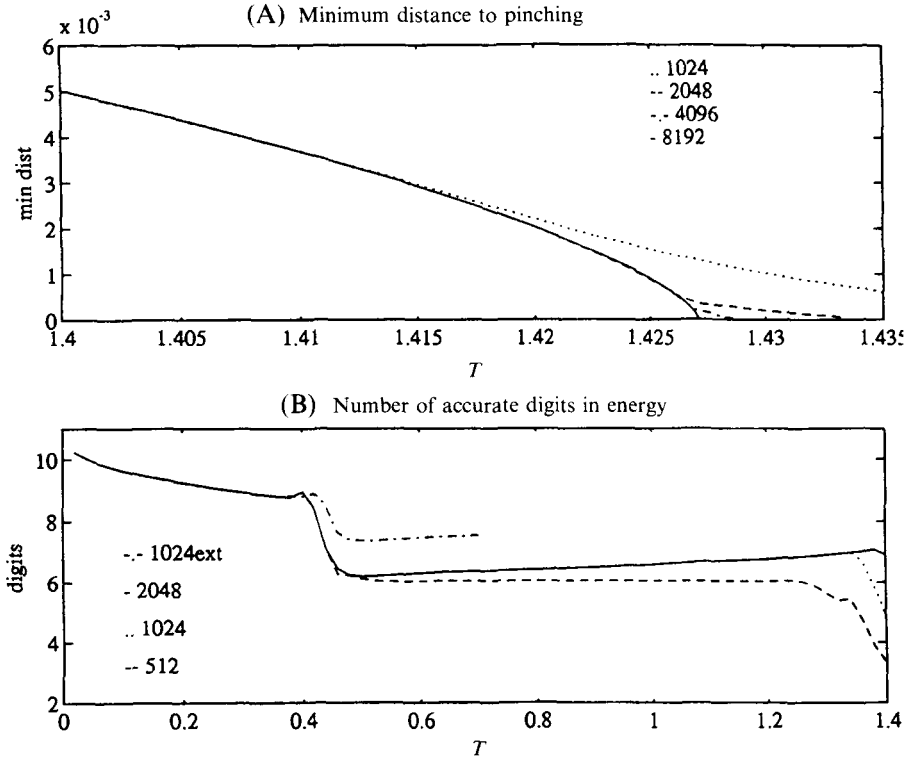

Fig. 8. Pinching in, and accuracy in the energy of, the inertial vortex sheet: (A) minimum width of the top pinching region, $\tau = 0.005$, $N = 1024$ with $\Delta t = 2.5 \times 10^{-4}$, $N = 2048$ with $\Delta t = 1.25 \times 10^{-4}$, $N = 4096$ with $\Delta t = 6.25 \times 10^{-5}$, $N = 8192$ with $\Delta t = 3.125 \times 10^{-5}$; (B) number of accurate digits in the energy, τ 0.005, $N = 512, N = 1024, N = 2048$ with $\Delta t = 1.25 \times 10^{-4}$, and $N = 1024$ with $\Delta t = 3.125 \times 10^{-5}$(1024ext). From Hou, Lowengrub and Shelley (1994).

through a rapid *compression* of vorticity along the sheet at a single isolated point (Moore, 1979; Krasny, 1986; Baker and Shelley, 1990; Shelley, 1992). Here the singularity occurs through a rapid *production* of vorticity that is associated with the surface tension. And indeed, the maximum vortex-sheet strength appears to diverge at the singularity time, unlike the $\tau = 0$ case. Further details, physical interpretation and modelling are given in Hou, Lowengrub and Shelley (1994) and Hou, Lowengrub and Shelley (to appear).

The second example we consider is the expanding bubble. This is a calculation of a gas bubble expanding into a Hele–Shaw fluid; see Figure 9. The dynamics of expanding bubbles in the radial geometry have attracted a great deal of attention due to the formation of striking patterns observed in experiments. In our set-up, the viscosity inside the bubble is set to zero, but

the viscosity outside the bubble is equal to 1. Therefore, there is a viscosity contrast $A_\mu = 1$. Thus the γ equation now reads

$$\gamma = -2A_\mu s_\alpha U^T + \tau\kappa_\alpha,$$

where U^T is the tangential velocity component of the interface velocity (u, v). In this case, γ is defined implicitly through an integral relation. An iterative scheme is needed to solve for γ. The initial condition is given by

$$(x_0(\alpha), y_0(\alpha)) = r(\alpha)(\cos\alpha, \sin\alpha),$$
$$\text{with } r(\alpha) = 1 + 0.1\sin 2\alpha + 0.1\cos\ 3\alpha.$$

See the innermost curve in Figure 9. This choice of initial condition is to avoid particular symmetry in the initial interface. The value of surface tension is $\tau = 0.001$, the time step is $\Delta t = 0.001$ and $N = 4096$. Figure 9 shows the expansion of this bubble from $t = 0$ to $t = 20$, printed at unit intervals of time. We can see that the interface develops oscillations in the moving front, and subsequently produces many fingers and pedals as time evolves. These petals expand outwards and eventually tip-split into two petals. This process repeats itself. In performing this calculation, we have done a careful resolution study. This calculation agrees very well with lower-resolution calculations. It is quite remarkable that we can now use such a large time step $\Delta t = 0.001$ for $N = 4096$. Without the new formulation, the time step would have been at least one thousand times smaller to achieve stability for an explicit method.

5.4. A note on computing beyond the singularity time

Topological changes or formation of singularities in free interfaces occur in many physical applications. For example , in crystal growth and thin-film growth, an initial smooth front can develop cusps and crack-like singularities, and isolated islands of film material can merge (Gray, Chisholm and Kaplan, 1993; Sethian, 1985; Snyder *et al.*, 1991; Spencer, Vorhees and Davis, 1991). Computing beyond the singularity time using front tracking methods is usually very difficult and complicated. Local grid surgery is required to reconnect the Lagrangian particles near the singularity region; see, for example, Unverdi and Tryggvason (1992). Also, how we reconnect the interfaces may affect the solution at later times. So it would be highly desirable to develop a more systematic framework for boundary-integral methods to compute beyond the (topological) singularity time. In the next section, we will discuss front capturing methods based on the level-set approach. But here we would like to exploit further what we can do within the framework of boundary-integral methods.

Here we propose a new approach to continue our boundary-integral calculation beyond the topological singularity. This borrows ideas from the

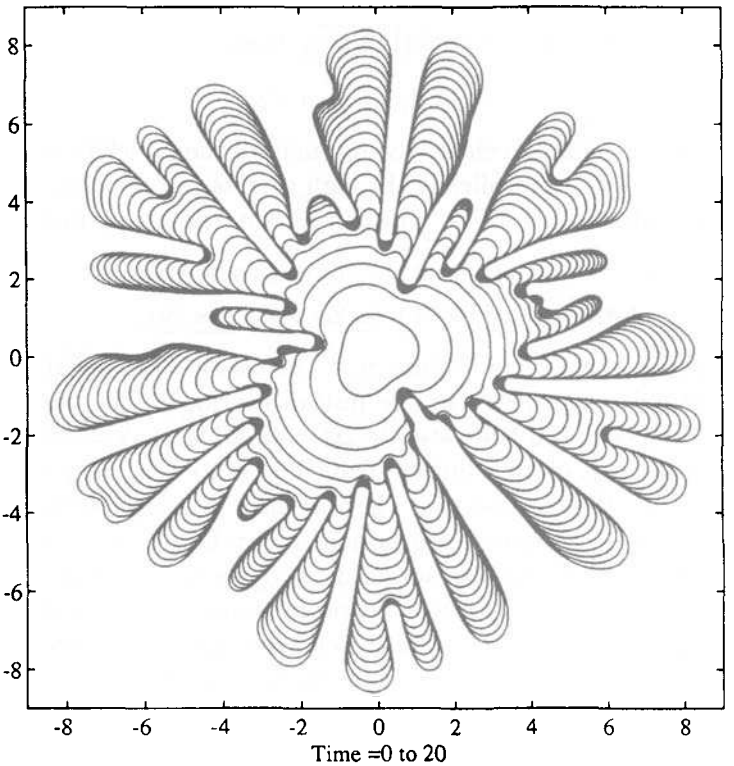

Fig. 9. An expanding Hele–Shaw bubble. $N = 4096, \Delta t = 0.001, \tau = 0.001$, $t = 0, 1, 2, \ldots, 20$. From Hou, Lowengrub and Shelley (1994).

level-set approach (see the next section). The idea is to use curvature regularisation, as has been successfully used for the level-set approach. By curvature regularisation, we mean that we add to the normal velocity component a term proportional to the local mean curvature, that is, $U' = U + \epsilon\kappa$. Here U is the normal component of the interface velocity, κ is the (mean) curvature and U' is the regularised normal velocity. We are interested in studying the limiting solution as $\epsilon \to 0^+$, beyond the singularity time.

To illustrate the idea, we take the example of motion by mean curvature. The normal velocity is given by $U = 1 + \epsilon\kappa$, where κ is local curvature. In the limit of $\epsilon = 0$, the equal arclength frame would choose a tangential velocity $T = \theta$. With this choice of T, our reformulated system of equations for θ and s_α becomes a variant of the viscous Burgers equation:

$$(s_\alpha)_t = 1 - \epsilon(\theta_\alpha)^2/s_\alpha, \tag{5.32}$$

$$\theta_t = \frac{\theta\theta_\alpha}{s_\alpha} + \frac{\epsilon}{s_\alpha}\left(\frac{\theta_\alpha}{s_\alpha}\right)_\alpha. \tag{5.33}$$

In the limit of $\epsilon = 0$, the θ equation becomes the inviscid Burgers equation, and s_α becomes constant (positive) in space. Now it is clear that a cusp or topological singularity corresponds to a shock discontinuity in the tangent angle. It is well known that an entropy condition is required to select the physical weak solution beyond the time a shock discontinuity is formed. For positive ϵ, the curvature regularisation plays exactly the same role as the viscosity regularisation. Thus using an upwinding scheme or high-order Godonov scheme for computing θ would give the correct continuation beyond the singularity. By applying curvature regularisation to a free surface directly, we do not need to introduce one extra space dimension as in the level-set approach. More accurate numerical methods can be designed since we only deal with the free surface and don't have to differentiate across the free surface. Also, the stiffness can be removed easily using our reformulated system.

We have used our formulation to reproduce some of the calculations presented in Osher and Sethian (1988) using the level-set formulation. We obtained the same results for computations of the cusp and corner singularities. In Figure 10, we plot the evolution of a sinusoidal initial condition propagating with unit normal velocity. The initial condition is given by $x(\alpha, 0) = \alpha, y(\alpha, 0) = -0.05 \sin(2\pi\alpha)$. $N = 128$, and an upwinding scheme was used to integrate the θ equation in time. Since the curve propagates into itself with unit normal velocity, a corner singularity is formed at later times. It is clear that applying an upwinding scheme to our reformulated system produced the entropy-satisfying continuation beyond the singularity time.

Merging of interfaces can also be handled similarly. We can determine accurately the time of merging by monitoring the minimum distance between the two interfaces, as we did for the vortex-sheet calculation. At the time of merging, we need to reparameterise the merged interface. This can be done by combining the original parameterisation of the two interfaces. For the merged interface, there is a jump discontinuity for θ at the point of contact. This will generate a cusp or corner singularity after the merging of the two interfaces. But using the curvature regularisation described above, the reformulated method can capture the cusp or corner singularities with no additional effort. And the entropy condition is satisfied automatically. Apparently, this idea can be applied to water waves, interaction of fluid bubbles and droplet formation. Detailed description and computational results will be presented elsewhere (Hou and Osher, 1994). Generalisation of this idea to three space dimensional problems is our active on-going research.

We would like to emphasise that curvature regularisation is a geometric (or topological) regularisation. It is frame-independent, and consequently it is an intrinsic regularisation. It has an important property of preserving the index of a curve. As a consequence, a curve cannot cross itself under the curvature regularisation. Of course, if we use curvature regularisation in the

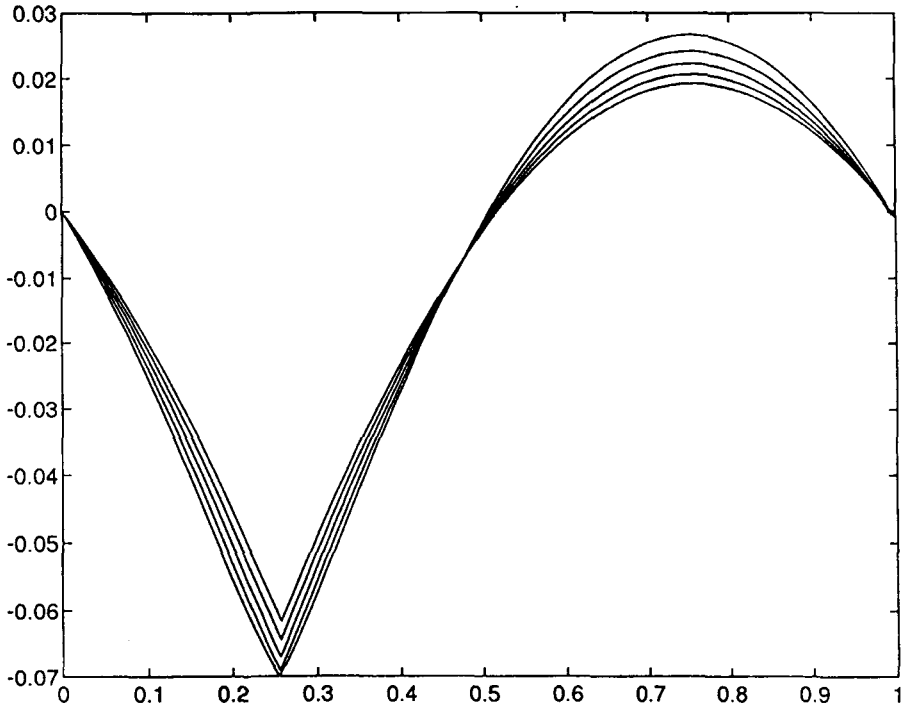

Fig. 10. Motion by mean curvature using reformulated front tracking method with curvature regularisation. The normal velocity $U = 1$. The initial condition is $x = \alpha, y = 0.05\sin(2\pi\alpha)$. $N = 128$. The upwinding scheme was used to integrate in time. From Hou and Osher (1994)

original Lagrangian frame, the differential point clustering of particles will result in a very stiff system to solve. So it is essential to apply curvature regularisation to our reformulated system in which an equal arclength frame is imposed dynamically. The curvature regularisation can also be used to regularise ill-posed problems. Using the point-vortex method approximation with curvature regularisation, we can compute beyond the Kelvin–Helmholtz singularity, and obtain a roll-up solution of vortex sheets. But it is more effective if a small vortex blob of the order of the mesh size is used. In Figure 11A, we present our vortex-sheet calculation using the point-vortex method and the curvature regularisation. The same initial condition as Krasny's was used. The curvature regularisation coefficient is 0.01. The solution is plotted at $t = 1.24$ with $N = 256$. This clearly gives a vortex-sheet roll-up solution. But it seems to require more resolutions to compute further in time. In Figure 11B, we present the same vortex-sheet calculation using a small blob. The blob size is equal to 0.01. The vortex-sheet positions at three different times are shown in Fig. 11B, with $N = 512$. The solutions

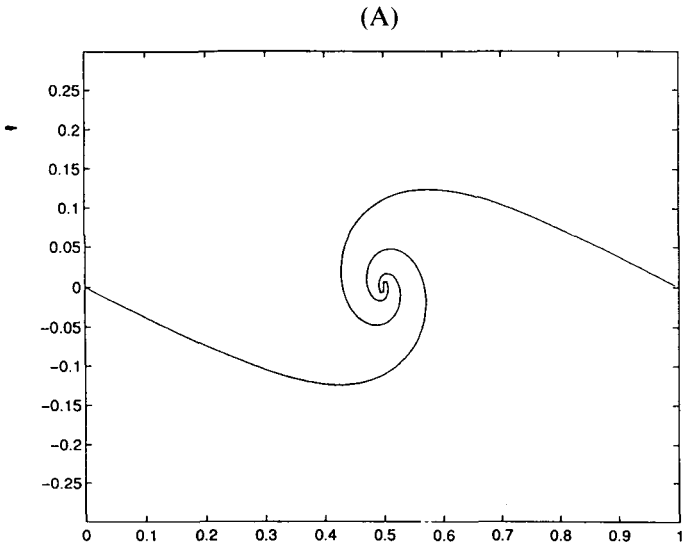

Fig. 11A. Vortex-sheet roll-up calculation using the point-vortex method and the curvature regularisation. The same initial condition as Krasny's was used. The curvature regularisation coefficient is 0.01. The solution is plotted at $t = 1.24$. $N = 256$. From Hou and Osher (1994).

are very similar to those obtained by Krasny using vortex-blob calculations with larger blobs. By using the curvature regularisation, it is possible to study the limiting solution as the regularisation parameters tend to zero simultaneously with the mesh size.

Curvature regularisation introduces a *dissipative* regularisation for the θ equation with respect to the *arclength variable*. It is important that such dissipative regularisation is with respect to the arclength variable. If we naïvely add a dissipative regularisation in the original Lagrangian frame α, the result is quite different. Such Lagrangian regularisation would allow interface self-crossing, producing a non-physical continuation beyond the Kelvin–Helmholtz singularity time (Hou and Osher, 1994).

6. The Level-Set Approach

The level-set approach is an effective front capturing method for computing free surfaces. It was originally introduced by Osher and Sethian in 1988. The basic idea is to consider the free surface as a zeroth-level set of some smooth function which is defined in one higher space dimension than the free surface. So advancing the free surface is reduced to advancing the level-set function. Since only the zeroth-level set is physically relevant to the free surface, there is a lot of freedom in advancing the level-set function away from the zeroth-level set. Such freedom can be exploited to design a

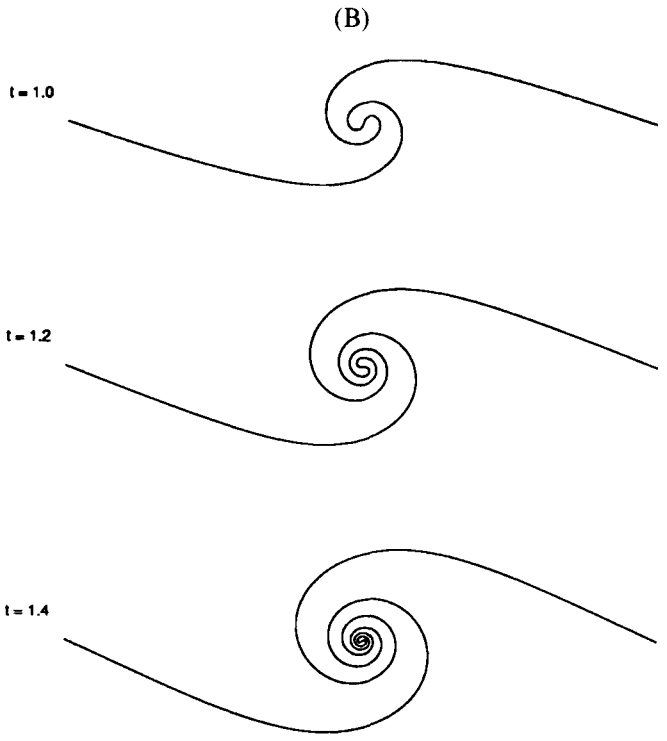

Fig. 11B. Vortex-sheet roll-up calculation using the curvature regularisation with a small vortex blob. The same initial condition as Krasny's was used. The curvature regularisation coefficient and the blob size are equal to 0.01. $N = 512$. The solutions are plotted at $t = 1.0, 1.2, 1.4$. The frame dimension of each plot is $0 \leq x \leq 1, -4 \leq y \leq 0.4$. From Hou and Osher (1994).

smooth level-set function throughout the numerical computation. Thus, a free surface may develop a topological singularity such as a cusp, a corner or merging of two surfaces; the level-set function remains relatively smooth (the level-set function is Lipschitz continuous at the singularity of the interface). Moreover, the level-set function satisfies a Hamilton–Jacobi-type equation, and curvature regularisation corresponds to an entropy condition. Therefore, high-order Godonov methods developed for hyperbolic conservation laws can be used to compute the level-set function. Unlike the front tracking approach, no special effort is required at the interface singularity. The interface is recovered at the end of the computation by locating the zeroth-level set. Generalisation to three space dimensional problems requires no additional effort.

In this section, we describe the level-set algorithm for propagating a curve or union of curves $\Gamma(t)$. We assume that the motions of these curves are completely determined by the normal velocity, V. Let B be a fixed domain

which contains the union of curves in all times of interest. The main idea is to construct a function $\phi(x,t)$ defined on B, such that the level set $\{\phi = 0\}$ corresponds to the moving curves $\Gamma(t)$, that is,

$$\Gamma(t) = \{x : \phi(x,t) = 0\}.$$

We now derive a partial differential equation for ϕ, which holds on $B \times [0,T]$. First, we need to construct a smooth extension of the normal velocity, V, of the curves to the entire domain of B such that

$$F(x,t) = V(x,t) \quad \text{for} \quad x \in \Gamma(t).$$

Now consider the motion of an arbitrary level set $\{\phi(\mathbf{x},t) = C\}$. We will follow the derivation of Osher and Sethian (1988). Let $\mathbf{x}(\alpha,t)$ be the Lagrangian trajectory of this level-set. This implies that

$$\phi(\mathbf{x}(\alpha,t),t) = C.$$

Differentiating the above relation with respect to time, we get

$$\phi_t + \frac{\partial \mathbf{x}}{\partial t} \cdot \nabla\phi = 0.$$

Note that $\nabla\phi$ is normal to the level set $\{\phi(\mathbf{x},t) = C\}$, and $\frac{\partial \mathbf{x}}{\partial t} \cdot n = F$, where $n = \nabla\phi/|\nabla\phi|$ is the unit normal vector to the level set $\phi = C$. This consideration implies that the evolution equation for the level-set function ϕ is given by

$$\phi_t + F|\nabla\phi| = 0, \tag{6.1}$$

$$\phi(x,0) = \text{given}. \tag{6.2}$$

Equation (6.1) yields the motion of $\Gamma(t)$ with normal velocity V on the level set $\phi = 0$. We refer to equation (6.1) as the level-set 'Hamilton–Jacobi' formulation.

One essential property of the level-set function is that it always remains a function, even if the free surface (corresponding to $\phi = 0$) changes topology, breaks, merges or forms sharp corners. Parameterisations of the boundary become multivalued or singular in these cases. Furthermore, since the level-set formulation is completely Eulerian, finite-difference approximations over a fixed grid may be used to discretise the equation in space and time. Thus, there is no need to explicitly track the free surface during a numerical calculation. The free surface is recovered only at the end of the computation.

To illustrate, suppose we wish to follow an initial curve $\Gamma(t=0)$ propagating with normal velocity $V = 1 - \epsilon\kappa$, where κ is the local curvature of the boundary. The curvature of the level curve passing through a point (x,y,t) is given by

$$\kappa = \nabla \cdot \left(\frac{\nabla\phi}{|\nabla\phi|} \right) = -\frac{\phi_y^2\phi_{xx} - 2\phi_x\phi_y\phi_{xy} + \phi_x^2\phi_{yy}}{(\phi_x^2 + \phi_y^2)^{3/2}}.$$

The minus sign occurs because we have initialised the surface so that $\nabla\phi$ points inwards and we want κ to be positive for a circle. The smooth extension of V to F is straightforward, and equation (6.1) becomes

$$\phi_t + (\phi_x^2 + \phi_y^2)^{1/2} = \epsilon\nabla \cdot \left(\frac{\nabla\phi}{|\nabla\phi|}\right)$$
$$\phi(x, y, t = 0) = \pm\text{distance from } (x, y) \text{ to } \Gamma(t = 0).$$

As shown in Sethian (1985), for $\epsilon > 0$, the parabolic right-hand side diffuses sharp gradients and forces ϕ to stay smooth for all time. This is not true for $\epsilon = 0$ and $F = 1$. A corner singularity must develop in time.

Thus the goal is to produce approximations to the spatial derivative that (1) do not smooth sharp corners artificially and (2) pick up the correct entropy solution when singularities develop. The schemes are motivated by the fact (Osher and Sethian 1988) that the entropy condition for propagating boundaries is identical to the one for hyperbolic conservation laws, where stable, consistent, entropy-satisfying algorithms have a rich history.

In discretising the term $F|\nabla\phi|$, we decompose F into two components:

$$F = F_A + F_G.$$

Here, F_A is an advection term containing that part of the velocity that is independent of the moving boundary, and F_G contains those terms that depend on the geometric properties of the boundary, such as the curvature and normal. We begin by splitting the influence of F, and rewrite the equation for ϕ as

$$\phi_t = -(F_A|\nabla\phi| + F_G|\nabla\phi|).$$

In two space dimensions, one can easily devise an iterative type of scheme based on dimension-by-dimension splitting (Osher and Sethian, 1988; Osher and Shu, 1991):

$$\phi_{ij}^{n+1} = \phi_{ij}^n - F_A\Delta t(\max(D_x^-\phi_{ij}, 0))^2(\min(D_x^+\phi_{ij}, 0))^2$$
$$+(\max(D_y^-\phi_{ij}, 0))^2(\min(D_y^+\phi_{ij}, 0))^2 - \Delta t F_G|\nabla\phi|.$$

Here we have not approximated the final term $F_G|\nabla\phi|$; one may use a straightforward centred difference approximation to this term. This is the first-order multi-dimensional algorithm described in Osher and Sethian (1988). High-order schemes have also been derived, see Osher and Shu (1991). In Figure 12 we show this technique applied to the case of a star propagating outwards with speed $F = 1$, $\Delta t = 0.01$, and a mesh size of 50 points in each direction in a box. The cusp singularities were captured properly. The curve became circular as it evolved (Osher and Sethian, 1988).

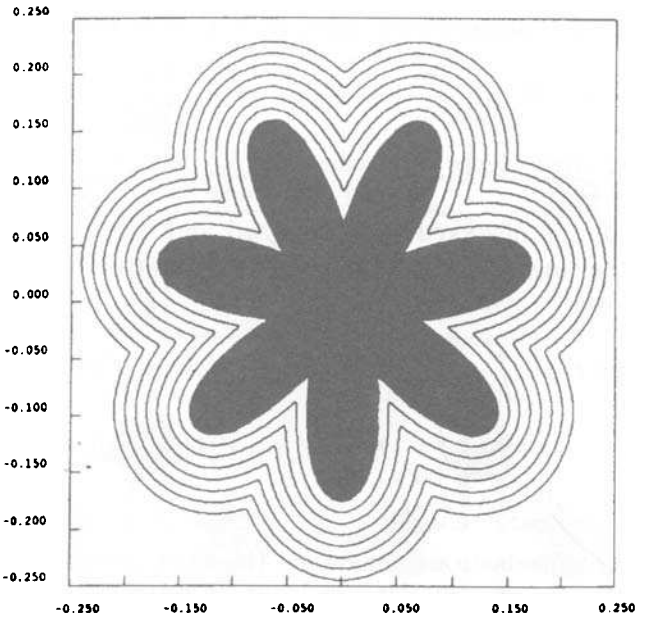

Fig. 12. Expanding star, $F(\kappa) = 1$, $t = 0.0, 0.7(0.01)$. $N = 50$. From Osher and Sethian (1988).

6.1. *Crystal growth and solidification*

We have described the boundary-integral formulation in Subsection 2.4. Here we describe how to extend the velocity V to a globally defined speed function F. Such an extension is needed to use the level-set formulation. What we will describe below is contained in the paper by Sethian and Strain (1992).

The most natural extension makes direct use of the integral equation

$$\epsilon_\kappa \kappa + \epsilon_V V + U + H \int_0^t \int_{\Gamma(t')} K(x, x', t - t') V(x', t') \mathrm{d}x' \mathrm{d}t' = 0, \quad (6.3)$$

for $x \in \Gamma(t)$. Each term in (6.3) can be evaluated anywhere in B, once V is known on $\Gamma(t')$ for $0 \leq t' \leq t$ and ϕ is known on B. Thus, given the set $\Gamma(t)$, plus all its previous positions and velocities for $0 \leq t' \leq t$, one could first solve an integral equation to find the velocity V for all points on $\Gamma(t)$ and then find $F(x, t)$ by solving the equation

$$\epsilon_\kappa \kappa(x, t) + \epsilon_V F(x, t) + U(x, t) + H \int_0^t \int_{\Gamma(t')} K(x, x', t - t') V(x', t') \mathrm{d}x' \mathrm{d}t' = 0,$$

for F throughout B. The curvature away from $\Gamma(t)$ is evaluated by

$$\kappa = \nabla \cdot \left(\frac{\nabla \phi}{|\nabla \phi|} \right) = \nabla \cdot n, \quad n = \frac{\nabla \phi}{|\nabla \phi|}.$$

These expressions make sense everywhere in B. This defines the extension of V away from $\Gamma(t)$.

Furthermore, it was observed by Greengard and Strain (1990) that one can decompose the single-layer potential into a history part $S_\delta V$ and a local part $S_L V$ as follows:

$$\begin{aligned} SV(x,t) &= \int_0^{t-\delta} \int_{\Gamma(t')} K(x,x',t-t')V(x',t')\mathrm{d}x'\mathrm{d}t' \\ &+ \int_{t-\delta}^{t} \int_{\Gamma(t')} K(x,x',t-t')V(x',t')\mathrm{d}x'\mathrm{d}t' \\ &\equiv S_\delta V + S_L V. \end{aligned}$$

Here δ is a small regularisation parameter. Heuristically, we try to separate the local part, which is causing the jump in the normal derivative of the potential, from the history part, which is smooth and independent of current velocity. It was shown (Sethian and Strain, 1992; Greengard and Strain, 1990) that the local part $S_L V$ can be approximated by

$$S_L V(x,t) = \sqrt{\delta/\pi} V(x,T) + O(\delta^{3/2}),$$

at point x on $\Gamma(t)$. The history part $S_\delta V$ depends only on values of V at times t' bounded away from the current time, $t' \leq t - \delta$. This is a smooth function. A fast summation method has been developed to evaluate the history part efficiently, requiring only $O(M^2)$ calculations per time step. Finite-difference approximations can also be used to obtain a fast evaluation of the history part; see Brattkus and Meiron (1992). Now we can define the extended velocity F explicitly through the history part of the single-layer potential:

$$F = \frac{-1}{\epsilon_V(n) + H\sqrt{\delta/\pi}} [\epsilon_\kappa \kappa + U + H S_L V].$$

We have reduced the equation of motion, with an $O(\delta^{3/2})$ error, to a pair of equations on fixed domain B:

$$\begin{aligned} &\phi_t + F|\nabla \phi| = 0, \\ &F = \frac{-1}{\epsilon_V(n) + H\sqrt{\delta/\pi}} [\epsilon_\kappa \kappa + U + H S_L V]. \end{aligned}$$

Numerical approximation of these coupled equations gives rise to a robust algorithm which can handle topological singularities, cusps, and corners.

In Figure 13, we plot a sequence of fingered growth under mesh refinement

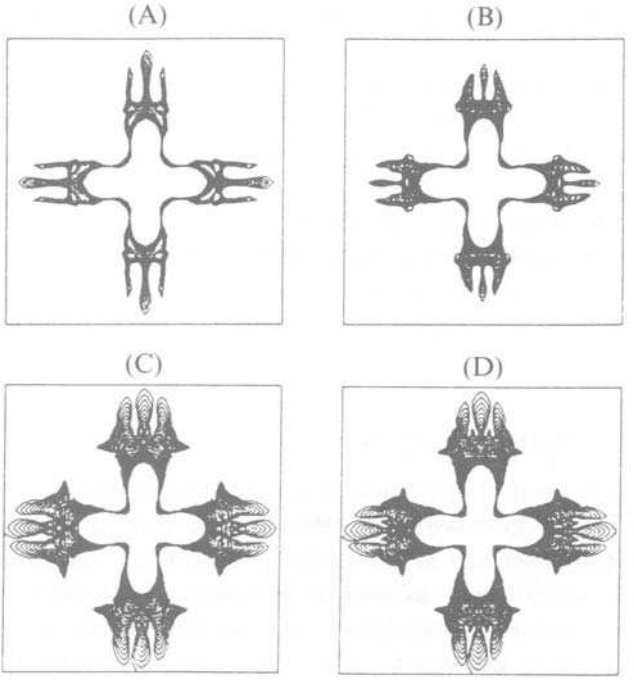

Fig. 13. Fingered crystal: effect of refining both grid size and time step, $H = 1, A = 0, \epsilon_\kappa = 0.001, \epsilon_V = 0.001, k_A = 0$: (A) 32×32 mesh, $\Delta t = 0.005$; (B) 48×48 mesh, $\Delta t = 0.005$; (C) 96×96 mesh, $\Delta t = 0.001\,25$; (D) 128×128 mesh, $\Delta t = 0.00125$. From Sethian and Strain (1992).

(Sethian and Strain, 1992). Here the physical parameters were specified as follows: $\epsilon_V = 0.001, \epsilon_\kappa = 0.001, H = 1$. There was no anisotropy in the coefficient, and the constant undercooling was set to be -1. In Figure 13A, a 32×32 grid was used with $\Delta t = 0.005$. In Figure 13B, a 48×48 grid was used with $\Delta t = 0.005$. In Figure 13C, a 96×96 grid was used with $\Delta t = 0.001\,25$. In Figure 13D, a 128×128 grid was used with $\Delta t = 0.001\,25$. On the coarsest mesh (32×32), only the gross features of the fingering and tip-splitting process are seen. As the numerical parameters are refined, the basic pattern emerges. It is clear that the resulting shapes are qualitatively the same, and there is little qualitative difference between Figure 13c and Figure 13d. We refer to Sethian and Strain (1992) for more details.

One disadvantage of this approach is that computing the normal velocity at each time step requires solving the boundary-integral problem. So it is not a completely Eulerian formulation. Since the boundary-integral problem is history dependent and the integration is non-local in space, it is usually very expensive. Even using the fast algorithm for heat potentials developed by Greengard and Strain (1990), numerical calculations by this

approach are still slower compared with finite-difference approximations for the heat equation. Recently, Osher and his co-workers (private communication) have developed a completely Eulerian level-set formulation to compute solidification problems. The method is in principle as fast as standard finite-difference methods for the heat equation. The preliminary results seem to be very encouraging.

Numerical study of unstable solidification has been a very active research area in the past decade. Other numerical studies of solidification problems include the works of Meiron (1986), Kessler and Levine (1986), Langer (1980), Karma (1986), Voorhees *et al.* (1988), Almgren (1993), Bratkkus and Meiron (1992), Greenbaum *et al.* (1993).

6.2. Level-set formulation for incompressible-fluid surfaces

We have described a number of boundary-integral methods for computing fluid interfaces in previous sections. We can see that they are very effective as long as the interface stays smooth. However, when the interface develops pinching singularity, as seen in Subsection 5.2, corners and topological changes, boundary-integral methods are difficult to compute beyond time singularities. Here we would like to present a level-set formulation for incompressible-fluid interfaces with discontinuous densities and viscosities. Detailed derivation can be found in Chang *et al.* (to appear). Here we just present the result in our reformulation.

The equations governing the motion of an unsteady, viscous, incompressible, immiscible two-fluid system are the Navier–Stokes equations. In conservation form, the equations are

$$\rho(\mathbf{u}_t + \nabla \cdot (\mathbf{uu})) = -\nabla p + \rho \mathbf{g} + \nabla \cdot (2\mu \mathbf{D}),$$

where $\mathbf{u}$ is velocity and ρ and μ are discontinuous density and viscosity fields respectively. $\mathbf{D}$ is the rate-of-deformation tensor whose components are $D_{ij} = \frac{1}{2}(u_{i,j} + u_{j,i})$. The density and viscosity are purely convected by the fluid velocity:

$$\frac{\partial}{\partial t}(\rho) + \nabla \cdot (\mathbf{u}\rho) = 0,$$

$$\frac{\partial}{\partial t}(\mu) + \nabla \cdot (\mathbf{u}\mu) = 0.$$

These equations are coupled to the incompressibility condition

$$\nabla \cdot \mathbf{u} = 0.$$

Denote the stress tensor by $\sigma(\mathbf{x})$, which is given by

$$\sigma(\mathbf{x}) = -p\mathbf{I} + 2\mu \mathbf{D},$$

where $\mathbf{I}$ is the identity matrix, $\mathbf{D}$ is the deformation tensor and p is the pressure. We let Γ denote the fluid interface. The effect of surface tension is to balance the jump of the normal stress along the fluid interface. This gives rise to a free-boundary condition for the discontinuity of the normal stress across Γ

$$[\sigma_{ij} n_j] \mid_\Gamma = \tau \kappa n_i, \tag{6.4}$$

where $[p]$ denotes the jump of p across the interface, κ is the curvature of Γ, τ is the surface-tension coefficient and $\mathbf{n}$ is a unit outward normal vector along Γ. Note that in the case of inviscid flows, the above jump condition is reduced to

$$[p] \mid_\Gamma = \tau \kappa. \tag{6.5}$$

In this case, the effect of surface tension is to introduce a discontinuity in pressure across the interface proportional to the (mean) curvature.

Our level-set formulation is based on the following observation. The effect of surface tension can be expressed in terms of a singular source function that is defined by our level-set function. This is similar in spirit to Peskin's formulation for the immersed boundary-value problem for blood flows through a heart valve (Peskin, 1977); see also Unverdi and Tryggvason (1992). Let us denote by ϕ the level-set function. The fluid interface Γ corresponds to the zero-level set of ϕ. In Chang *et al.* (to appear), we derived a completely Eulerian level-set formulation for multi-fluid interface problems with surface tension. The evolution equations are given by

$$\rho(\mathbf{u}_t + \nabla \cdot \mathbf{uu}) = -\nabla p + \rho \mathbf{g} + \nabla \cdot (2\mu \mathbf{D}) + \tau \kappa(\phi) \nabla \phi \delta(\phi), \tag{6.6}$$

$$\frac{\partial}{\partial t} \phi + \mathbf{u} \cdot \nabla \phi = 0, \tag{6.7}$$

where $\delta(\phi)$ is a one-dimensional Dirac Delta function and ϕ is chosen in such way that $\nabla \phi$ is in the outward normal direction when evaluated on Γ. The curvature $\kappa(\phi)$ can be expressed by ϕ and its derivatives

$$\kappa(\phi) = -\frac{\phi_y^2 \phi_{xx} - 2\phi_x \phi_y \phi_{xy} + \phi_x^2 \phi_{yy}}{(\phi_x^2 + \phi_y^2)^{\frac{3}{2}}}. \tag{6.8}$$

Our level-set formulation was partially motivated by the work of Unverdi and Tryggvason (1992). The work of Unverdi and Tryggvason was formulated as a vortex-in-cell method. The free surface is tracked explicitly by following the Lagrangian markers of the free surface. A fixed underlying grid is used to invert the Poisson equation. The interface velocity is obtained by grid/particle interpolation, in the same way as we described in the previous section on the VIC method. But in this semi-Lagrangian formulation, the coupling between the Delta function source term and the momentum equations is *non-local*. If $\mathbf{x}(s,t)$ is a parameterisation of the fluid inter-

face Γ, with s being the *arclength* variable and t being the time variable, and $\delta(\mathbf{x})$ is the two-dimensional Dirac Delta function, then the momentum equations become

$$\rho(\mathbf{u}_t + \nabla \cdot (\mathbf{uu})) = -\nabla p + \rho \mathbf{g} + \nabla \cdot (2\mu \mathbf{D}) + \int_\Gamma \tau \kappa(\mathbf{x}(s,t)) \delta(\mathbf{x} - \mathbf{x}(s,t)) \mathbf{n} ds. \tag{6.9}$$

Note that the singular source term is a 2-D Delta function and it is non-local. This is in contrast with the local and 1-D Delta function source term. In fact, equation (6.9) was not derived explicitly in Unverdi and Tryggvason (1992). It was based on our derivation of the level-set reformulation that we gave an independent derivation of (6.9). Also, consistency of equation (6.9) with the original interface problem requires s to be an arclength variable. Since $\mathbf{x}(s,t)$ is advected by the fluid velocity, s will not remain as an arclength variable even if it is so chosen initially. Therefore, if a Lagrangian variable α is used to parameterise the interface, that is, $\mathbf{x}(\alpha, t)$, then a factor $|\mathbf{x}_\alpha|$ should be added on to the integration with respect to α. This point was not clearly stated before, and it caused some confusion in the literature.

After the completion of our work on the level-set formulation, the work of Brackbill, Kothe and Zemach (1992) was brought to our attention. They have derived a continuum method for modelling surface tension for multi-fluid flows which is almost the same as our formulation if we replace the Dirac Delta function by a regularised one. Brackbill *et al.* used a 'colour' function to describe the smoothed interface. The colour function changes continuously in the transition region of finite thickness. Brackhill *et al.*'s derivation was based on a physical argument.

We now describe how to discretise the level-set formulation. Assume that we have chosen the initial level-set function such that $\phi < 0$ defines region 1 of the fluid, and $\phi > 0$ defines region 2. Further, we assume that ρ_1 and ρ_2 are the constant densities in region 1 and region 2, respectively, and μ_1 and μ_2 are the constant viscosities in region 1 and region 2 respectively. Then we have $\rho = \rho_1 + (\rho_2 - \rho_1)H(\phi)$, where H is the Heaviside function that satisfies $H(x) = 1$ for $x > 0$ and $H(x) = 0$ for $x < 0$. Similarly, we have $\mu = \mu_1 + (\mu_2 - \mu_1)H(\phi)$. In numerical computations, we approximate H by a regularised Heaviside function, and approximate δ by a regularised Delta function, just as in Peskin (1977). The regularised Delta function $\delta_\epsilon(x)$ has support in $\{|x| \leq \epsilon\}$. Typically, we choose $\epsilon = 4h$ in our calculations.

The evolution equations can be solved by a projection method. In its most basic form, the projection method requires the solution of advection–diffusion equations, which are then projected onto the space of divergence-free vector fields. The projection uses the Hodge decomposition which states that any vector $\mathbf{V}$ can be uniquely decomposed into a divergence-free field $\mathbf{V}_d$ and a gradient field ∇p, that is, $\mathbf{V} = \mathbf{V}_d + \nabla p$. Moreover $\mathbf{V}_d$ is or-

thogonal to the gradient field. For more detailed descriptions of projection methods and their applications, we refer to Chorin (1968) and Bell, Colella and Glaz (1989) and the review paper by Gresho and Sani (1987). For our problem, density is not a constant in the entire domain. A modification of the standard projection method is required. A second-order projection method for variable density has been introduced by Bell and Marcus (1992), and it has been applied successfully to a number of interesting multi-fluid interface problems.

From the evolution equations (6.7), we have $\mathbf{u}_t = L\mathbf{u} - \nabla p/\rho$. As in Bell and Marcus (1992), we introduce a density-weighted inner product such that we can decompose $\mathbf{V}$ into $\mathbf{V}_d$ and $\nabla p/\rho$. In the density-weighted norm, $\mathbf{V}_d$ is orthogonal to ∇p. Given a vector $\mathbf{V}$, we define our projection operator as $\mathbf{P}_d(\mathbf{V}) = \mathbf{V}_d$. Since the Hodge decomposition is unique and $\mathbf{u}_t$ is divergence free, we have $\mathbf{u}_t = \mathbf{P}_d(L\mathbf{u})$. In order to compute the projection, we take the divergence of both sides of the equation $\mathbf{V} = \mathbf{V}_d + \nabla p/\rho$ to obtain

$$\nabla \cdot \left(\frac{1}{\rho}\nabla p\right) = \nabla \cdot \mathbf{V}.$$

The orthogonality condition implies the boundary condition $\partial p/\partial n = 0$ on the boundary. Another way to compute the projection is to take the curl of both sides of the equation $\mathbf{V} = \mathbf{V}_d + \nabla p/\rho$. This also gives a variable elliptic problem for p with a different boundary condition. We refer to Bell and Marcus (1992) for more detailed discussions.

The convection terms can be approximated by high-order ENO schemes Harten *et al.* (1987) or by other high-order Godunov schemes. Apparently, our level-set formulation works for both two-dimensional and three-dimensional problems. There are no additional complications to extend the method to three-dimensional problems.

To obtain an effective method, it is important to keep the level-set function as smooth as possible at all times. For this reason, it is desirable to keep the level-set function as a signed distance function from the moving surface. This also ensures that the regularised surface has a finite thickness of order ϵ for all time. However, even if we initialise the level-set function ϕ as a signed distance from the free surface, the level-set function in general will not remain a distance function at later times. In Sussman, Smereka and Osher (to appear), an iterative procedure was proposed to reinitialise the level-set function at each time step so that the reinitialised level-set function remains a distance function from the front. Specifically, given a level-set function, ϕ_0, at time t, solve for the steady-state solution of the equation

$$\begin{aligned} \frac{\partial}{\partial t}\phi &= \operatorname{sgn}(\phi_0)(1 - |\nabla\phi|), \\ \phi(\mathbf{x}, 0) &= \phi_0(\mathbf{x}), \end{aligned}$$

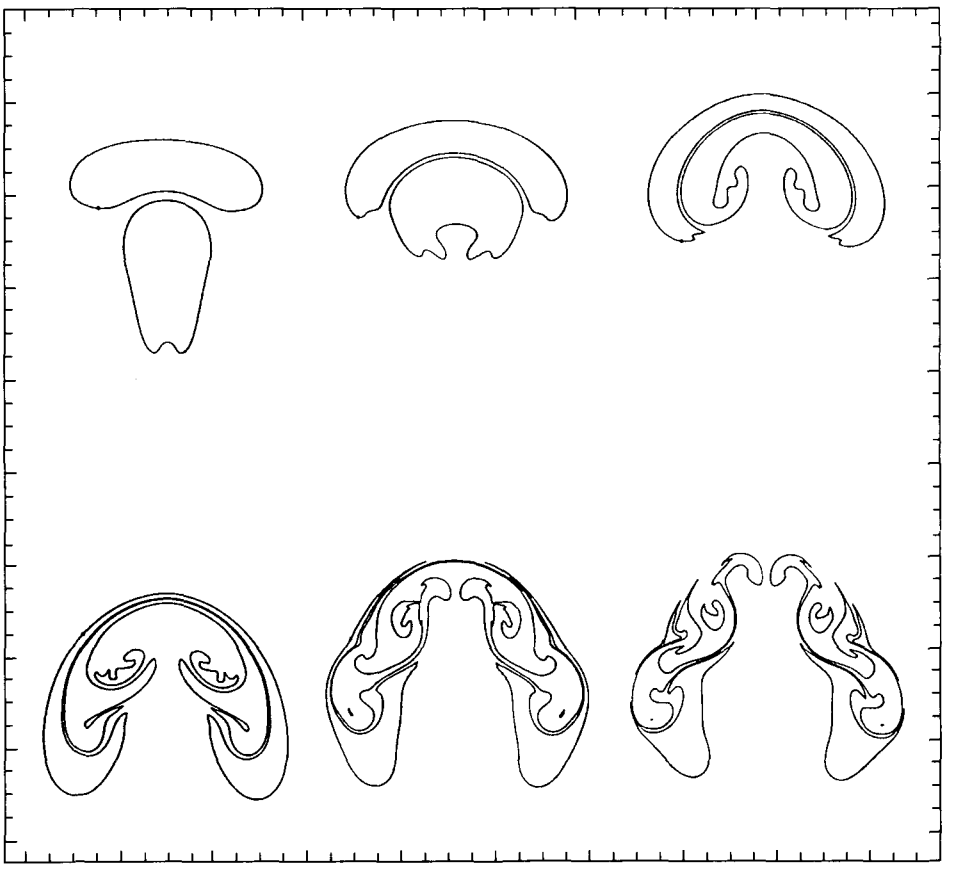

Fig. 14. Fourth-order difference approximations for two-fluid bubbles with different densities. The density ratio is 1:60:3600, with the bottom bubble being the lightest. The viscosity is equal to 0.000 125 in all fluids. $t = 0.1, 0.15, 0.2$ for the first row ($N = 256$), and $t = 0.275, 0.325, 0.35$ for the second row ($N = 512$). From Chang *et al.* (to appear).

where sgn is the sign function. The solution ϕ has the same zero-level set as ϕ_0, and satisfies $|\nabla\phi| = 1$, and so is a distance function for the front. It was found in Sussman, Smereka and Osher (to appear) that such reinitialisation is crucial in maintaining the accuracy of large-time integrations, especially when the density ratio between the two fluids is large. In Sussman, Smereka and Osher, the motion of bubbles in water and falling water drops in air were studied numerically using our level-set formulation, together with the reinitialisation procedure described above. The density ratio is 1 to 1000. The numerical results were in good agreement with some experimental results.

In Figure 14, we illustrate the method by considering the interaction of

two fluid bubbles with different densities using 256×256 grid points. The density for the bubble on the top is 60, the density for the bubble on the bottom is 1 and the background density is 3600. The initial interfaces of the bubbles are elliptical in shape. A Bousinesqu approximation was used in these calculations. We assume that viscosities are the same in all fluids and are equal to 0.000 125. The problem is set up in such a way that both bubbles rise in time and the bottom bubble rises the fastest. As the bottom bubble rises in time, we see that the top portions of the bubble interfaces are almost in contact. But they cannot merge into a single bubble in this case because the densities are different for these two bubbles. In this calculation, we labelled the two interfaces with two different level-set values. That is, Γ_1 corresponds to $\phi = c_1$ and Γ_2 corresponds to $\phi = c_2$, with $c_1 \neq c_2$. In the mean time, the bubble in the bottom develops a roll-up. We plot the solutions at $t = 0.1, 0.15, 0.2, 0.275, 0.325, 0.35$. We increase our numerical resolutions to 512×512 for times larger than $t = 0.2$. Part of the interface that has rolled up pinches off before $t = 0.275$; two smaller bubbles are detached from the bottom bubble, and have their own dynamics. As the region between the top portions of two bubbles becomes thinner and thinner in time, they eventually pinch off at $t = 0.325$ and $t = 0.35$ respectively. In the process, many small-scale structures are produced due to the unstable stratification of the fluids.

REFERENCES

A. Almgren, T. Buttke and P. Colella (1994), 'A fast adaptive vortex method in 3 dimensions', *J. Comp. Phys.*, **113**, 117–200.

R. Almgren (1993), 'Variational algorithms and pattern-formation in dendritic solidification', *J. Comp. Phys.*, **106**, 337–354.

R. Almgren, W.-S. Dai and V. Hakim (1993), 'Scaling behaviour in anisotropic Hele–Shaw flow', *Phys. Rev. Lett.*, **71**, 3461–3464.

C. Anderson (1985), 'A vortex method for flows with slight density variations', *J. Comp. Phys.*, **61**, 417–444.

C. Anderson (1986), 'A method of local corrections for computing the velocity due to a distribution of virtex blobs', *J. Comp. Phys.*, **62**, 111–123.

C. Anderson and C. Greengard (1985), 'On vortex methods', *SIAM J. Numer. Anal.*, **22**, 413–440.

U. Ascher, S Ruuth and B. Wetton, 'Implicit–explicit methods for time-dependent PDE's', to appear in *SIAM J. Numer. Anal.*

G. Baker (1979), 'The 'cloud-in-cell' technique applied to the roll-up of vortex sheets', *J. Comp. Phys.*, **31**, 76–95.

G. Baker (1983), Generalized vortex methods for free-surface flows, in *Waves on Fluid Interfaces*, (R. E. Meyer, ed.), Academic Press pp. 53–81.

G. Baker, R. Caflisch and M. Siegal, 'Singularity formation during the Rayleigh–Taylor instability', to appear *J. Fluid Mech.*

G. Baker, D. Meiron and S. Orszag (1982), 'Generalized vortex methods for free-surface flow problems', *J. Fluid Mech.*, **123**, 477–501.

G. R. Baker and M. J. Shelley (1990), 'On the connection between thin vortex layers and vortex sheets', *J. Fluid Mech.*, **215**, 161–194.

G. Baker and A. Nachbin, 'Stable methods for vortex sheet motion in the presence of surface tension', to appear in *J. Comp. Phys.*

J. T. Beale and A. Majda (1982), 'Vortex methods, I: Convergence in three dimensions', *Math. Comp.*, **32**, 1–27.

J. T. Beale, T. Y. Hou and J. S. Lowengrub (1993a), 'Growth rates for the linear motion of fluid interfaces far from equilibrium', *Comm. Pure Appl. Math.*, **46**, 1269–1301.

J. T. Beale, T. Y. Hou and J. S. Lowengrub, 'Convergence of a boundary integral method for water waves', to appear in *SIAM J. Num. Anal.*

J. T. Beale, T. Y. Hou and J. S. Lowengrub (1993b), On the well-posedness of two fluid interfacial flows with surface tension, *Singularities in Fluids, Plasmas and Optics*, (eds. R. C. Caflisch and G. C. Papanicolaou), Kluwer Academic, London, pp. 11–38.

J. T. Beale, T. Y. Hou, J. Lowengrub and M. Shelley, 'Spatial and temperal stability issues for interfacial flows with surface tension', to appear in *J. Math. Computer Modelling*, Vol. 20, No. 10/11, pp. 1–27, 1994.

J. T. Beale, T. Y. Hou and J. S. Lowengrub, Two Fuid Flows with Surface Tension, Part 1: Growth Rates of the Linearized Motion Far From Equilibrium; Part 2: Convergence of Boundary Integral Methods, in preparation, Applied Math., Caltech.

J. B. Bell, P. Colella and H. M. Glaz (1989), 'A 2nd order projection method for the incompressible Navier–Stokes equations', *J. Comp. Phys.*, **85**, 257–283.

J. B. Bell and D. L. Marcus (1992), 'A second-order projection method for variable-density flows', *J. Comp. Phys.*, **101**, 334–348

M. Benamar and Y. Pomeau (1986), 'Theory of dendritic growth in a weakly undercooled melt', *Europhys. Lett.*, **2**, 307–314.

A. L. Bertozzi and P. Constantin (1993), 'Global regularity for vortex patches, *Comm. Math. Phys.*', **152**, 19–28.

G. Birkhoff (1962), 'Helmholtz and Taylor instability', in *Proc. Symp. Appl. Math.*, **13**, 55–76, Vol. XIII, Publ. American Math. Society, Providence, R.I.

J. U. Brackbill, D. B. Kothe and C. Zemach (1992), 'A continuum method modeling surface tension', *J. Comp. Phys.*, **100**, 335–354.

K. Brattkus and D. I. Meiron (1992), 'Numerical simulation of unsteady crystal growth', *SIAM J. Appl. Math.*, **52**, 1303–1320.

T. F. Buttke (1989), 'The observation of singularities in the boundary of patches of constant vorticity', *Phys. Fluids A*, **1**, 1283–1285.

R. Caflisch and O. Orellana (1988), 'Long time existence for a slightly perturbed vortex sheet', *Comm. Pure Appl. Math.*, **39**, 807–838.

R. Caflisch and O. Orellana (1989), 'Singularity solutions and ill-posedness for the evolution of vortex sheets', *SIAM J. Math. Anal.*, **20**, 293–307.

R. Caflisch and J. Lowengrub (1989), 'Convergence of the vortex method for vortex sheets', *SIAM J. Numer. Anal.*, **26**, 1060–1080.

R. Caflisch, X. Li and M. Shelley (1993), 'The collapse of an axisymmetrical, swirling vortex sheet', *Nonlinearity*, **6**, 843–867

R. Caflisch, N. Ercolani, T. Y. Hou and Y. Landis (1993), 'Multi-valued solutions and branch point singularities for nonlinear and elliptic systems', *Comm Pure Appl Math.*, **46**, 453–499.

R. Caflisch, T. Y. Hou and J. Lowengrub (1994), Almost Optimal Convergence of the Point Vortex Method for Vortex Sheets Using Numerical Filtering, preprint, Dept of Math., Univ. of Minnesota, submitted to *Math. Comput.*

G. Gaginalp and P. C. Fife (1988), 'Dynamics of layered interfaces arising from phase boundaries', *SIAM J. Appl. Math.*, **48**, 506–518.

J. Chadam and P. Ortoleva (1983), 'The stabilizing effect of surface tension on the development of the free-boundary in a planar, one-dimensional, Cauchy–Stefan problem', *IMA J. Appl. Math.*, **30**, 57–66.

Y. C. Chang, T. Y. Hou, B. Merriman and S. Osher, 'Eularian capturing methods based on a level set formulation for incompressible fluid interfaces', to appear in *J. Comp. Phys.*

H. Ceniceros and T. Y. Hou, Convergence of a Non-stiff Boundary Integral Method for Interfacial Flows with Surface Tension, preprint, Applied Math., Caltech.

J.-Y. Chemin (1993), 'Presistency of geometric structures in bidimensional incompressible fluids', *Ann. Sci. EC*, **26**, 517–542.

D. L. Chopp (1993), 'Computing minimal surfaces via level set curvature flow,' *J. Comp. Phys.*, **106**, 77–91.

A. Chorin (1968), 'Numerical solution of the Navier–Stokes equations', *Math. Comput.*, **22**, 745–762.

A. Chorin (1973), 'Numerical study of slightly viscous flow', *J. Fluid Mech.*, **57**, 785–796.

A. Chorin and P. S. Bernard (1973), 'Discretization of a vortex sheet, with an example of roll-up', *J. Comp. Phys.*, **13**, 423–429.

J. P. Christiansen (1973), 'Numerical simulation of hydrodynamics by the method of point vortices', *J. Comp. Phys.*, **13**, 363–379.

P. Constantin, P. D. Lax and A. Majda (1985), 'A simple one dimensional model for the three dimensional vorticity equations', *Comm. Pure Appl. Math.*, **38**, 715–724.

P. Colella and P. R. Woodward (1984), 'The piecewise parabolic method (PPM) for gas dynamical simulations', *J. Comp. Phys.*, **54**, 174–201.

G. H. Cottet (1988), 'On the convergence of vortex methods in two and three dimensions', *Ann. Insti. H. Poincaré*, **5**, 641–672.

G. H. Cottet, J. Goodman and T. Y. Hou (1991), 'Convergence of the grid free point vortex method for the 3-D Euler equations', *SIAM J. Numer. Anal.*, **28**, 291–307.

G. H. Cottet (1987), 'Convergence of a vortex in cell method for the two-dimensional Euler equations', *Math. Comp.*, **49**, 407–425.

W. Craig (1985), 'An existence theory for water waves and the Bousinesq and the Kortewegde–de Vries scaling limits', *Comm. Partial Diff. Eqns.*, **10**, 787–1003.

W. Craig and C. Sulem (1993), 'Numerical simulation of Gravity Waves, *J. Comp. Phys.*', **108**, 78–83.

W. J. A. Dahm, C. E. Frieler and G. Tryggvason (1992), 'Vortex structure and dynamics in near field of a coaxial jet', *J. Fluid Mech.*, **241**, 371–402.

W.-S. Dai and M. J. Shelley (1993), 'A numerical study of the effect of surface tension and noise on an expanding Hele–Shaw bubble', *Phys. Fluids A*, **5(9)**, 2131–2146.

J.-M. Delort (1991), 'Existence de nappes de tourbillon en dimension deux', *J. Amer. Math. Soc.*, **4**, 553–586.

R. DiPerna and A. Majda (1987a), 'Concentration in regularizations for 2-D incompressible flow', *Comm. Pure Appl. Math.*, **40**, 301–345.

R. DiPerna and A. Majda (1987b), 'Oscillations and concentrations in weak solutions of the incompressible fluid equations', *Comm. Math. Phys.*, **108**, 667–689.

J. W. Dold (1992), 'An efficient surface-integral algorithm applied to unsteady gravity waves', *J. Comp. Phys.*, **103**, 90–115.

D. G. Dommermuth and D. K. P. Yue (1987), 'A high order spectral method for the study of nonlinear gravity waves'. *J. Fluid Mech.*, **184**, 267–288.

C. I. Draghicescu (1994), 'An efficient implementation of particle methods for the incompressible Euler equations', *SIAM J. Numer. Anal.*, **31**, 1090–1108.

D. G. Dritschel (1989), 'Contour dynamics and contour surgery – Numerical algorithms for extended, high-resolution modelling of vortex dynamics in two-dimensional, inviscid, incompressible flows', *Comp. Phys. Review*, **10**, 77–146.

D. G. Dritschel and M. E. McIntyre (1990), 'Does contour dynamics go singular?' *Phys. Fluids A*, **2**, 748–753.

J. Duchon and R. Robert (1986), 'Solution globales avec nape tourbillionaire pour les equations d's Euler dans le plan', *C. R. Acad. Sc. Paris*, **302**, Series I. 5, 183–186.

J. Duchon and R. Robert (1988), 'Global vortex sheet solutions of Euler equations in the plane', *J. Diff. Eqn.*, **73**, 215–224.

D. Ebin (1988), 'Ill-posedness of the Rayleigh–Taylor and Helmholtz problems for incompressible fluids', *Comm. PDE*, **13**, 1265–1295.

L. C. Evans and J. Spruck (1991), 'Motion of level sets by mean-curvature, I', *J. Diff. Geom.*, **33**, 635–681.

L. C. Evans and J. Spruck (1992), 'Motion of level sets by mean-curvature, II', *Tran. Amer. Math. Soc.*, **330**, 321–332.

J. D. Fenton and M. M. Rienecker (1982), 'A Fourier method for solving nonlinear water-wave problems: Application to solitary-wave interactions', *J. Fluid Mech.*, **118**, 411–443.

P. T. Fink and W. K. Soh (1978), 'A new approach to roll-up calculations of vortex sheets', *Proc. Roy. Soc. London A.*, **362**, 195–209.

M. Glozman, Y. Agnon and M. Stiassnie (1993), 'High-order formulation of the water-wave problem', *Physica D*, **66**, 347–367.

R. Goldstein, A. Pesci and M. Shelley (1993), 'Topology transitions and singularities in viscous flows', *Phys. Rev. Lett.*, **70**, 3043–3046.

J. Goodman, T. Y. Hou and J. Lowengrub (1990), 'The convergence of the point vortex method for the 2-D Euler equations', *Comm. Pure and Appl. Math.*, **43**, 415–430.

J. Goodman, T. Y. Hou and E. Tadmor (1994), 'On the stability of the unsmoothed Fourier method for hyperbolic equations', *Numer. Math.*, **67**, 93–129.

L. J. Gray, M. F. Chisholm and T. Kaplan (1993), Morphological stability of thin films, in *Boundary Element Technology VIII*, (H. Pina and C. A. Brebbia, eds.), Southampton, UK, Computational Mechanics Publications, pp. 181–190.

A. Greenbaum, L. Greengard and G. B. McFadden (1993), 'Laplace's equation and the Dirichlet–Neumann map in multiply connected domains', *J. Comp. Phys.*, **105**, 267–278.

L. Greengard and V. Rokhlin (1987), 'A fast algorithm for particle summations', *J. Comp. Phys.*, **73**, 325–348.

L. Greengard and J. Strain (1990), 'A fast algorithm for the evaluation of heat potentials', *Comm. Pure Appl. Math.*, **43**, 949–963.

P. M. Gresho and R. L. Sani (1987), 'On pressure boundary conditions for the incompressible Navier–Stokes equations', *Internat. J. Numer. Methods Fluids*, **7**, 1111–1145.

D. Gottlieb and S. A. Orszag (1977), *Numerical Analysis of Spectral Methods: Theory and Applications*, CBMS–NSF Regional Conference Series in Applied Mathematics **26**, SIAM Publ., Philadelphia.

M. E. Gurtin (1986), 'On the 2-phase stefan problem with interfacial energy and entropy', *Arch. Ration. Mech. Anal.*, **96**, 199–241.

O. Hald (1979), 'Convergence of vortex methods II', *SIAM J. Numer. Anal.*, **16**, 726–755.

O. Hald (1991), Convergence of vortex methods, in *Vortex Methods and Vortex Motion*, (Gustafson and Sethian, eds.), SIAM publications, Philadelphia, pp. 33–58.

A. Harten, B. Engquist, S. Osher and S. R. Chakravarthy (1987), 'Uniformly high order accurate essentially non-oscillatory schemes, III', *J. Comp. Phys.*, **71**, 231–303.

J. J. L. Higdon and C. Pozrikidis (1985), 'The self-induced motion of vortex sheets', *J. Fluid Mech.*, **150**, 203–231.

T. Y. Hou and J. Lowengrub (1990), 'Convergence of a point vortex method for 3-D Euler equations', *Comm. Pure Appl. Math.*, **43**, 965–981.

T. Y. Hou and S. Osher (1994), *Computing Topological Singularities Using a Tracking Method: Geometric regularization*, preprint, Applied Math., Caltech.

T. Y. Hou, J. S. Lowengrub and M. J. Shelley (1994), 'Removing the stiffness from interfacial flows with surface tension', *J. Comp. Phys.*, **114**, 312–338.

T. Y. Hou, J. S. Lowengrub and M. J. Shelley, *The Roll-up and Self-intersection of Vortex Sheets Under Surface Tension*, preprint, Courant Institute.

T. Y. Hou, J. S. Lowengrub and R. Krasny (1991), 'Convergence of a point vortex method for vortex sheets', *SIAM J. Numer. Anal.*, **28**, 308–320.

Y. Kaneda (1990), 'A representation of the motion of a vortex sheet in a three dimensional flow', *Phys. Fluids A*, **2**, 458–461.

A. Karma (1986), 'Wavelength selection in dendritic solidification', *Phys. Rev. Lett.*, **57**, 858–861.

R. M. Kerr (1988), 'Simulation of Rayleigh–Taylor flows using vortex blobs', *J. Comput. Phys.*, **76**, 48–84.

D. A. Kessler and H. Levine (1986), 'Stability of dendritic crystals', *Phys. Rev. Lett.*, **57**, 3069–3072.

P. Koumoutsakos (1993), Direct Numerical Simulations of Unsteady Separated Flows Using Vortex Methods, Ph.D. thesis, Graduate School of Aeronautics, Caltech.

R. Krasny (1986a), 'A study of singularity formation in a vortex sheet by the point vortex approximation', *J. Fluid Mech.*, **167**, 65–93.

R. Krasny (1986b), 'Desingularization of periodic vortex sheet roll-up', *J. Comp. Phys.*, **65**, 292–313.

R. Krasny (1987), 'Computation of vortex sheet roll-up in the Trefftz plane', *J. Fluid Mech.*, **184**, 123–155.

H.-O. Kreiss and J. Oliger (1979), 'Stability of the Fourier method', *SIAM J. Num. Anal.*, **16**, 421–433.

J. S. Langer (1980), 'Instabilities and pattern formation in crystal growth', *Rev. Modern Phys.*, **52**, 1–28.

J. S. Langer (1986), 'Existence of needle crystals in local models of solidification', *Phys. Rev. A*, **33**, 435–441.

A. Leonard (1980), 'Vortex methods for flow simulation', *J. Comp. Phys.*, **37**, 289–335.

J. G. Liu and Z. P. Xin, *Convergence of Vortex Methods for Weak Solutions to the 2-D Euler Equations with Vortex Sheet Data*, preprint, Courant Institute.

M. S. Longuet-Higgins and E. D. Cokelet (1976), 'The deformation of steep surface waves on water, I. A numerical method of computation', *Proc. Roy. Soc. London A*, **350**, 1–26.

A. Majda (1986), 'Vorticity and the mathematical theory of incompressible fluid flow', *Comm. Pure Appl. Math.*, **39**, 5187–5220.

D. I. Meiron (1986), 'Boundary Integral formulation of the two-dimensional symmetric model of dendritic growth', *Physica-D*, **23**, 329–339.

D. I. Meiron, G. R. Baker and S. A. Orszag (1982), 'Analytic structure of vortex sheet dynamics, 1. Kelvin–Helmholtz instability', *J. Fluid Mech.*, **114**, 283–298.

W. Mulder, S. Osher and J. Sethian (1992), 'Computing interface motion in compressible gas dynamics', *J. Comp. Phys.*, **100**, 209–228.

D. W. Moore (1979), 'The spontaneous appearance of a singularity in the shape of an evolving vortex sheet', *Proc. R. Soc. Lond. Ser. A*, **365**, 105–119.

D. W. Moore (1981), 'On the point vortex method'. *SIAM J. Sci. Stat.*, **2**, 65–84.

D. W. Moore (1978), 'The equations of motion of a vortex layer of small thickness', *Stud. Appl. Math.*, **58**, 119–140.

D. W. Moore (1985), Numerical and analytical aspects of Helmholtz instability. In Theoretical and Applied Mechanics, *Proc. XVI IUTAM* (eds., Niodsen and Olhoff), pp. 263.

W. Mullins and R. Sekerka (1963), 'Morphological stability of a particle growing by diffusion or heat flow', *J. Appl. Phys.*, **34**, 323–329.

A. L. New, P. McIver and D. H. Peregrine (1985), 'Computations of overturning waves', *J. Fluid Mech.*, **150**, 233–251.

M. Nitsche and R. Krasny (1994), *A Numerical Study of Vortex Ring Formation at the Edge of a Circular Tube*, preprint, Dept. of Math., Univ. of Michigan.

S. Osher and J. Sethian (1988), 'Fronts propagating with curvature-dependent speed: Algorithms based on Hamilton–Jacobi formulations', *J. Comp. Phys.*, **79**, 12–49.

S. Osher and C. W. Shu (1991), 'High order essentially nonoscillatory schemes for Hamilton–Jacobi equations', *J. Comp. Phys.*, **28**, 907–922.

S. Osher, private communication.

L. Paterson (1981), 'Radial fingering in a Hele–Shaw cell', *J. Fluid Mech.*, **113**, 513–519.

L. Paterson (1985), 'Fingering with miscible fluids in a Hele–Shaw cell', *Phys Fluids.*, **28**, 26–30.

P. Pelcé (1988), *Dynamics of Curved Fronts*, Academic Press, Inc., San Diego.

D. H. Peregrine (1983), 'Breaking waves on beaches', *Ann. Rev. Fluid Mech.*, **15**, 149–178.

C. Peskin (1977), 'Numerical analysis of blood flow in the heart', *J. Comp. Phys.*, **25**, 220–252.

C. Pozrikidis (1992), *Boundary Integral and Singularity Methods for Linearized Viscous Flow*, Cambridge University Press.

C. Pozrikidis and J. J. L. Higdon (1985), 'Nonlinear Kelvin–Helmholtz instability of a finite vortex layer', *J. Fluid Mech.*, **157**, 225–263.

A. Prosperetti, L. A. Crum and H. C. Pumphrey (1989), 'The underwater noise of rain', *J. Geophys. Res.*, **94** , 3255–3259.

D. A. Pugh (1989), Development of Vortex Sheets in Boussinesq Flows – Formation of Singularities, Ph.D. Thesis, Imperial College, London

D. I. Pullin (1979), 'Vortex ring formation at tube and orifice openings', *Phys. Fluids*, **22**, 401–403.

D. I. Pullin (1982), 'Numerical studies of surface tension effects in nonlinear Kelvin–Helmholtz and Rayleigh–Taylor instability', *J. Fluid Mech.*, **119**, 507–532.

R. Rangel and W. Sirignano (1988), 'Nonlinear growth of the Kelvin–Helmholtz instability: effect of surface tension and density ratio', *Phys. Fluids*, **31**, 1845–1855.

S. N. Rauseo, P. D. Barnes, Jr and J. V. Maher (1987), 'Development of radial fingering patterns', *Phys. Rev. A*, **35**, 1245–1251.

A. J. Roberts (1983), 'A stable and accurate numerical method to calculate the motion of a sharp interface between fluids', *IMA J. Appl. Math.*, **31**, 13–35.

L. Rosenhead (1932), 'The point vortex approximation of a vortex sheet', *Proc. Roy. Soc. London Ser. A*, **134**, 170–192.

P. G. Saffman and G. I. Taylor (1958), 'The penetration of a fluid into a porous medium of Hele–Shaw cell containing a more viscous fluid', *Proc. Roy. Soc. London Ser. A*, **245**, 312–329.

L. W. Schwartz and J. D. Fenton (1982), 'Strongly nonlinear waves', *Ann. Rev. Fl. Mech.*, **14**, 39–60.

M. Shelley (1992), 'A study of singularity formation in vortex sheet motion by a spectrally accurate vortex method', *J. Fluid Mech.*, **244**, 493–526.

J. A. Sethian (1985), 'Curvature and the evolution of fronts', *Comm. Math. Phys.*, **101**, 487–499.

J. Sethian and J. Strain (1992), 'Crystal growth and dendritic solidification', *J. Comp. Phys.*, **98**, 231-253.

A. Sidi and M. Israeli (1988), 'Quadrature methods for periodic singular and weakly singular Fredholm integral equations', *J. Sci. Comp.*, **3**, 201–231.

C. W. Snyder, B. G. Orr, D. Kessler and L. M. Sander (1991), 'Effect of strain on surface morphology in highly strained InGaAs', *Phys. Rev. Lett.*, **66**, 3032–3035.

B. J. Spencer, P. W. Voorhees and S. H. Davis (1991), 'Morphological instability in epitaxially dislocation-free solid films', *Phys. Rev. Lett.*, **67**, 3696–3999.

B. J. Spencer and D. I. Meiron (1994), 'Nonlinear Evolution of the stress-driven morphological instability in a 2-dimensional semi-infinite solid', *Act. Met. Mat.*, **42**, 3629–3641.

M. Stiassnie and L. Shemer (1984), 'On modifications of the Zakharov equation for surface gravity waves', *J. Fluid Mech.*, **143**, 47–67.

J. Strain (1989), 'A boundary integral approach to unstable solidification', *J. Comp. Phys.*, **85**, 342–389.

P. Sulem, C. Sulem, C. Bardos and U. Frisch (1981), 'Finite time analyticity for the two and three dimensional Kelvin–Helmholtz instability', *Comm. Math. Phys.*, **80**, 485–516.

M. Sussman, P. Smereka and S. Osher, 'A level set approach for computing solutions to incompressible 2-phase flow', to appear in *J. Comp. Phys.*

E. Tadmor (1987), 'Stability analysis of finite difference, pseudospectral and Fourier–Galerkin approximations for time dependent problems', *SIAM Review*, **29**, 525–555.

G. I. Taylor (1950), 'The instability of liquid surfaces when accelerated in a direction perpendicular to their planes', *Proc. Roy. Soc. London Ser. A.*, **201**, 192–196.

G. Tryggvason and H. Aref (1983), 'Numerical experiments on Hele–Shaw flow with a sharp interface', *J. Fluid Mech.*, **136**, 1–30.

G. Tryggvason (1988), 'Numerical simulations of the Rayleigh–Taylor instabilities', *J. Comp. Phys.*, **75**, 253–282.

G. Tryggvason (1989), 'Simulations of vortex sheet roll-up by vortex methods', *J. Comp. Phys.*, **80**, 1–16.

G. Tryggvason , W. J. A. Dahm and K. Sbeih (1991), 'Fine structure of vortex sheet roll-up by viscous and inviscid simulation', *J. Fluid Eng.*, **113**, 31–36.

S. O. Unverdi and G. Tryggvason (1992), 'A front-tracking method for viscous, incompressible, multi-fluid flows', *J. Comp. Phys.*, **100**, 25–37.

A. van de Vooren (1980), 'A numerical investigation of the rolling-up of vortex sheets', *Proc. Roy. Soc. London Ser. A*, **373**, 67–91.

L. van Dommelen and E. A. Rundensteiner (1989), 'Fast, adaptive summation of point forces in the two-dimensional Poisson equation', *J. Comp. Phys.*, **83**, 126–147.

T. Vinje and P. Brevig (1981), 'Numerical simulation of breaking waves', *Adv. Water Resources*, **4**, 77–82.

P. W. Voorhees, G. B. McFadden, R. F. Boisvert and D. I. Meiron (1988), 'Numerical simulation of morphological development during Ostwald ripening', *Acta Metall.*, **36**, 207–222.

P. W. Voorhees (1992), 'Ostwald ripening of 2-phase mixtures', *Annual review of Material Sci.*, **22**, 197–215.

B. J. West, K. A. Brueckner and R. S. Janda (1987), 'A new numerical method for surface hydrodynamics', *J. Geophys. Res. C*, **92**, 11803–24.

R. W. Yeung (1982), 'Numerical methods in free-surface flows', *Ann. Rev. Fl. Mech.*, **14**, 395–442.

V. I. Yudovich (1963), 'Non-stationary flow of an ideal incompressible liquid', *Zh. Vych. Mat.*, **3**, 1032–1066 (in Russian)

N. J. Zabusky, M. H. Hughes and K. V. Robert (1979), 'Contour dynamics for the Euler equations in two dimensions', *J. Comp. Phys.*, **30**, 96–106.

N. J. Zabunksy and E. A. Overman (1983), 'Regularization of contour dynamics algorithms , 1 Tangential regularization', *J. Comp. Phys.*, **52**, 351–373.